International MUON Collider Collaboration

March 9, 2022
https://muoncollider.web.cern.ch

The physics case of a 3 TeV muon collider stage

(Preliminary Draft)

Submitted to the Proceedings of the US Community Study
on the Future of Particle Physics (Snowmass 2021)

Editors:
J. de Blas[1], *D. Buttazzo*[2], *R. Capdevilla*[3,4], *D. Curtin*[3], *R. Franceschini*[5], *F. Maltoni*[6,7], *P. Meade*[8], *F. Meloni*[9], *S. Su*[10], *E. Vryonidou*[11], *A. Wulzer*[12]

Authors:
List being defined??

Signatories:
List being defined??

[1]CAFPE and Departamento de Física Teórica y del Cosmos, Universidad de Granada, Granada, Spain
, [2]INFN, Sezione di Pisa, Italy
, [3]Department of Physics, University of Toronto, Canada
, [4]Perimeter Institute for Theoretical Physics, Waterloo, Ontario, Canada
, [5]Dipartimento di Matematica e Fisica and INFN, Università degli Studi Roma Tre
, [6]Dipartimento di Fisica e Astronomia, Alma Mater Studiorum - Università di Bologna, Italy
, [7]CP3, Université catholique de Louvain, Louvain-la-Neuve, Belgium
, [8]C. N. Yang Institute for Theoretical Physics, Stony Brook University, Stony Brook, USA
, [9]Deutsches Elektronen-Synchrotron DESY, Hamburg, Germany
, [10]Department of Physics, University of Arizona, Tucson, Arizona 85721, USA
, [11]University of Manchester, Manchester, United Kingdom
, [12]Dipartimento di Fisica e Astronomia, Università di Padova

Abstract

In the path towards a muon collider with center of mass energy of 10 TeV or more, a stage at 3 TeV emerges as an appealing option. Reviewing the physics potential of such collider is the main purpose of this document. In order to outline the progression of the physics performances across the stages, a few sensitivity projections for higher energy are also presented.

There are many opportunities for probing new physics at a 3 TeV muon collider. Some of them are in common with the extensively documented physics case of the CLIC 3 TeV energy stage, and include probing higgsino thermal dark matter, measuring the Higgs trilinear coupling and testing the possible composite nature of the Higgs boson and of the top quark at the 20 TeV scale or more.

Other opportunities are unique of a 3 TeV muon collider, and stem from the fact that muons are collided rather than electrons. This is exemplified by studying the potential to explore the microscopic origin of the current g-2 and B-physics anomalies, which are both related with muons.

Contents

1 Introduction

Muons can be accelerated in rings up to very high energies, without fundamental limitation from synchrotron radiation. The recently formed International Muon Collider Collaboration (IMCC) [1] targets the design of muon colliders with a center of mass energy E_{cm} of 10 TeV or slightly more (10+ TeV), which seem feasible with technologies that can be made available in the near future. The highest E_{cm} muon colliders can reach, possibly subject to more radical advances in accelerator technologies, is not yet known and will be assessed.

The physics potential of 10+ TeV muon colliders has been investigated quite extensively over the past two years [**?**, 2–14]. While much is still to be done, the emerging picture [2–6] is that a 10+ TeV muon collider combines the advantages of proton and of e^+e^- colliders, thanks to the large energy available for direct exploration and to the perspectives for precise measurements within the Standard Model (SM) and beyond. Furthermore the simultaneous availability of energy and precision offers unique opportunities for new physics discovery and characterization. All this, at a single collider and on a feasible timescale. The extraordinary physics potential of a 10+ TeV muon collider unquestionably poses the urgency of investing in a complete design study [2].

On the other hand, strategic considerations suggest that a first stage of the muon collider with lower E_{cm} could facilitate and accelerate the development of the project. It is worth emphasizing in this context that muon colliders can be built in stages, in spite of being circular colliders. Indeed, the muon production and cooling complex can be used at all energies, and the muon acceleration proceeds through a sequence of rings, which can be reused at higher energy. The final collider ring of the lower energy collider can not be reused for the higher energy stage, but this might have a minor impact on the total cost. The advantage of a low E_{cm} first stage mainly stems from the significant reduction of the initial investment. This could give easier and faster access to the necessary financial resources. Furthermore the reduced energy target allows, if needed, to make compromises on technologies that might not yet be fully developed, avoiding potential delays.

When discussing the staging options it should be taken into account that lepton collisions at around 250 GeV can be more easily obtained with circular or linear e^+e^- machines, and with a much higher luminosity than what muon colliders can achieve. So while there is evidently a compelling physics case for a leptonic 250 GeV "Higgs factory" at that energy, muon colliders are not the best option. Linear e^+e^- colliders can also reach the TeV scale, up the 3 TeV energy of the last stage of the CLIC project [15]. The luminosity attainable by a muon collider of 3 TeV is comparable to the one of CLIC. Therefore a muon collider with $E_{\text{cm}} = 3$ TeV, operating at the maximal energy for which an e^+e^- machine has ever been designed, emerges as a natural first stage of the muon collider project.

A fascinating alternative for a first muon collider [16, 17] is to operate it very close to Higgs pole, $E_{\text{cm}} = m_H = 125$ GeV, in order to study the lineshape of the Higgs particle. The larger Yukawa coupling of the muon offers in this case a competitive advantage to muon colliders relative to e^+e^- machines at the same energy. However the Higgs is a rather narrow particle, with a width over mass ratio Γ_H/m_H as small as $3 \cdot 10^{-5}$. The muon beams would thus need a comparably small energy spread $\Delta E/E = 3 \cdot 10^{-5}$ for the program to succeed. Engineering such tiny energy spread might perhaps be possible, however it poses a challenge for the accelerator design that is peculiar of the Higgs pole collider and of no relevance for higher energies, where a much higher permille-level spread is perfectly adequate for physics.

For this reason, the Higgs pole muon collider is not among the targets of the IMCC. Nevertheless in this document we review its physics potential, assuming the feasibility of the small beam energy spread $\Delta E/E = 3 \cdot 10^{-5}$. We also assume a relatively large integrated luminosity, to be however collected in a short enough time not to delay the upgrade to higher energy. We also assume that the Beam Induced Backgrounds (BIB) from muon decays can be mitigated, while the BIB impact at the Higgs pole muon collider has never been studied and is expected to be more severe than at 3 TeV.

The main goal of the present report is to review the physics potential of a 3 TeV muon collider, with 1 ab^{-1} integrated luminosity if not otherwise specified. Results at 10+TeV energy are also described, occasionally, in order to outline the progression of the physics performances across the stages. The material is collected from different sources, including invited contributions that summarize, adapt and extend recent papers on muon collider physics. Some of these papers were initiated in preparation for this report, and part of the material results from dedicated work and appears here for the first time.

The physics opportunities of the 3 TeV muon collider overlap in part with the ones of CLIC, extensively documented in Ref. [18] and summarized in [19, 20] in preparation for the 2020 update of the European Strategy for Particle Physics. There are however important differences between the two projects that need to be taken into account.

First, the CLIC stage at 3 TeV is the last of a series of three, which include in particular a stage at 380 GeV that is quite effective for precise measurements of Higgs (and top) properties. The muon collider precision on the determination of the Higgs coupling should thus be reassessed and can not be inferred from CLIC results.

Second, CLIC targets 5 ab^{-1} luminosity at 3 TeV, while only 1 ab^{-1} is currently foreseen for the 3 TeV muon collider in the baseline design target. This difference is partly compensated by the absence of beamstrahlung at the muon collider, which instead entails a significant reduction of the high-energy luminosity peak at CLIC. However it can result in a significant degradation of the muon collider performances for those studies that do not rely very strongly on collisions at the highest energy. On the contrary, for studies that do require high energy collisions and that are not strongly sensitive to the integrated luminosity, like direct searches, CLIC sensitivity projections generically apply.

Third, muon colliders pose a novel challenge for detector design, due to the copious BIB from the decay products of the muons in the colliding beams. Since these challenges have never been encountered and addressed before, a design of the muon collider detector and an assessment of its performances is not yet available, unlike for CLIC. Promising preliminary results and directions for further progress, described in Ref.s [21,22], suggest that reconstruction efficiencies and resolutions comparable to the one of the CLIC detector should be achievable eventually. Most of the studies we present are based on these assumed performances, encapsulated in the muon collider Delphes card [**?**].

Some results are instead obtained with the full simulation of a preliminary muon collider detector, under realistic BIB conditions. In particular, full simulation estimates of Higgs signal-strength measurements are described in Section 2 and compared with the estimates based on Delphes. Moreover in Section 5.1 we review a search for disappearing tracks that successfully implements a BIB mitigation strategy for this challenging signal. The remarkable conclusion is that the 3 TeV muon collider is sensitive to the minimal higgsino dark matter candidate.

The fourth and most obvious difference with CLIC is that the 3 TeV muon collider collides muons rather than electrons. Engineering muon anti-muon collisions for the first time is in itself a tremendous opportunity in the quest for generic exploration of new physics. Concretely, there are plenty of motivated scenarios where new physics couples more strongly to muons than to electrons. One of them might be waiting for a muon collider to be discovered.

The current g-2 and B-physics anomalies offer additional motivations for muon-filic new physics scenarios, that result in several opportunities for the muon collider that are specific of muon collisions, to be reviewed in this document. Obviously the anomalies could be resolved by new experiments and theoretical calculations in few years, before the muon collider is built. Alternatively, they could be strengthened and become a primary driver of particle physics research. We will see that muon colliders offer excellent perspectives for progress on the muon anomalies already at 3 TeV, with a very competitive time scale. This further supports the urgency of investing now in a complete muon collider design study.

This report illustrates the 3 TeV muon collider physics case under three different perspectives, along the lines described below. A concise summary of our key findings is provided in Section 11.

Higgs and effective field theory

Editors: J. de Blas, P. Meade and E. Vryonidou

While the direct search of new heavy particles is perhaps one of the main physics motivator of a multi-TeV muon collider, such a machine would also bring opportunities in terms of performing precise measurements of SM processes and thus explore new physics in an indirect way. This is of particular interest for Higgs physics, which is crucial from the point of view of learning about models addressing the hierarchy problem, as these tend to predict deviations on the Higgs interactions. At the HL-LHC these will be bounded to be below few percent, so a machine capable of bringing down such contraints to the permille level is needed to make substantial progress in this front. This is the target of most of the currently proposed Higgs factories, e^+e^- operating tipically at energies $\sqrt{s} = 240$ GeV. As we will see, such precision can also be obtained under certain assumptions via the Higgs measurements at a high energy muon collider. In Section 2, we will discuss the current prospects for Higgs physics measurements at high-energy muon colliders, discussing also the potential of the low energy option operating at the Higgs pole. These prospects will be then used to estimate the projected reach in precision for single and multi-Higgs interactions.

The programme of Higgs measurements that would be possible at a muon collider, with the possibility of testing BSM deformations of the Higgs properties with a precision at the permile level, represents however only part of the physics potential of a muon collider in terms of exploring new physics effects indirectly. The so-called SM Effective Field Theory (SMEFT) helps in putting these measurements into a more global context from the point of view of constraints on new physics. In the SMEFT, the SM is complemented by higher-dimensional gauge-invariant operators involving only SM fields, suppressed by the scale associated to new physics, typically denoted by Λ. The very minimal assumptions involved in its construction, makes the SMEFT a powerful tool in terms of parameterizing general BSM deformations that could show up in SM processes. It can also help in providing guiding principles in the design of observables to study, based on the type of new physics scenarios of interest and taking into account the technical capabilites of the experimental facilities. The access to very high energies at a muon collider brings additional physics opportunities in this regard. Indeed, the contributions of the SMEFT operators to physical processes are suppressed by $(q/\Lambda)^n$ with $q = v, E$. Thus, for those effects that growth with the energy in a given process, one could exploit the energy reach of a multi-TeV collider to set precision constraints in the corresponding operator, even if experimental accuracy is limited. In Section 3 of this report we will perform a global EFT interpretation of the projections available at muon colliders, where apart from the Higgs results we also discuss the gains that one could obtain with respect to the HL-LHC for a few of these *high energy probes* of new physics. These results will then be interpreted in terms of constraints over a few classes of new physics scenarios.

Beyond the SM

Editors: R. Franceschini, F. Meloni and S. Su

A 3 TeV muon collider also serves as a direct discovery machine for new physics beyond the SM by searching for new particles that carry electroweak charges. In the simplest SM plus a real singlet extension (Sec. 4.1.1), extra heavy singlet mixes with the SM Higgs. Single production of the heavy scalar with the subsequent decay into two SM Higgses provides the most sensitive channel, which can be used to explore the small mixing cases, exceeding the sensitivity of the Higgs factories for small mass region. Reaches at higher center of mass energy could be extended further. Such setup has also been studied under the consideration of strong first order electroweak phase transition. For the two Higgs doublet extension of the SM (Sec. 4.1.2), pair production of the BSM Higgses, as well as single production in association with pair of fermions, and radiative production have been studied at a muon collider. At 3 TeV, production via annihilation dominates, while VBF production becomes more important at higher center of mass energies. Reach up to the pair production threshold is possible when all four fermion final states channels are used. Single production modes can extend the reach further, especially in regions with enhanced Yukawa couplings. For the Inert Doublet Model (Sec. 4.1.3) with the light neutral BSM Higgs being a possible dark matter candidate, the semileptonic final states with missing energy signal provides the best reach. Reach of charged Higgs mass up to 1 TeV is possible at a 3 TeV muon collider. Electroweak states of the Minimal Supersymmetric Standard Model (Sec. 4.1.4) can also be studied at a muon collider with the dominant pair production mode. For electroweakinos, as well as selectrons and smuons, reach up to half of the center of mass energy can be achieved even with small mass splittings. The reach for staus is slightly worse given the difficulty in identifying the hadronic tau final states.

The possibility that dark matter is a weakly interacting particle has been a main driver for theory and experiments in search of physics beyond the Standard Model. Particle colliders have the unique capability to produce dark matter in a controlled environment and potentially study this new form of matter in great detail, testing fully its interactions with the SM and possible further new physics states. Among the most studied dark matter candidates there are general admixtures of weak doublets, triplets and uncharged weak singlets. Most notably this possibility arises in supersymmetric extensions of the SM. However, a weakly charged n-plet can also be added to the SM just to provide a dark matter candidate, resulting in very sharply defined BSM scenarios with sharp predictions on the dark matter mass and on its other properties.

The typical mass range for such dark matter candidates is around the TeV scale, therefore a muon collider at 3 TeV has a unique chance to produce and discover dark matter. Notable fermionic candidates are the 1.05 TeV pure doublet, the higgsino dark matter of supersymmetry, and the 2.9 TeV Majorana pure triplet, the wino dark matter of supersymmetry. Section 5.1 reports sensitivity to exclude pure higgsino dark matter at the 3 TeV muon collider searching for direct evidences of its very characteristic stub-track signature. A discovery can be attained running at a slightly higher center of mass energy around 3.5 TeV, still at the nominal 1 ab^{-1} luminosity, or by running for a longer period at 3 TeV until around 10 ab^{-1} are accumulated.

The sensitivity to pure higgsino dark matter is a key result for physics potential of the 3 TeV muon collider, as this dark matter candidate yields spin-independent cross-sections on nuclei below the so-called neutrino floor of direct DM detection experiment.

As discussed in Section 4.2.1 the direct search for dark matter can be carried out more generally looking for dark matter particles produced in association with SM states, that we denote as X. For $X = \gamma$ and $X = W^{\pm}$ the muon collider has a potential to put stringent bounds on dark matter candidates and can exclude, or add to the hints of discovery of, a higgsino dark matter running at 3 TeV and collecting around 5 ab^{-1}.

The picture is further enriched by the precision measurements that can be carried at the 3 TeV muon collider, as described in Sec. 4.2.2. Indeed, the precision measurements of angular distributions and total rates for simple processes $\mu^+\mu^- \to f\bar{f}, VV, Vh + X$ can yield further evidence for dark matter production. E.g. a 3 TeV muon collider can exclude, or add to the hints of discovery of, a higgsino dark matter running at 3 TeV and collecting around 10 ab^{-1}.

The multi-channel sensitivity to higgsino dark matter of the 3 TeV muon collider is a showcase of the the muon collider potential to discover weakly charged dark matter. This potential extends to other weakly charged candidates. Indeed the precision measurements described in Sec. 4.2.2 offer sensitivity to further dark matter candidates, e.g. a fermionic Dirac weak triplet 2.0 TeV dark matter, already with 1 ab^{-1} of integrated luminosity. Further dark matter candidates can be probed systematically in all the three modes described above by increasing the accumulated luminosity or increasing the center of mass energy, or both.

Muon-specific opportunities

Editors: D. Buttazzo, R. Capdevilla and D. Curtin

Lepton flavour universality is not a fundamental property of Nature. In fact, even in the SM, the only known non-gauge interactions – the Yukawa interactions with the Higgs field – violate flavour universality maximally, both in the lepton and in the quark sector. The Higgs boson couples significantly to the third generation of fermions, while its couplings to lighter generations are negligible. It is therefore conceivable that new physics in the multi-TeV range, if it exists, also distinguishes the three families of fermions; this is even more the case if new physics is somehow related to the Higgs and to the physics of Electroweak symmetry breaking. If that is the case, a muon collider would be able to explore physics scenarios that are not accessible to any other machine that collides first-generation particles.

Several hints of lepton flavour non-universality have been observed in the last decade. Intriguingly enough, most of these hints are observed in processes that involve muons. One is the muon anomalous magnetic moment (g-2), that shows an enduring discrepancy with the Standard Model prediction. Another hint comes from $b \to s$ transitions, with several semi-leptonic and leptonic decay rates of B mesons that show a difference between electron and muon final states, thus providing evidence of flavored new interactions that violate lepton flavor universality. All these anomalies could be confirmed in the next few years, providing a clear evidence of new physics coupled to muons. Sections 6 and 7 report the sensitivity of a muon collider to new physics aiming to explain these anomalies, both from an effective field theory perspective and in the context of specific models.

Section 6 covers the muon g-2. We will present the muon collider sensitivity to the various new physics scenarios that can explain the anomaly, which could have origin in a vast range of mass scales, from the GeV to a hundreds to TeV. By doing this we will be able to establish a no-lose theorem for a muon collider program, in case the presence of new physics in the g-2 will be confirmed in the forthcoming years. A 3 TeV muon collider could probe in a model-independent way scenarios where new physics interacts mainly with the second generation of fermions. At the same time, all the models with TeV-scale new physics can be probed via direct production. Further indirect constraints on well-motivated models with heavy new physics come from Higgs physics. The remaining possible new physics interpretations of the muon g-2 will be accessible to muon beam dumps experiments, that can efficiently discover light new particles, and to muon colliders of higher energy. A 10 TeV muon collider can fully test new physics in semi-leptonic interactions, and all models that respect minimal flavor violation and do not create a fine tuning problem in the muon mass. Finally, the endgame of this program is a 30 TeV muon collider that can directly probe the dipole operator responsible for the anomalous magnetic moment, closing the window on any possible heavy new physics that might be responsible for the anomaly.

Section 7 covers the B-physics anomalies. We will study the sensitivity of a muon collider to the possible new physics interpretations. A muon collider running at an energy of about 6 TeV has the opportunity to provide a true *no-lose* theorem, being able to test the nightmare scenario where only the four-fermion interactions needed to explain the anomaly are present. This extreme scenario, although not truly motivated from a theoretical perspective, could not be tested by any other collider, including a 100 TeV hadron machine. If some realistic flavor structure is assumed, the same result can be obtained already at an energy of 3 TeV or less. Both in a model-independent approach and in concrete motivated models, a muon collider would cover all corners of the parameter space that are not accessible to the HL-LHC.

Finally, in sections 8, 9, and 10 we will study further muon-specific opportunities including lepton flavor violation, Higgs physics and extended Higgs sectors, and weakly interacting dark sectors. All these studies focus on scenarios where new physics communicates with the Standard Model through the muon portal, where muon colliders have a clear advantage over any other type of collider.

2 Higgs physics at muon colliders

At high-energy muon colliders, as the virtual electroweak gauge boson content of the muon beam becomes relevant, vector boson fusion (VBF) becomes the most important channel for production of SM particles. This is illustrated in Figure 1, which shows how the growth with the energy of VBF Higgs production clearly outmatches the usual higgsstrahlung process dominant at low-energy e^+e^- Higgs factories. An initial estimate for the precision that would be possible for Higgs measurements via W boson fusion (WBF, $\mu^+\mu^- \to h\bar{\nu}\nu$) and Z boson fusion (ZBF, $\mu^+\mu^- \to h\mu^+\mu^-$) has been recently presented on [4]. These were obtaining including fast detector simulation but they neglect backgrounds, both physics as well as the beam-induced ones. The latter are however suppressed by a cut $|\eta| < 2.5$, equivalent to vetoing physics objects within 10 degrees of the beam, as suggested by 1.5 TeV muon collider studies [23]. These estimates are currently being extended to include the effects of physics backgrounds [24]. Note that in order to distinguish between WBF and ZBF, one must be able to tag the forward muons beyond $|\eta| \approx 2.5$. The projected sensitivities for the main Higgs decays in single H production are estimated at the few percent level at 3 TeV with 1 ab^{-1}, whereas at 10 TeV with 10 ab^{-1}, precisions a t the permile level would be possible for the main decay channels ($b\bar{b}$, WW^*). While the 3 TeV numbers could be considered comparable to the HL-LHC, the use of different production mechanisms makes both machines quite complementary, as we will see in the Higgs coupling interpretation presented below. It must be noted that there are currently no available projections for sensitivities of ttH production and hence, for processes direct sensitivity to the Top Yukawa coupling, y_t. As suggested by Fig. 1, $VV \to ttH$ would again dominate over the standard ttH production. In [4] only $WBF\ ttH$ was used to infer an estimate precision in the rate at 10 TeV with 10ab^{-1}, yielding an uncertainty of 12%. Even if a combination of all VBF channels would return an estimate of ~ 2500 events, as shown in Fig. 1, a proper study including backgrounds is required to extract a precision for y_t which, in any case, does not seem to be far beyond the HL-LHC estimate of a few percent. This precision could benefit from a combination in global study including other VBF processes sensitive to y_t, e.g. $WW \to t\bar{t}$.

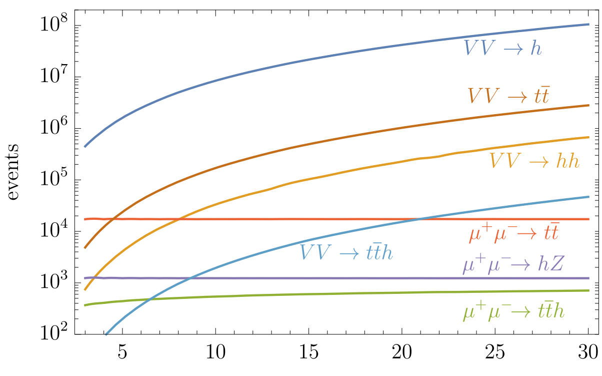

Fig. 1: Expected number of events for different processes at a muon collider, as a function of the centre-of-mass energy, for integrated luminosities $L = 10\,\text{ab}^{-1}(E_{\rm cm}[\text{TeV}]/10\text{ TeV})^2$. Figure courtesy of A. Wulzer.

Relatively high rates are also accesible to high-energy colliders for multi-Higgs processes via VBF production. This is particularly the case for $\mu^+\mu^- \to HH\bar{\nu}\nu$ at 10 TeV 10 ab^{-1}, where a total of $3 \cdot 10^6$ HH events would be produced. These could be used to obtain a determination of the triple Higgs coupling λ_3. Assuming the uncertainties associated to single Higgs couplings are kept under control by single Higgs processes (see below), in table 1 we collect the expected precisions for the exclusive determination of the trilinear Higgs coupling, obtained using the likelihood from the recent study in Ref. [6]. This uses the information from the differential distribution in M_{HH} in $\mu^+\mu^- \to HH\bar{\nu}\nu$. (See also Ref. [25], which reports similar results). As can be seen, the trilinear Higgs coupling could be

Table 1: 68% probability sensitivity to the h^3 coupling at a muon collider at different energies. Derived using the likelihood from the study in [6]. (We note that the likelihood at 3 TeV is non-Gaussian, with a second minimum for $\delta\kappa_\lambda > 0$, so the 68% probability interval is quite different from the 1-σ limits computed with reference to the mode of the distribution $\delta\kappa_\lambda^{1\sigma,\ 3\mathrm{TeV}} \in [-0.17, 0.18]$. See text for details.)

	3 TeV μ-coll. L≈ 1 ab^{-1}	10 TeV μ-coll. L= 10 ab^{-1} 68% prob. interval	14 TeV μ-coll. L≈ 20 ab^{-1}	30 TeV μ-coll. L= 90 ab^{-1}
$\delta\kappa_\lambda$	[-0.27,0.35] ∪ [0.85,0.94] →[-0.15,0.16] (2× L)	[-0.035, 0.037]	[-0.024, 0.025]	[-0.011, 0.012]

determined at 68% probability at 3 TeV with a precision of several tenths of percent, but still better than the projected error from the HL-LHC of $\sim 50\%$. We also note that the presence of a second minimum in the κ_λ log-likelihood "deforms" the expected 68% probability intervals with respect to the standard 1σ bounds, valid for a Gaussian distribution, which would suggest a more precise result of $\approx 18\%$. The influence of this second minimum could be easily alleviated by an increase in luminosity by roughly a factor of two. This would bring a similar improvement in the bounds, as opposed to the expected $\sqrt{2}$ reduction in the size of the interval, and also single out the solution around $\delta\kappa_\lambda = 0$ at 68% probability, yielding a precision for κ_λ of 15%. On the other hand the higher energy and luminosity of the 10 TeV options would bring a determination at the $\sim 5\%$ level precision, better thant CLIC at 3 TeV, and comparable to what would be possible at a 100 TeV hadron collider [26]. For comparison, we also report the projected sensitivities at even higher centre-of-mass energies, 14 and 30 TeV, where a one percent level determination could be possible.

Beyond double Higgs production, a multi-TeV $\mu^+\mu^-$ collider could use triple-Higgs production to gain sensitivity to the quartic Higgs coupling, λ_4, as recently explored in Ref. [27]. The cubic and quartic Higgs interaction are related in the SM and extensions were electroweak symmetry breaking is linearly realized (described at low energies by a SMEFT Lagrangian). If this is not the case, new physics could modify λ_3 and λ_4 indepedendently. The quartic coupling is directly tested at leading order via, e.g. $\mu^+\mu^- \to HHH\bar{\nu}\nu$, which has a cross section of 0.31 (4.18) ab at $\sqrt{s} = 3$, (10) TeV [27]. For realistic luminosities, this makes a 3 TeV option unable to probe the quartic coupling, but this could be tested at 10 TeV to a precision of tens of percent with integrated luminosities of several tens of ab.

Finally, we comment on the possibility of, as a first stage before a high energy muon collider. operating at significantly low energies, as this could be advantageous from the accelerator perspectives. In particular, one could operate around the Higgs pole $\sqrt{s} = 125$ TeV, which also brings the question of what would be the physics benefits of performing s-channel Higgs measurements. Indeed, unlike other collider options, a $\sqrt{s} = 125$ GeV $\mu^+\mu^-$ collider could perform on-shell Higgs physics directly via $\mu^+\mu^- \to H$ production which, in particular, brings the opportunity of a direct model-independent measurement of the Higgs width (as opposed to, e.g. e^+e^- Higgs factories where this could be determined indirectly, by exploiting the measurement of the inclusive ZH cross section in combination with all the other exclusive rates). With a resonant $\mu^+\mu^- \to H$ cross section of 70 pb, reduced to about 22 pb when taking into account a beam energy spread $R = 0.003\%$ together with the effects of initial state radiation, a luminosity at the level of several fb^{-1} would yield order 10^{-5} Higgses, limiting a priori the statistical reach in terms of precision Higgs physics compared to the Higgs factory runs at the different future colliders that have been proposed, where an order of magnitude larger in the number of Higgs events are expected. The direct measurement of the width at the percent level can partially compensate this loss in terms of pure statistics, though, as it directly normalizes all rates, whereas the normalization at other future H factories comes from a direct measurement of a particular coupling. The expected precision in different channels, together with an optimized study of the determination of the Higgs lineshape from a threshold scan have been performed in [28]. This includes the main physics backgrounds but ignores the beam-induced ones which, as in the high-energy case, are simply suppressed by a ten degree cut around the beam.

In what follows we interpret the available projections for single Higgs processes at muon colliders in terms of sensitivity to modifications of the Higgs boson couplings, to illustrate the expected improvements at the different stages, and compared to the knowledge that will be available at the end of the LHC era.

2.1 Higgs coupling precision

To illustrate the potential of the muon collider in measuring the properties of the Higgs boson, we show in Table 2 the results of a series of fits to the single Higgs couplings in the so-called κ framework,[*] where the cross sections, decomposed as follows

$$(\sigma \cdot \mathrm{BR})(i \to \mathrm{H} \to f) = \frac{\sigma_i \cdot \Gamma_f}{\Gamma_H}, \tag{1}$$

are parameterized in terms of scaling parameters κ,

$$(\sigma \cdot \mathrm{BR})(i \to \mathrm{H} \to f) = \frac{\sigma_i^{SM} \kappa_i^2 \cdot \Gamma_f^{SM} \kappa_f^2}{\Gamma_H^{SM} \kappa_H^2} = \frac{\kappa_i^2 \cdot \kappa_f^2}{\kappa_H^2} \quad , \tag{2}$$

and where we will assume, for the purposes of this sections that the Higgs boson only into SM final states, i.e. $\kappa_H^2 \equiv \sum_j \kappa_j^2 \Gamma_j^{\mathrm{SM}} / \Gamma_H^{\mathrm{SM}}$. Note that the muon collider option operating at 125 GeV offers the possibility of a model-independent measurement of the Higgs width, allowing to close a fit where the Higgs width is a free parameter, $\Gamma_H = \frac{\Gamma_H^{\mathrm{SM}} \cdot \kappa_H^2}{1-(BR_{\mathrm{new}})}$. A comparison of the results at the different machines releasing the constraint that Γ_H contains only SM channels is thus not possible and here we will restrict to the case $BR_{\mathrm{new}} = 0$. The results for the fits at different colliders are presented in Table 2 and illustrated in Figure 2. We compare with the expected precision at the HL-LHC[†], which is also combined with the projections at the different variants of the muon colliders, to show the impact of the muon collider measurements in the knowledge of the different coupling modifiers.

From the results, it is clear that any incarnation of a muon collider with the considered settings would be able to bring a significant improvement in the knowledge of the several of the Higgs couplings. This is particularly the case for the multi-TeV options for the couplings to vector bosons Z, W, where subpercent precisions could be achieved, reaching the permile level for the 10 TeV option. Comparatively, the precision of the same couplings for the 125 GeV option is somewhat worse. The main gain from the 125 GeV setup, apart from the width which is not taken into account in these fits, would be a subpercent determination of the muon coupling. For any other coupling, it typically underperforms compared to the 3 TeV results, unless high luminosities are collected. (We show the 125 GeV results for both 5 and 20 fb^{-1}, from [28].) It is also worth noting the complementarity with future e^+e^- factories, in particular with the 10 TeV option. Given the different main modes of electroweak production of the Higgs at each facility (ZH at e^+e^- and WBF at a multi-TeV $\mu^+\mu^-$), each are more sensitive to either κ_Z (for e^+e^-) or κ_W (for $\mu^+\mu^-$) and in combination are able to bring both to a precision of one permile (or even below if one assumes custodial symmetry relations).

Finally, and as explained above, we should mention that the estimates for some couplings, in this case $\kappa_{t,Z\gamma}$, are limited by the lack of inputs for processes sensitive to them (ttH and $H \to Z\gamma$) so the numbers presented here should not be taken as representative of the physics potential of the muon colliders.

[*]The fits presented in this chapter have been performed using the `HEPfit` code [29].

[†]We use the same inputs as in [19], with the exception of the channels $H \to$invisible. We use the S2 projections for systematic uncertainties, as explained in [30].

Table 2: Results from the κ fit assuming no BSM contributions to the Higgs width.

Coupling	HLLHC	HLLHC + 125 GeV μ-coll. 5 / 20 fb^{-1}	HLLHC + 3 TeV μ-coll. 1 ab^{-1}	HLLHC + 10 TeV μ-coll. 10 ab^{-1}	HLLHC + 10 TeV μ-coll. + e^+e^- H fact (240/365 GeV)
κ_W	1.7	1.3 / 0.9	0.4	0.1	0.1 /
κ_Z	1.5	1.3 / 1.0	0.9	0.4	0.1
κ_g	2.3	1.7 / 1.4	1.4	0.7	0.6
κ_γ	1.9	1.6 / 1.5	1.3	0.8	0.8
κ_c	-	12 / 5.9	7.4	2.3	1.1
κ_b	3.6	1.6 / 1.0	0.9	0.4	0.4
κ_μ	4.6	0.6 / 0.3	4.3	3.4	3.2
κ_τ	1.9	1.4 / 1.1	1.3	0.6	0.4 /
$\kappa_t^\dagger$	3.3	3.1 / 3.1	3.1	3.1	3.1
$\kappa_{Z\gamma}^\dagger$	10	10 / 10	10	10	10
$\Gamma_H^\ddagger$	5.3	2.7 / 1.7	1.5	0.5	0.4

† No input used for μ collider.
‡ Prediction assuming only SM Higgs decay channels. Not a free parameter in the fits.

3 Effective Field Theory interpretations

In this section we present a global interpretation of the projections for different types of measurements at a high-energy muon collider in terms of an effective field theory constructed assuming any new degrees of freedom are much heavier than the electroweak scale and that at low energies the particles and symmetries are those of the SM, i.e. the so called SMEFT. While a full study in terms of the general SMEFT truncated at the dimension-6 level is not possible with the available set of projections for physics processes at a muon collider, a reasonably global fit can be closed when combining that information with the expected information that will be available by the end of the HL-LHC era, plus making a series of extra assumptions about the new physics. In particular, following what was done as part of the ESG studies [19, 20], we adopt the following dimension-6 EFT Lagrangian:

$$\begin{aligned}\mathcal{L}_{\rm SILH} =& \frac{c_\phi}{\Lambda^2}\frac{1}{2}\partial_\mu(\phi^\dagger\phi)\partial^\mu(\phi^\dagger\phi) + \frac{c_T}{\Lambda^2}\frac{1}{2}(\phi^\dagger \overleftrightarrow{D}_\mu\phi)(\phi^\dagger\overleftrightarrow{D}^\mu\phi) - \frac{c_6}{\Lambda^2}\lambda(\phi^\dagger\phi)^3\\ &+\sum_f\left(\frac{c_{y_f}}{\Lambda^2}y^f_{ij}\phi^\dagger\phi\bar{\psi}_{Li}\phi\psi_{Rj}+\text{h.c.}\right)\\ &+\frac{c_W}{\Lambda^2}\frac{ig}{2}\left(\phi^\dagger\overleftrightarrow{D}^a_\mu\phi\right)D_\nu W^{a\,\mu\nu}+\frac{c_B}{\Lambda^2}\frac{ig'}{2}\left(\phi^\dagger\overleftrightarrow{D}_\mu\phi\right)\partial_\nu B^{\mu\nu}\\ &+\frac{c_{\phi W}}{\Lambda^2}igD_\mu\phi^\dagger\sigma_a D_\nu\phi W^{a\,\mu\nu}+\frac{c_{\phi B}}{\Lambda^2}ig'D_\mu\phi^\dagger\sigma_a D_\nu\phi B^{\mu\nu}\\ &+\frac{c_\gamma}{\Lambda^2}g'^2\phi^\dagger\phi B^{\mu\nu}B_{\mu\nu}+\frac{c_g}{\Lambda^2}g_s^2\phi^\dagger\phi G^{A\,\mu\nu}G^A_{\mu\nu}\\ &-\frac{c_{2W}}{\Lambda^2}\frac{g^2}{2}(D^\mu W^a_{\mu\nu})(D_\rho W^{a\,\rho\nu})-\frac{c_{2B}}{\Lambda^2}\frac{g'^2}{2}(\partial^\mu B_{\mu\nu})(\partial_\rho B^{\rho\nu})\\ &+\frac{c_{3W}}{\Lambda^2}g^3\varepsilon_{abc}W^{a\ \nu}_{\mu}W^{b\ \rho}_{\nu}W^{c\ \mu}_{\rho}.\end{aligned} \tag{3}$$

While this just contains a subset of the operators of the more general dimension-six SMEFT, the operators in (3) are of special relevance for several BSM types of scenarios. For the purpose of this chapter we will focus, in particular, in the case of the Universal Composite Higgs scenarios and $U(1)$ extensions of the SM.

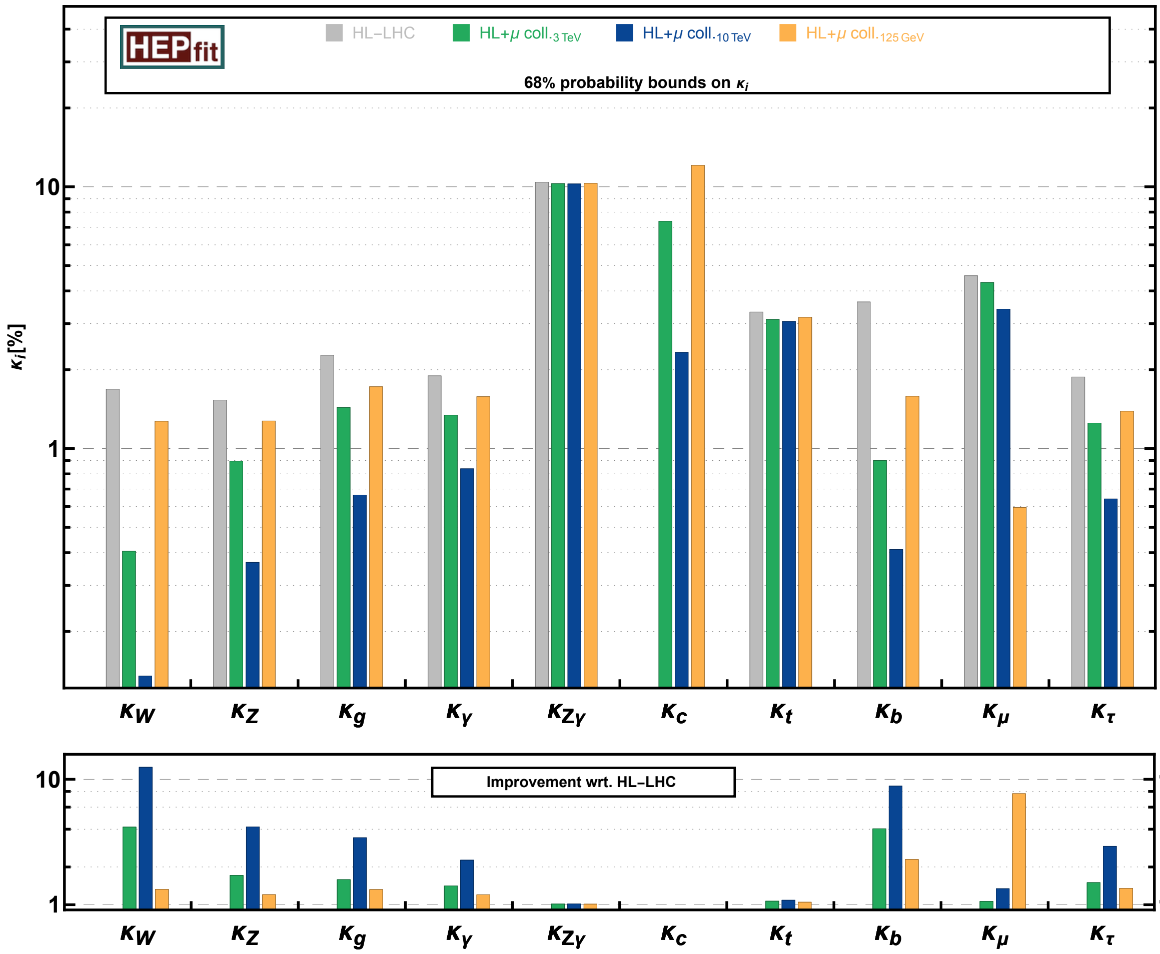

Fig. 2: Sensitivity to modified Higgs couplings in the κ framework. We show the marginalized 68% probability reach for each coupling modifier.

In the EFT fits to Eq. (3) we include the following set of experimental inputs and projections:

- The complete set of electroweak precision measurements from LEP/SLD, including the projected measurements of the W mass at the HLLHC. We also include the aTGC constraints from LEP2.
- The HLLHC projections for single Higgs signal strengths and double Higgs production from [30]. We assume the S2 scenario for the projected experimental and theory systematics.
- Also from the HLLHC, the projections from two to two fermion processes, expressed in terms of the W and Y oblique parameters, from Ref. [31], and the high energy diboson study from [32].
- The expected precision for single-Higgs observables at the 3 and 10 TeV muon colliders from the preliminary results of [24].
- As in the HLLHC case, we also include the projections from high-energy measurements in two to two fermion processes, expressed in terms of W and Y from [33], and in diboson processes $\mu^+\mu^- \to ZH, W^+W^-$, $\mu\nu \to WH, WZ$ from Ref. [6, 33].
- The expected precision for the Higgs self-coupling from the measurement of the di-Higgs invariant mass in $\mu^+\mu^- \to \bar{\nu}\nu HH$ from Ref. [6]. (See also [25].)

In all cases we asume the projected experimental measurements to be centerd around the SM prediction. The assumptions in terms of theory uncertainties follow the same setup as in [19].

The results of these EFT fits are summarized in Table 3 and Figure 3. We also include in the table and figure the projections obtained from the HLLHC measurements (also included in the $\mu^+\mu^-$ collider results), to show the improvement in the reach for the different operators, shown explicitly in the lower panel of Figure 3. This is clear for $\mathcal{O}_\phi$ due to the increase in precision in the knowledge of the HVV couplings and, in particular, for the operators $\mathcal{O}_{W,B}$ and $\mathcal{O}_{2B,2W}$, which induce growing with energy effects in diboson and difermion processes, respectively, and thus benefit from the high energy reach of the 3 and 10 TeV muon colliders. As in the κ analysis, we must also note that the improvements in other operators, e.g. $\mathcal{O}_{yu}$ which modifies the Top Yukawa coupling, do not represent a fair assessment of the muon collider potential, due to the absence of projections for the processes that would impose the leading constraints on them, e.g. ttH. Finally, it should be noted that all projections included here correspond to the case where the muon collider beams are unpolarized. The presence of polarization could bring extra information, i.e. allow to test extra directions in the SMEFT parameter space, as it basically doubles the number of observables, e.g. solving flat directions that appear in unpolarized observables due to cancellations []. In particular, as explained in [6] it would benefit the reach of the $\mathcal{O}_{W,B}$ operators from the diboson high-energy measurements.

Table 3: 68% probability reach on the different Wilson coefficients in the Lagrangian Eq. (3) from the global fit. In parenthesis we give the corresponding results from a fit assuming only one operator is generated by the UV physics.

	HL-LHC	HL-LHC + μ collider 3 TeV (1 ab^{-1})	HL-LHC + μ collider 10 TeV (10 ab^{-1})
$\frac{c_\phi}{\Lambda^2}$ [TeV^{-2}]	0.52	0.12	0.039
	(0.28)†	(0.11)	(0.029)
$\frac{c_T}{\Lambda^2}$ [TeV^{-2}]	0.0056	0.0021	0.0019
	(0.0019)	(0.0019)	(0.0019)
$\frac{c_W}{\Lambda^2}$ [TeV^{-2}]	0.32	0.014	0.0012
	(0.021)	(0.0049)	(0.00044)
$\frac{c_B}{\Lambda^2}$ [TeV^{-2}]	0.33	0.022	0.0019
	(0.026)	(0.0079)	(0.00073)
$\frac{c_{\phi W}}{\Lambda^2}$ [TeV^{-2}]	0.31	0.035	0.025
	(0.033)	(0.032)	(0.019)
$\frac{c_{\phi B}}{\Lambda^2}$ [TeV^{-2}]	0.32	0.19	0.18
	(0.19)	(0.19)	(0.18)
$\frac{c_\gamma}{\Lambda^2}$ [TeV^{-2}]	0.0054	0.0047	0.0031
	(0.0041)	(0.0039)	(0.0027)
$\frac{c_g}{\Lambda^2}$ [TeV^{-2}]	0.0012	0.0011	0.00068
	(0.00052)	(0.00042)	(0.00022)

	HL-LHC	HL-LHC + μ collider 3 TeV (1 ab^{-1})	HL-LHC + μ collider 10 TeV (10 ab^{-1})
$\frac{c_{y_e}}{\Lambda^2}$ [TeV^{-2}]	0.25	0.2	0.1
	(0.2)	(0.18)	(0.095)
$\frac{c_{y_u}}{\Lambda^2}$ [TeV^{-2}]	0.58	0.48	0.29
	(0.24)	(0.19)	(0.088)
$\frac{c_{y_d}}{\Lambda^2}$ [TeV^{-2}]	0.46	0.15	0.06
	(0.25)	(0.12)	(0.053)
$\frac{c_{2B}}{\Lambda^2}$ [TeV^{-2}]	0.087	0.0036	0.00031
	(0.075)	(0.0029)	(0.00026)
$\frac{c_{2W}}{\Lambda^2}$ [TeV^{-2}]	0.0087	0.00097	0.000084
	(0.0076)	(0.00077)	(0.00007)
$\frac{c_{3W}}{\Lambda^2}$ [TeV^{-2}]	1.7	1.7	1.6
	(1.7)	(1.7)	(1.6)
$\frac{c_6}{\Lambda^2}$ [TeV^{-2}]	8.4	4.6	0.65
	(7.8)	(4.4)	(0.6)

† As explained in [19], due to the treatment of systematics/theory uncertainties in the HLLHC inputs, this number must be taken with caution, as it would correspond to an effect below the dominant theory uncertainties. A more conservative estimate accounting for 100% correlated theory errors would give $c_\phi/\Lambda^2 \sim 0.42$ TeV^{-2}.

3.1 Interpretation in terms of BSM benchmark scenarios

For the case of composite Higgs scenarios we assume the new dynamics is parameterized in terms of a single coupling, $g_\star$, and mass, $m_\star$. As in [19], we use the following illustrative assumptions for the power counting and contributions of the new physics to the different Wilson coefficients in (3):

$$\frac{c_{\phi,6,y_f}}{\Lambda^2} = \frac{g_\star^2}{m_\star^2}, \qquad \frac{c_{W,B}}{\Lambda^2} = \frac{1}{m_\star^2}, \qquad \frac{c_{2W,2B}}{\Lambda^2} = \frac{1}{g_\star^2}\frac{1}{m_\star^2},$$
$$\frac{c_T}{\Lambda^2} = \frac{y_t^4}{16\pi^2}\frac{1}{m_\star^2}, \quad \frac{c_{\gamma,g}}{\Lambda^2} = \frac{y_t^2}{16\pi^2}\frac{1}{m_\star^2}, \quad \frac{c_{\phi W,\phi B}}{\Lambda^2} = \frac{g_\star^2}{16\pi^2}\frac{1}{m_\star^2}, \quad \frac{c_{3W}}{\Lambda^2} = \frac{1}{16\pi^2}\frac{1}{m_\star^2}. \tag{4}$$

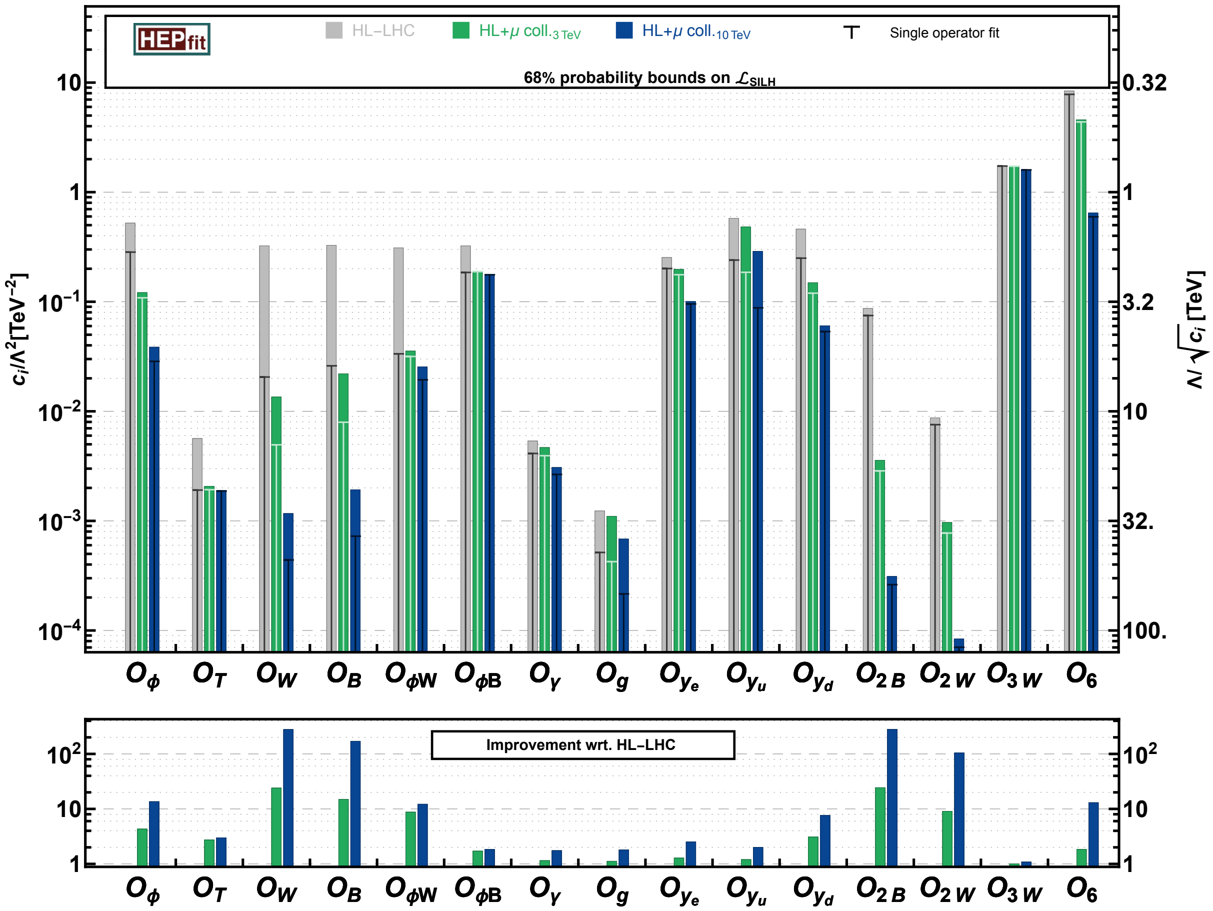

Fig. 3: Global fit to the EFT operators in the Lagrangian (3). We show the marginalized 68% probability reach for each Wilson coefficient c_i/Λ^2 in Eq. (3) from the global fit (solid bars). The reach of the vertical "T" lines indicate the results assuming only the corresponding operator is generated by the new physics.

and projecting the EFT likelihood onto the $(g_\star, m_\star)$ plane we obtain the exclusion regions in the right panel in Figure 4 for the different muon collider options, combined and in comparison with the HL-LHC reach. We also show the results interpreted in terms of extra vector bosons, using as a representative example the case of an universal Z' coupling to the hypercharge current, also considered in [20]. In this case the dimension-6 effective Lagrangian only receives tree-level contributions to the operator with coefficient $c_{2B}/\Lambda^2 = g_{Z'}^2/g'^4 M_{Z'}^2$. The corresponding indirect constraints in the $(g_{Z'}, M_{Z'})$ plane are shown in the left panel of Figure 4.

Whereas the bounds on the Z' example considered here are going to be clearly dominated by the high-energy measurements of the $\mu^+\mu^- \to f\bar{f}$ and the induced constraints on the Y parameter, the situation is more complex for the case of composite Higgses. The contributions from the different processes are shown separately in Figure 4, highlighting the complementarity of the different processes, which the diboson constraints setting the overall mass reach indepedendtly of $g_\star$, extended for low (high) values of $g_\star$ by the difermion (Higgs) bounds. Going back to Figure 4, it is clear that, while the 3 TeV option would clearly outperform the HLLHC, the real leap in terms of indirect sensitivity comes with the 10 TeV option, thanks to the significantly higher energy reach, which boosts the constraining power of difermion and diboson processes on W, Y and $C_{B,W}$, respectively.

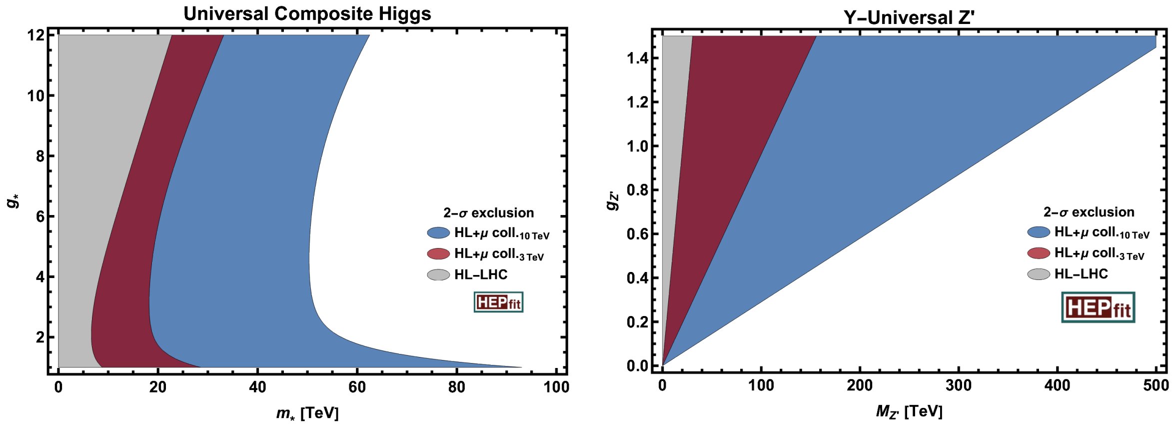

Fig. 4: (Left) Comparison of the global reach for universal composite Higgs models at the HL-LHC and the a high-energy muon collider (combined with the HL-LHC constraints). The figure compares the 2-σ exclusion regions in the $(g_\star, m_\star)$ plane from the fit presented in Figure 3, using the SILH power-counting described in Eq. (4) (Right) The same for a BSM extension with a massive replica of the $U(1)_Y$ gauge boson in the $(g_{Z'}, m_{Z'})$ plane from the fit presented in Figure 3.

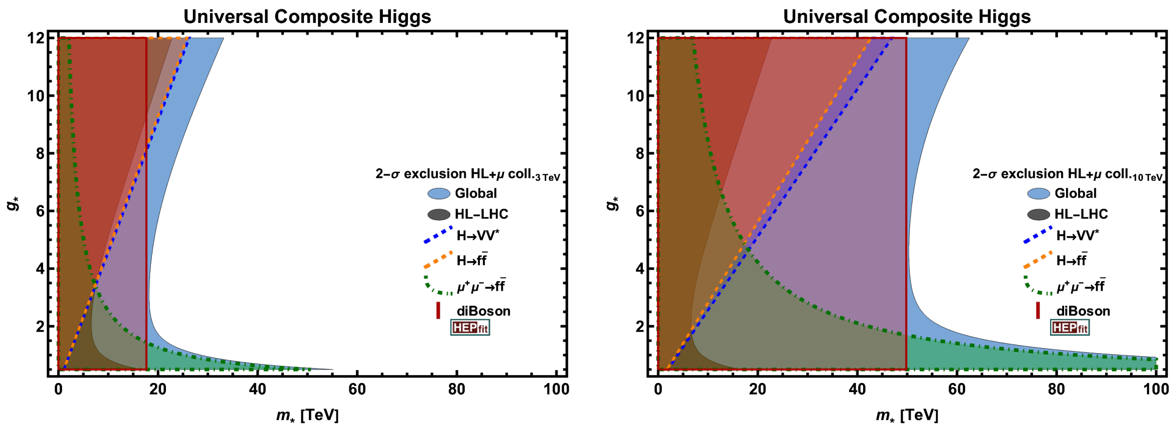

Fig. 5: (Left) 2-σ exclusion regions in the $(g_\star, m_\star)$ plane from the fit presented in Figure 3, using the SILH power-counting described in Eq. (4) and below (solid regions). The solid and dashed lines denote the contributions to the constraints from different processes. The results correspond to the combination of the HL-LHC with the 3 TeV muon collider. (Right) The same for the 10 TeV muon collider.

4 Direct Searches for New Physics

4.1 Extended Higgs Sectors

4.1.1 SM plus a singlet extension

The simplest extension of the SM Higgs sector is the SM Higgs sector plus an extra real singlet. In the case when the extra singlet mixes with the SM Higgs doublet with mixing parameter $\sin\gamma$, the SM-like Higgs couplings are modified, and the extra heavy scalar S can be singly produced, which decays to a pair of SM gauge bosons or SM-like Higgses. Considering the Vector Boson fusion production $VV \to S$, the most sensitive channel at a high energy lepton collider is $S \to hh \to 4b$ [7]. The 95% C.L. exclusion reach for CLIC 3 TeV with 3 ab^{-1} luminosity is shown in Fig. 6 (taken from Ref. [20]) as blue solid curve, which is better than the direct reach of HL-LHC once $\sin^2\gamma < 0.1$. Comparing to the sensitivity of indirect measurements of the SM-like Higgs couplings at future colliders, which are indicated by the dashed horizontal lines in the plot, 3 TeV CLIC can test new resonances down to couplings correlated to

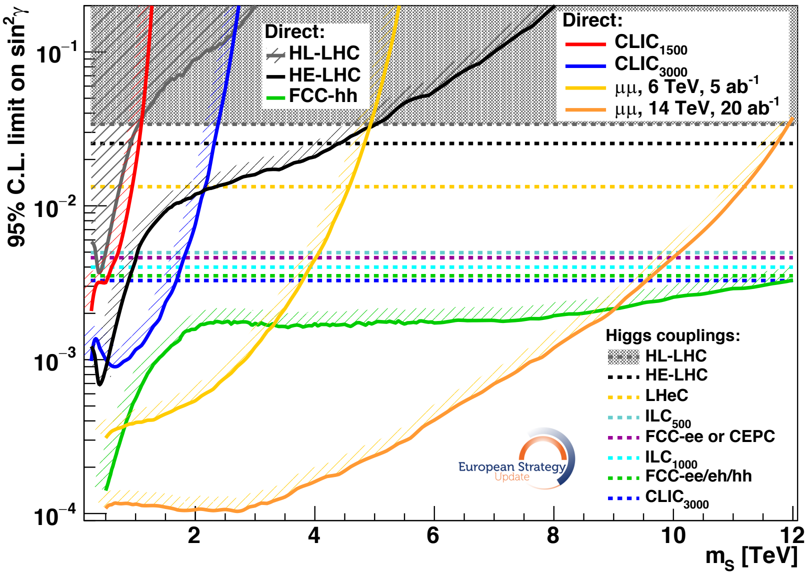

Fig. 6: The direct (solid curves) and indirect (dotted curves) 95 % C.L. reach [20] of heavy singlet mixed with the SM Higgs doublet at various future colliders.

a deviation in the Higgs couplings smaller than 0.1%. The sensitivity in $\sin^2\gamma$ is better than that of the Higgs precision measurements at $m_S < 2$ TeV. 3 TeV muon collider reach would be slight worse given a smaller luminosity of 1 ab^{-1}. Higher energy muon collider has better reach in both $\sin^2\gamma$ and m_S, surpassing that of Higgs precision measurements for $m_S < 4(10)$ TeV for 6(14) TeV muon collider.

SM plus a real singlet extension can also provide a strong first order electroweak phase transition (FOEWPT), which is essential for the electroweak baryogenesis mechanism to explain the observed cosmological matter-antimatter asymmetry [8, 9]. In the left panel of Fig. 7, the colored solid curves show the muon collider 95% C.L. exclusion reach for VBF production with di-Higgs decay modes and $4b$ final states. A 3 TeV muon collider (1 ab^{-1}) has a sensitivity more than one order of magnitude better than the HL-LHC (13 TeV, 3 ab^{-1}). It also covers most of the points that generate a strong FOEWPT, which are indicated by the dots. Comparing to the reach of future Gravitational Wave experiment LISA (red and green points), majority of those points falls with the 3 TeV muon collider reach. Furthermore, the muon colliders also have significant sensitivity to the blue data points which are beyond the reach of the LISA. Higher energy muon collider can extend the reach further. The reaches in the SM-like Higgs coupling measurements on $\delta\kappa_3$ and $\delta\kappa_V$ are shown in the right panel of Fig. 7 for muon collider with various center of mass energy as well as Higgs factory CEPC. While the reach of the 3 TeV muon collider is worse than that of the Higgs factory for $\delta\kappa_V$, the reach for muon collider with higher center of mass energy is better.

4.1.2 Two Higgs Doublet Model

In the framework of Two Higgs Doublet Model (2HDM) [34], the scalar sector consists of 5 physical scalars: the SM-like Higgs h, and the non-SM ones $H, A, H^\pm$ with $m_h = 125$ GeV after the electroweak symmetry breaking. The tree-level couplings of Higgs bosons are determined by two parameters: the mixing angle between the neutral CP-even Higgs bosons α and $\tan\beta = v_2/v_1$, with $v_{1,2}$ being the vacuum expectation value for two Higgs doublets. The un-suppressed gauge couplings of the Higgses with the SM gauge bosons typically involve two non-SM Higgses, for example, ZHA or $W^\pm H^\mp H$. The Yukawa couplings of the non-SM like Higgses with the SM fermions depends on how the two Higgs doublets are coupled to the leptons and quarks, giving rise to four different types of 2HDMs, namely Type-I, Type-II, Type-L and Type-F.

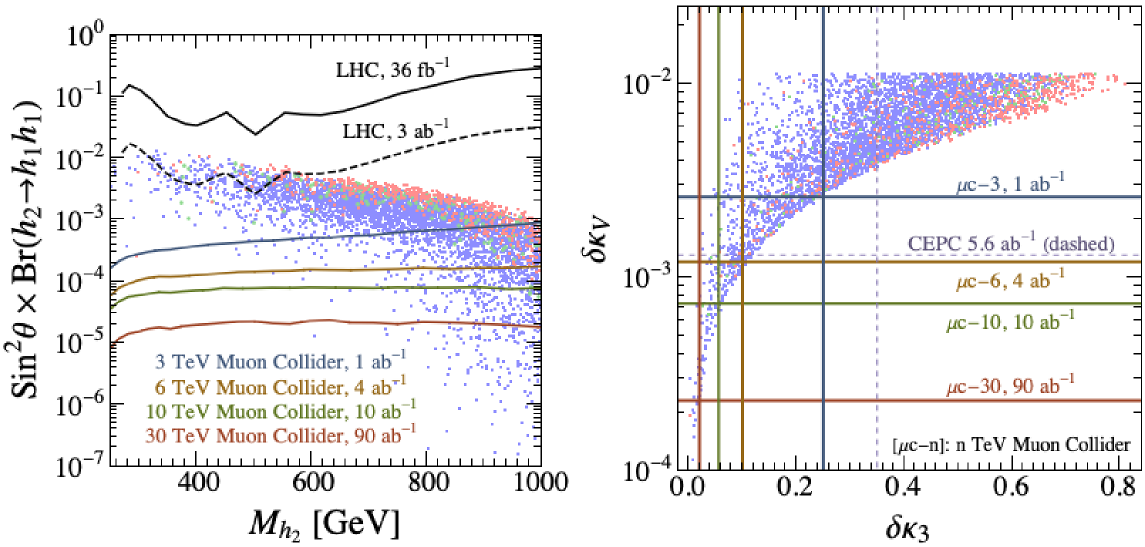

Fig. 7: Direct (left panel) and indirect reach (right panel) on the SM plus real scalar singlet scenario for muon colliders with various center of mass energy. Dots indicate points with successful FOEWPT, while red, green and blue dots represent signal-to-noise ratio (SNR) for gravitational eave detection of $[50, +\infty)$, $[10, 50)$ and $[0, 10)$, respectively. Results are taken from [8].

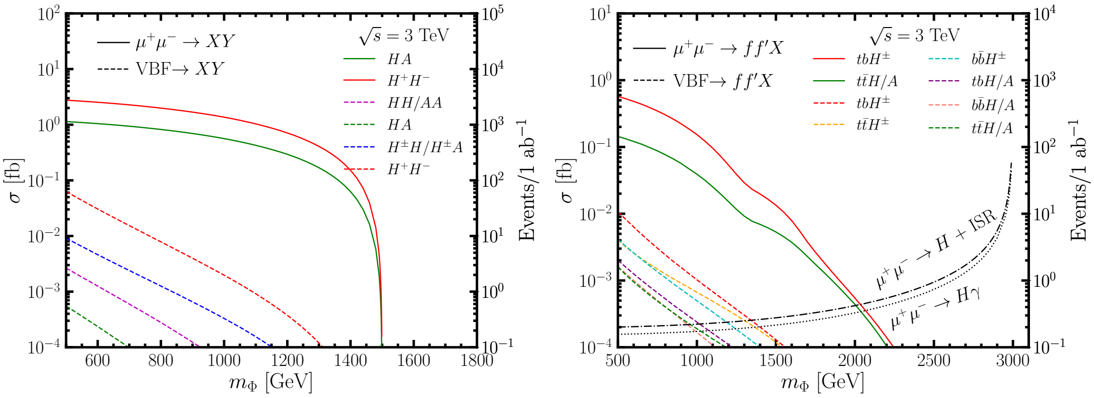

Fig. 8: Cross sections versus the non-SM Higgs mass for $\sqrt{s} = 3$ TeV for pair production (left panel), single production with a pair of fermions and radiative return production (right panel) for $\tan\beta = 1$ under the alignment limit of $\cos(\alpha - \beta) = 0$. Plot is produced by authors of Ref. [10].

Once crossing the pair production threshold, the heavy Higgs bosons can be produced in pair via the $\mu^+\mu^-$ annihilation as well as Vector Boson Fusion (VBF):

$$\mu^+\mu^- \to \gamma^*, Z^* \to H^+H^-, \quad \mu^+\mu^- \to Z^* \to HA, \tag{5}$$

$$\mu^+\mu^- \to V_1V_2\, \mu^+(\bar{\nu})\mu^-(\nu),\ V_1V_2 \to H^+H^-, HA, H^\pm H/H^\pm A, HH/AA, \tag{6}$$

The production cross section as a function of the non-SM like Higgs masses for $\sqrt{s} = 3$ TeV for various channels are shown in the left panel of Fig. 8 under the alignment limit of $\cos(\alpha - \beta) = 0$. The annihilation processes dominate at $\sqrt{s} = 3$ TeV. For higher center of mass energies, VBF channels become more and more important [10], especially for light scalar masses. The annihilation process can be separated from the VBF process by comparing the invariant mass distribution of the Higgs pair, which is approximately equal to the collider c.m. energy $m_{\Phi_1\Phi_2} \approx \sqrt{s}$ for the direct annihilation process, while peaked near the threshold $m_{\Phi_1\Phi_2} \approx m_{\Phi_1} + m_{\Phi_2}$ for the VBF process. Considering the dominant decay channel of non-SM Higgs into third generation fermions, the SM backgrounds can be sufficiently suppressed. Reach up to pair production threshold is possible at all $\tan\beta$ region, when all four fermion final states channels are used. Comparing with HL-LHC reach for Type-II 2HDM, 3 TeV muon collider reach exceeds that of the HL-LHC [35], except for very small value of $\tan\beta < 2$ above the pair production mass threshold.

In the parameter region with enhanced Higgs Yukawa couplings or beyond the Higgs pair production threshold, single production of non-SM Higgs with a pair of fermions could play an important role. The production cross section for fermion associated production are shown in the right panel of Fig. 8 for both the annihilation and VBF processes, with $\tan\beta = 1$ and $\cos(\alpha - \beta) = 0$. The dominant channel is $tbH^{\pm}$, followed by $t\bar{t}H/A$. Note that there are strong $\tan\beta$ dependence on the production cross section, depending on the types of 2HDM [10].

Radiative return $\mu^+\mu^- \to \gamma H$ offers another production channel for the non-SM Higgs, especially in regions with enhanced $H\mu^+\mu^-$ coupling. The cross section increases as the heavy Higgs mass approaches the collider c.m. energy, closer to the s-channel resonant production. The production cross section is shown as the black curves in the right panel of Fig. 8.

In summary, non-SM Higgses can be copiously produced at 3 TeV muon collider. For pair production, 95% C.L. exclusion reaches in the Higgs mass up to the production threshold of $\sqrt{s}/2$ are possible when channels with different final states are combined. Including single production modes can extend the reach further. With the combination of both the production mechanisms and decay patterns, we found that the intermediate and large $\tan\beta$ values offer great discrimination power to separate Type-I and Type-L from Type-II/F. To further identify either Type-II or Type-F, we need to study the subdominant channels with τ final states, which could be sizable in the signal rate in Type-II [10].

4.1.3 Inert Doublet Model

Inert Doublet Model (IDM) is an extension of the SM with the second Higgs doublet carries an extra discrete Z_2 symmetry and couples to the SM gauge boson only. The lightest of the extra neutral scalars is a good candidate for a Dark Matter particle. The production of IDM scalars at lepton colliders is dominated by production of neutral scalar pair $\mu^+\mu^- \to HA$ or charged scalar pair $\mu^+\mu^- \to H^+H^-$ via the SM gauge interactions. The subsequent decay of $A \to HZ$ and $H^{\pm} \to HW^{\pm}$ leads to HHZ and HHW^+W^- final states, with H being identified as the dark matter particle of missing energy signal. The leptonic final states have limited reach at high energy lepton colliders. The discovery reach is only about 500 GeV for scalar mass at 3 TeV collider, given the small leptonic final states branching fractions, and the decreasing of production cross section with the increasing center of mass energy [36, 37]. Considering the semi-leptonic final states [38], the signal statistical significance for charged Higgs pair production is shown in Fig. 9 for CLIC 1.5 TeV and 3 TeV with 4 ab^{-1} integrated luminosity. Most of the scenarios considered in the study with $m_H^{\pm}$ up to about 1 TeV can be be discovery at more than 5 σ level for a 3 TeV collider. The 3 TeV muon collider reach is similar.

4.1.4 MSSM electroweak states

Electroweak states in supersymmetric models can be pair produced at a muon collider. The dominant production for Wino-like NLSP with Bino-like LSP are $\mu^+\mu^- \to \chi_1^+\chi_1^-, \chi_0^2\chi_1^0$, with $\chi_1^{\pm}$ and χ_2^0 being Wino-like states. Sensitivity up to pair production mass threshold of $\sqrt{s}/2$ are possible even for $m_{\chi_1^{\pm}} - m_{\chi_1^0}$ as low as 1 GeV, with no loss in acceptance [18]. In comparison, the HL-LHC reach is about 1 TeV for the Wino NLSP, with Bino-LSP mass up to about 500 GeV [39].

For the case when the Higgsino-like states are the NLSP and LSP, the electroweakinos exhibit a compressed spectrum with a production cross section smaller than that of the Wino case. The high energy lepton collider allow a reach close to the pair production threshold: about 1.3 TeV for CLIC3000 with the mass splitting down to about 0.5 GeV. The muon collider 3 TeV reach would be similar [20].

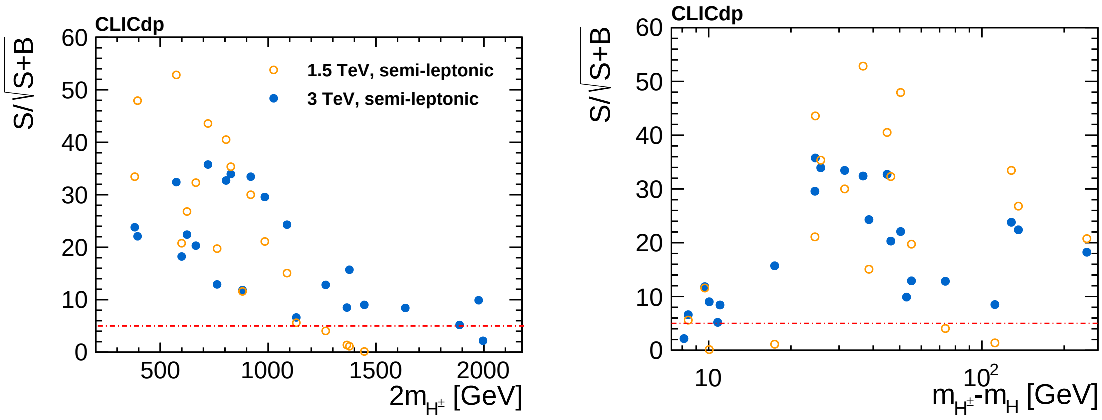

Fig. 9: Signal statistical significance for various IDM benchmark points [38] at high energy lepton collider for charged Higgs pair production and semi-leptonic final states.

Table 4: Thermal mass, in TeV, for pure SU(2) n-plet dark matter WIMP. Effects of bound states and Sommerfeld enhancement of the annihilation cross-section are included from Ref. [11, 40]. The neutral component of complex scalars and Dirac fermions can have a tiny electric charge. In some cases it is also possible to assign a non-zero hypercharge consistently with direct searches of dark matter.

n	Dirac	Majorana	Complex Scalar	Real Scalar
2	1.08	-	0.58	-
3	2.0 & 2.4	2.86	1.6 & 2.5	2.53
4	4.79(9)	-	4.98(5)	-
5	8.8(4)	13.6(5)	11.5(7)	15.4(7)

In comparison, the HL-LHC reach highly depends on the mass splitting, only about 350 GeV for mass splitting between 1.6 to 50 GeV [39]. Searches based on the disappearing charge tracks for pure Higgsino states will be covered in Section 5.1.

The reach for selectron and smuon is about its pair production kinematic threshold of 1.5 TeV for a 3 TeV muon collider. The reach for stau is slightly worse, given the identification of hadronically decaying τ. CLIC3000 can reach up to stau of about 1.25 TeV and $\Delta m(\tilde{\tau}, \chi_1^0) = 50$ GeV [20]. The muon collider reach is similar.

4.2 Dark Matter

The possibility that Dark Matter is a massive particle charged under electroweak interactions is one of the major themes of research in Dark Matter. Cosmogenic Dark Matter can be observed in ultra-low noise underground detectors into which it is possible to detect directly the DM interaction with the SM matter in the detector. Additionally, DM can be searched in DM-rich astrophysical environments, where the DM pairs can annihilate and give rise to observables signals in cosmic ray observatories. These experimental investigation are promising and actively pursued, but suffer few potential roadblocks. Cosmic rays observation can be hampered by large uncertainties about astrophysical quantities and astrophysical processes that can mimic dark matter signals. Furthermore, the unknown density distribution of the dark matter that undergoes annihilation brings in additional uncertainty. Lab-based direct detection of cosmogenic dark matter has the inherent problem of being a very low momentum transfer process even when Dark Matter is quite heavy, hence background rejection is very challenging.

The possibility to produce dark matter particles in the laboratory and study them with precise particle detectors is a unique capability of particle colliders. The great challenge for particle colliders is to produce these particles with sufficient rate to result in a statistically significant observation. The case of Weakly Interacting Massive Particles (WIMPs) dark matter is particularly useful to gauge the efficacy of particle colliders to test dark matter. In fact WIMPs must feel the weak interactions of the SM, as they use them to be in equilibrium in the early Universe plasma. The WIMP relic abundance is set by the (known) strength of the weak interactions coupling and the (unknown) mass of the WIMP. Therefore, for simple models in which the WIMP is a pure $SU(2)_W$ n-plet it is possible to sharply predict the mass of the dark matter particle, see Tab. 4 for some examples. As a general rule, the larger the n-plet the larger the mass of the WIMP. Smaller masses can be attained for a mixture of an n-plet e.g. with a state not charged under $SU(2)_W$. Therefore, testing the reach for pure $SU(2)_W$ n-plet is an excellent benchmark for particle colliders, as it demands to reach the highest mass for a given class of dark matter candidates.

A crucial phenomenological parameter for the detection of WIMP dark matter at colliders is the mass splitting between the neutral component of the dark matter n-plet and other electrically charged and neutral components of the multiplet. When this mass splitting is comparable or greater than the detector threshold, typically around 10 GeV, there is a good chance that the production of states furnishing the n-plet will give detectable signals, one example is the iDM of Section 4.1.3.

4.2.1 Mono-X

When the mass-splitting between the dark matter particle and the other states of the multiplets is below the detectable threshold, none of the particles in the dark matter multiplet leaves a detectable trace in the detector. This makes the production of dark matter observable only "by contrast", e.g. observing a bunch of particles apparently recoiling against nothing. At a muon collider the reaction is

$$\mu^+\mu^- \to \chi\chi + X\,,$$

where X denotes any particle or set of particles allowed by the interactions and χ is a generic state belonging to the dark matter n-plet.

Searches for general electroweak states have been studied for several types of observables particles X accompanying the production of Dark Matter. The signal for $X = \gamma, W, Z, \mu^\pm, \mu\mu$ have been studied in [11, 12], finding that the a 3 TeV muon collider is in general very sensitive to the production of new electroweak matter.

Figure 10 summarizes the reach illustrating in the left panel the luminosity needed to reach the 95% CL exclusion of electroweak matter of a given mass in several production modes $X = \gamma, \mu, \mu\mu$. Among these, the mono-γ search is the one placing the best bound for states heavier than about 500 GeV. The right panel shows the mass reach at fixed luminosity $1\ \mathrm{ab}^{-1}$ and includes the mono-W channel, which is most effective for the same mass range in which mono-γ leads the exclusion and in some cases exceeds mono-γ results. All in all, the combination of these two channels, especially thanks to different levels of signal-over-background ratio and sources of possible systematics, can provide best mass reach for some DM candidates.

4.2.2 Indirect reach through SM rates

Pure WIMP DM n-plets for $n \geq 3$ are too heavy to be directly produced in pairs at the 3 TeV muon collider at their thermal mass, see Tab. 4. However, these heavy DM candidates can leave observable effects as their off-shell propagation modifies the rate and the distributions of SM processes such as

$$\mu^+\mu^- \to f\bar{f}\,, \tag{7}$$
$$\mu^+\mu^- \to Zh\,, \tag{8}$$
$$\mu^+\mu^- \to W^+W^-\,, \tag{9}$$

and possible higher order processes such as $\mu^+\mu^- \to WWh$. Measuring the total rate of eqs.(7-9) and using differential information on the angular distribution of the channels in which the charge of the final

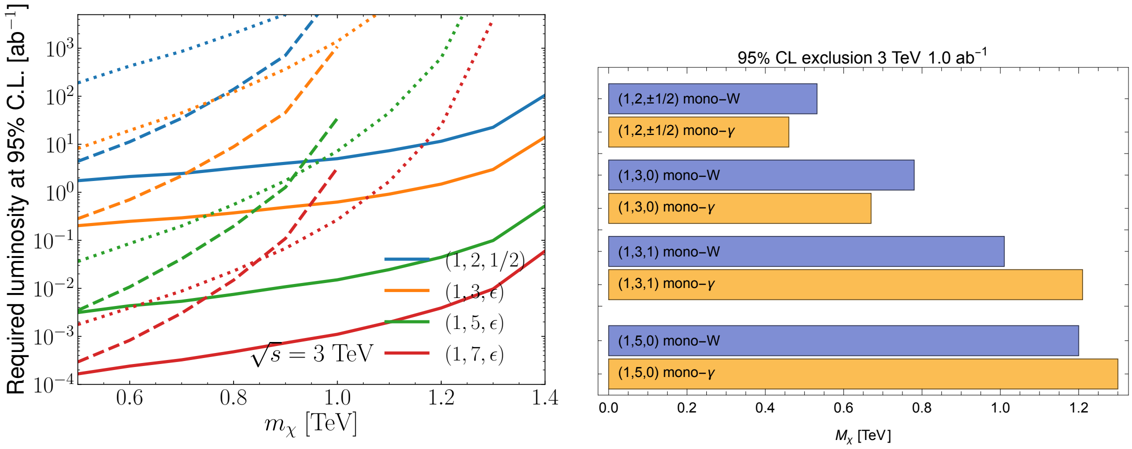

Fig. 10: Direct reach on electroweak states in mono-X signals. Left: Luminosity needed to exclude a Dirac fermion DM candidate [12] for $X = \gamma$ (solid), $X = \mu$ (dotted), $X = \mu\mu$ (dashed). Right: Mass reach on a fermionic DM candidate (assumed Majorana when $Y = 0$, Dirac otherwise) at fixed 1 ab^{-1} luminosity for the 3 TeV muon collider for $X = \gamma$ and $X = W$ [11].

states $f = e, \mu$ can be tagged reliably, it is possible to put bounds at 95% CL for the existence of new matter n-plets (see Refs. [13, 41] for muon collider specific studies).

In Fig. 11 we report the minimal luminosity necessary to exclude a thermal pure Wino dark matter (brown bands) as a function of the collider center of mass energy. These studies are helped by the presence of left-handed fermions initial states, which source larger weak-boson mediated scattering. Therefore it is interesting to study the effect of beam polarization. In the figure the lighter colored lines give the necessary luminosity for an exclusion at a machine capable of 30% left-handed polarization on the μ^- beam and -30% for the μ^+ beam. Even this modest polarization of the beams can cut significantly the luminosity required for the exclusion.

Figure 11 also shows the reach for a Dirac doublet with zero hyper-charge through the same observables. Neglecting hyper-charge contributions this is the same as the reach for a Higgsino. This reach is complementary to that from direct searches of all sorts, as it does not depend on the Higgsino mass splitting and the search final states that it results into. Thus the indirect search can complement the reach discussed in Section 5.1 from stub-tracks as it has no dependence on the Higgsino life-time.

The shaded area indicates that the search for new electroweak matter is based on such a luminosity high enough to have statistical uncertainties at the 0.1% level for some channel. This may require a careful evaluation of possible systematics.

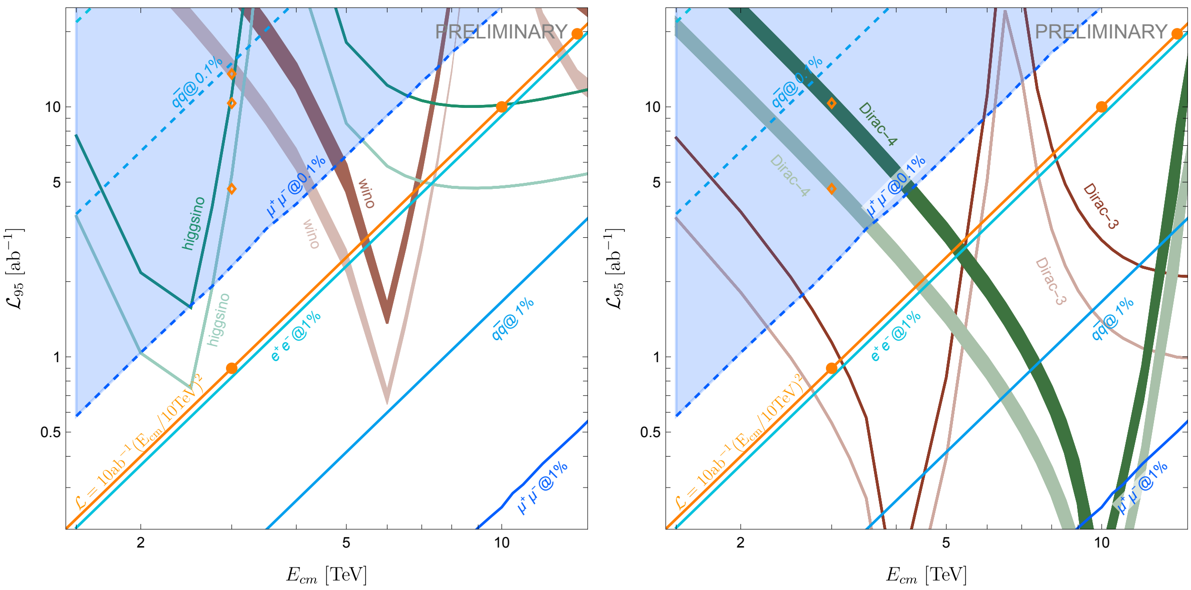

Fig. 11: Minimal luminosity to exclude a thermal pure Higgsino or Wino dark matter (left panel) a 2.0 TeV Dirac triplet or 4.8 TeV Dirac 4-plet as function of the collider center of mass energy [41] (hypercharge of the Higgsino and Dirac n-plets not taken into account). Lighter color lines are for polarized beams. The thickness of the Wino and Dirac 4-plet bands covers the uncertainty on the thermal mass calculations. Diagonal lines mark the precision at which the total rate of the labeled channels are going to be measured. The shaded area indicates that at least one channel is going to be measured with 0.1% uncertainty and systematic uncertainties need to be evaluated.

5 Unconventional signatures

The search for long-lived particles (LLPs) has recently become a priority in the particle physics community [42, 43]. LLPs appear in a variety of models and yield a large range of signatures at colliders. Depending on the LLP quantum numbers and lifetime, these can span from LLP decay products appearing in the detector volume, even outside of the beam crossings, to metastable particles with anomalous ionisation disappearing after a short distance.

This wide range of experimental signatures is strongly intertwined with the development of detector technologies and the design of the final detector layout. For example, the development of timing-sensitive detectors is crucial both to suppress the abundant beam-induced backgrounds and to detect the presence of heavy, slow-moving, particles that are traveling through the detector. A lively R&D programme is ongoing to develop the reconstruction algorithms that will profit from these new technologies.

For heavy particles, whose production cross sections are dominated by the annihilation s-channel, there are two main features that make searches for unconventional signatures particularly competitive at a muon collider when compared to other future proposed machines like the FCC-hh. The produced particles tend to be more centrally distributed, impinging on the regions of the detector where reconstruction is comparatively easier, and furthermore tend to have more "mono-chromatic" Lorentz boosts which can lead to effectively larger average observed lifetimes for the produced BSM states.

Searches for LLPs that decay within the volume of the tracking detectors (e.g. decay lengths between 1 mm and 500 mm) are particularly interesting as they directly probe the lifetime range motivated by compelling dark matter models.

5.1 Search for disappearing tracks

The higgsino is among the most compelling dark matter candidates, with tight connections to the naturalness of the weak scale, which could lead to LLPs being produced in particle collisions. In scenarios where all other supersymmetric partners are decoupled, the higgsino multiplet consists of an SU(2)-doublet Dirac fermion. Due to loop radiative corrections, the charged state $\tilde{\chi}^{\pm}$ splits from the neutral one $\tilde{\chi}_1^0$ by 344 MeV, giving rise to a mean proper decay length of 6.6 mm for the relic favoured mass of 1.1 TeV [44]. The $\tilde{\chi}^{\pm}$ can then travel a macroscopic distance before decaying into an invisible $\tilde{\chi}_1^0$ and other low-energy Standard Model fermions.

Searches at the LHC are actively targetting this scenario [45–49], but are not expected to cover the relic favoured mass [20, 50]. A muon collider operating at a multi-TeV centre-of-mass energies would provide a perfect tool to look for these particles.

The production of pairs of electroweakinos at a MuC proceeds mainly via an s-channel photon or off-shell Z-boson, with other processes, such as vector boson fusion, being subdominant. The prospects for such a search were investigated in detail in Ref. [14] exploiting a detector simulation based on GEANT 4 [51] for the modelling of the response of the tracking detectors, which are crucial in the estimation of the backgrounds. The simulated events were overlaid with beam-induced background events simulated with the MARS15 software [52].

The analysis strategy relies on requiring one ($\mathrm{SR}^{\gamma}_{1t}$) or two ($\mathrm{SR}^{\gamma}_{2t}$) disappearing tracks in each event in addition to a 25 GeV ISR photon. Additional requirements are imposed on the transverse momentum and angular direction of the reconstructed tracklet and on the distance between the two tracklets along the beam axis in the case of events with two candidates. The expected backgrounds are extracted from the full detector simulation and the results are presented assuming a 30% (100%) systematic uncertainty on the total background yields for the single (double) tracklet selections. The corresponding discovery prospects and 95% CL exclusion reach are shown in Figure 12 for each of the two selection strategies discussed above.

Both event selections are expected to cover a wide range of higgsino masses and lifetimes, well in excess of current and expected collider limits. In the most favourable scenarios, the analysis of 1 ab^{-1} of

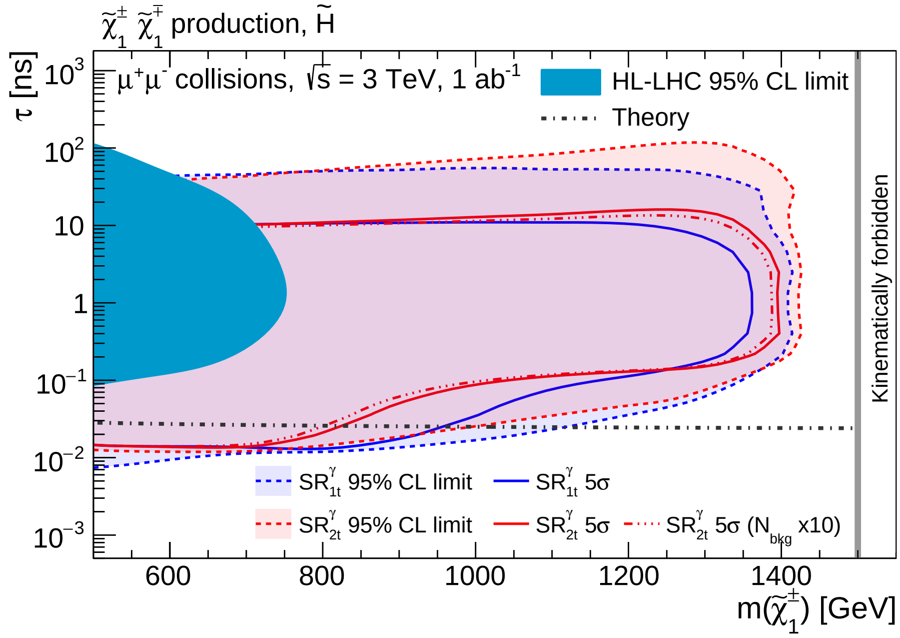

Fig. 12: Expected sensitivity using 1 ab^{-1} of 3 TeV $\mu^+\mu^-$ collision data as a function of the $\tilde{\chi}^{\pm}$ mass and mass difference with the lightest neutral state, assuming a mass-splitting equal to 344 MeV, as per a pure-higgsino scenario [14].

3 TeV muon collisions is expected to allow the discovery $\tilde{\chi}^{\pm}$ masses up to a value close to the kinematic limit of $\sqrt{s}/2$. The interval of lifetimes covered by the experimental search directly depends on the layout of the tracking detector, i.e. the radial position of the tracking layers, and the choices made in the reconstruction and identification of the tracklets, i.e. the minimum number of measured space-points. Considering the current detector design [53], 1 ab^{-1} of 3 TeV muon collisions would be allow to exclude the higgsino thermal target at 95% but not to discover it. Approximately 10 ab^{-1} are necessary to discover the thermal higgsino at 5σ, if no improvements on the background rejection are made, as show in Figure 13. Figure 14 extends the result of Ref. [14] exploring the possibilities of collecting data at a modified centre-of-mass energy, or assuming an improved background rejection in SR^{γ}_{1t} by one order of magnitude. A pure higgsino with a mass of 1.1 TeV can be probed at the 5-σ level by a 2.85 TeV muon collider with 1 ab^{-1} of data and better background rejection, or by a 3.55 TeV collider with the nominal background expectation, guaranteeing the discovery of thermal higgsino dark matter, if present in nature.

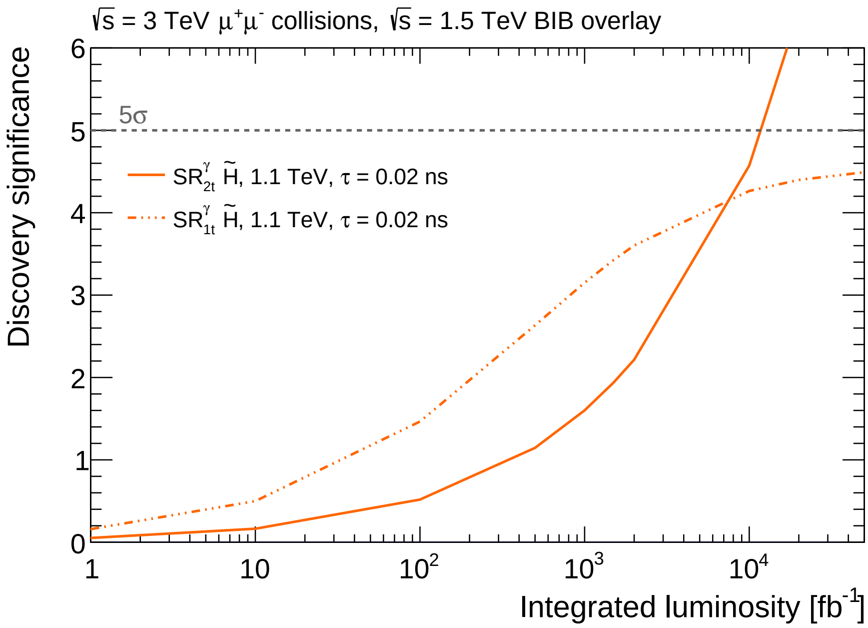

Fig. 13: Expected sensitivity to the higgsino relic favoured mass as a function of the collected integrated luminosity for 3 TeV $\mu^+\mu^-$ collisions.

6 The muon anomalous magnetic moment

The anomalous magnetic moment of the muon has provided, over the last ten years, an enduring hint for new physics (NP). The experimental value of $a_\mu = (g_\mu - 2)/2$ from the E821 experiment at the Brookhaven National Lab [54] was recently confirmed by the E989 experiment at Fermilab [55, 56], yielding the experimental average $a_\mu^{\rm EXP} = 116592061(41) \times 10^{-11}$. The comparison of this value with the Standard Model (SM) prediction $a_\mu^{\rm SM} = 116591810(43) \times 10^{-11}$ [57–67] shows an interesting $4.2\,\sigma$ discrepancy

$$\Delta a_\mu = a_\mu^{\rm EXP} - a_\mu^{\rm SM} = 251\,(59) \times 10^{-11}\,. \tag{10}$$

In the following, we refer to this as the g-2 anomaly. Current and forthcoming plans to unveil this anomaly include reducing the experimental uncertainty by a factor of four at E989, comparisons between phenomenological and Lattice determinations of the Hadronic Vacuum Polarization contribution to g-2 [68–78], and new experiments aiming to probe the same physics [79, 80]. If all these efforts confirm the presence of NP, given the huge level of precision in the muon g-2 measurement, it would be highly desirable to have an independent test of the same NP effects not affected by the hadronic and experimental uncertainties entering the low-energy determination of the muon g-2. The MuC is an appropriate laboratory for this task.

There are several ways in which a MuC can provide a powerful high-energy test of the muon g-2:

- If the physics responsible for Δa_μ is heavy enough, an Effective Field Theory (EFT) description holds up to the high energies of a MuC. In this case, scattering cross-sections induced by the NP effective operators grow at high energies (analogously to the case of weak-interaction cross-sections below the W boson mass), so that a measurement with $\mathcal{O}(1)$ precision at a sufficiently high energy will be sufficient to disentangle NP effects from the SM background. These considerations are completely independent from the specific underlying model.
- In most motivated models of NP, new particles responsible for Δa_μ are light enough to be directly produced in $\mu^+\mu^-$ collisions at the typical MuC energies. In this case, a MuC would be able to discover NP by directly looking for the new states. Under conservative assumptions, a complete

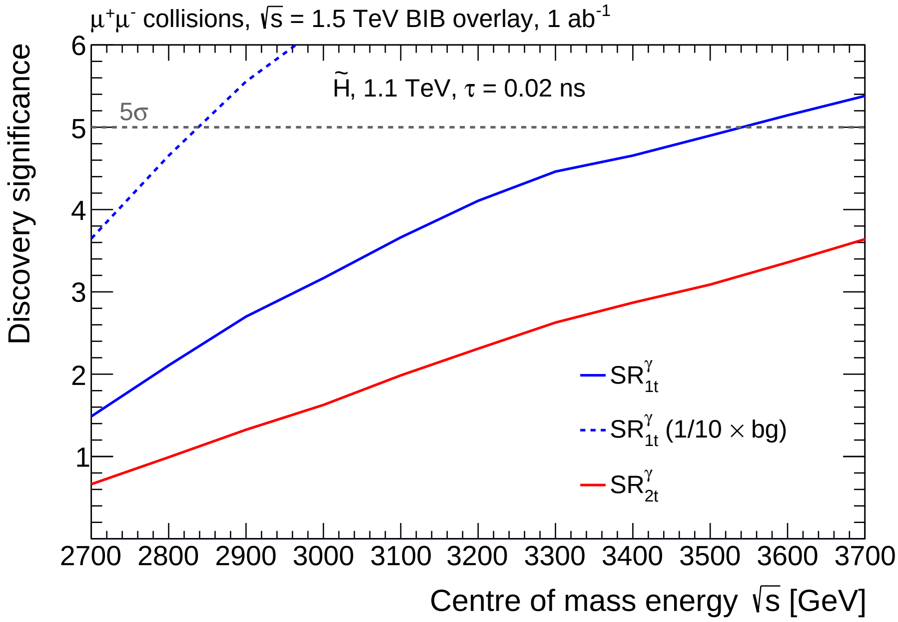

Fig. 14: Expected sensitivity to the higgsino relic favoured mass using 1 ab^{-1} of $\mu^+\mu^-$ collision data as a function of the collision energy.

classification of the particles that are able to give rise to the observed value of Δa_μ, and of their experimental signatures, is possible.

– Additional effects in muon couplings to SM gauge and Higgs bosons, correlated with the muon g-2, can also be present at a level that can be probed by precision measurements at a MuC. Some of these effects can be predicted in a model-independent way, others arise in specific, motivated models.

These three strategies together allow us to formulate a *no-lose theorem* for a high-energy MuC, in case the experimental anomaly in the muon g-2 is really due to NP. The physics case of a high-energy determination of Δa_μ, which is unique of a MuC, thus represents a striking example of the complementarity and interplay of the high-energy and high-intensity frontiers of particle physics, and it highlights the far reaching potential of a MuC to probe NP.

6.1 High-energy probes of the muon g-2

Heavy NP contributions to g-2 arise from the dimension-6 dipole operator $\left(\bar{\mu}_L \sigma_{\mu\nu} \mu_R\right) H F^{\mu\nu}$, [81] where H is the neutral component of the Higgs field and $F^{\mu\nu}$ is the electromagnetic field strength tensor. After electroweak (EW) symmetry breaking H is replaced by its vacuum expectation value $v = 174$ GeV, and one obtains the prediction $\Delta a_\mu^{\rm NP} \sim (g_{\rm NP}^2/16\pi^2) \times (m_\mu v/\Lambda^2)$, where $g_{\rm NP}$ is the typical coupling of the NP sector. Therefore, the NP chiral enhancement $v/m_\mu \sim 10^3$ with respect to the SM weak contribution, together with the assumption of a new strong dynamics with $g_{\rm NP} \sim 4\pi$, bring the sensitivity of the muon g-2 to NP scales of order $\Lambda \sim 100\,$TeV [82, 83]. Directly detecting new particles at such high scales is far beyond the capabilities of any foreseen collider. Nevertheless, a MuC running at energies of several TeV would enable to probe NP in the muon g-2 in a completely model-independent way. Indeed, the very same dipole operator that generates Δa_μ unavoidably induces also a NP contribution to the scattering process $\mu^+\mu^- \to h\gamma$. Measuring the cross-section for this process would thus be equivalent to measuring Δa_μ. This would however be a direct determination of the NP contribution, not hampered by the hadronic uncertainties that affect the SM prediction of a_μ.

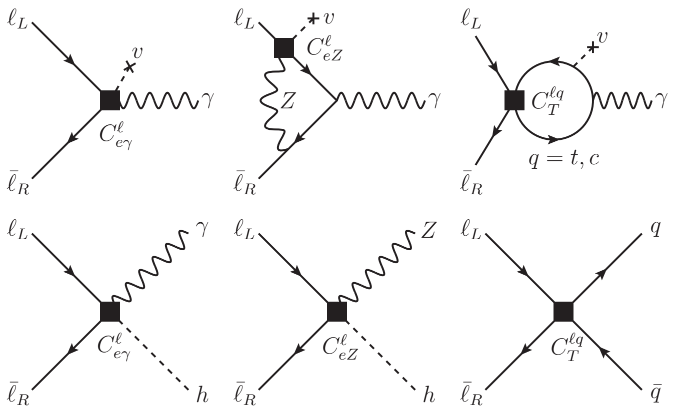

Fig. 15: *Upper row:* Feynman diagrams contributing to the leptonic g-2 up to one-loop order in the Standard Model EFT. *Lower row:* Feynman diagrams of the corresponding high-energy scattering processes. Dimension-6 effective interaction vertices are denoted by a square.

New interactions emerging at a scale Λ larger than the EW scale can be described at energies $E \ll \Lambda$ by an effective Lagrangian containing non-renormalizable $SU(3)_c \otimes SU(2)_L \otimes U(1)_Y$ invariant operators. The relevant effective Lagrangian contributing to g-2, up to one-loop order, reads [81]

$$\mathcal{L} = \frac{C^\ell_{eB}}{\Lambda^2}\,(\bar\ell_L \sigma^{\mu\nu} e_R) H B_{\mu\nu} + \frac{C^\ell_{eW}}{\Lambda^2}\,(\bar\ell_L \sigma^{\mu\nu} e_R)\tau^I H W^I_{\mu\nu} + \frac{C^\ell_T}{\Lambda^2}(\bar\ell_L \sigma_{\mu\nu} e_R)(\overline{Q}_L \sigma^{\mu\nu} u_R) + h.c. \quad (11)$$

The Feynman diagrams relevant g-2 are displayed in figure 15. They lead to the following result

$$\Delta a_\ell \simeq \frac{4 m_\ell v}{e\Lambda^2}\left(C^\ell_{e\gamma} - \frac{3\alpha}{2\pi}\frac{c_W^2 - s_W^2}{s_W c_W}\, C^\ell_{eZ} \log\frac{\Lambda}{m_Z}\right) - \sum_{q=c,t} \frac{4 m_\ell m_q}{\pi^2}\frac{C^{\ell q}_T}{\Lambda^2} \log\frac{\Lambda}{m_q}, \quad (12)$$

where s_W, c_W are the sine and cosine of the weak mixing angle, $C_{e\gamma} = c_W C_{eB} - s_W C_{eW}$ and $C_{eZ} = -s_W C_{eB} - c_W C_{eW}$. Additional loop contributions from the operators $H^\dagger H W^I_{\mu\nu} W^{I\mu\nu}$, $H^\dagger H B_{\mu\nu} B^{\mu\nu}$, and $H^\dagger \tau^I H W^I_{\mu\nu} B^{\mu\nu}$ can be neglected because they are suppressed by the lepton Yukawa couplings. We assume for simplicity C_{eB}, C_{eW} and C_T to be real. We also include the one-loop renormalization effects to $C^\ell_{e\gamma}$, which is the only operator that generates electromagnetic dipoles at tree-level

$$C^\ell_{e\gamma}(m_\ell) \simeq C^\ell_{e\gamma}(\Lambda)\left(1 - \frac{3y_t^2}{16\pi^2}\log\frac{\Lambda}{m_t} - \frac{4\alpha}{\pi}\log\frac{m_t}{m_\ell}\right). \quad (13)$$

Numerically, we find that

$$\frac{\Delta a_\mu}{3\times 10^{-9}} \approx \left(\frac{250\ \text{TeV}}{\Lambda}\right)^2 \left(C^\mu_{e\gamma} - 0.2 C^{\mu t}_T - 0.001 C^{\mu c}_T - 0.05 C^\mu_{eZ}\right).$$

A few comments are in order:

- The Δa_μ discrepancy can be solved for a NP scale up to $\Lambda \approx 250$ TeV. This requires a strongly coupled NP sector where $C^\mu_{e\gamma}$ and/or $C^{\mu t}_T \sim g^2_{\rm NP}/16\pi^2 \sim 1$ and a chiral enhancement v/m_μ compared with the weak SM contribution. As we shall see, this NP can be tested through high-energy processes such as $\mu^+\mu^- \to h\gamma$ or $\mu^+\mu^- \to q\bar q$ (with $q = c, t$) at a MuC.
- If the underlying NP sector is weakly coupled, $g_{\rm NP} \lesssim 1$, then $C^\mu_{e\gamma}$ and $C^{\mu t}_T \lesssim 1/16\pi^2$, implying $\Lambda \lesssim 20$ TeV to solve the g-2 anomaly. In this case, a MuC could still be able to directly produce NP particles [82]. Yet, the study of the processes $\mu^+\mu^- \to h\gamma$ and $\mu^+\mu^- \to q\bar q$ could be crucial to reconstruct the effective dipole vertex $\mu^+\mu^-\gamma$.

– If the NP sector is weakly coupled, and further Δa_μ scales with lepton masses as the SM weak contribution, then $\Delta a_\mu \sim m_\mu^2/16\pi^2\Lambda^2$. Here, the experimental value of Δa_μ can be accommodated only provided that $\Lambda \lesssim 1$ TeV. For such a low NP scale the EFT description breaks down at the typical multi-TeV MuC energies, and new resonances cannot escape from direct production.

The main contribution to Δa_μ comes from the dipole operator $O_{e\gamma} = \left(\bar\ell_L \sigma_{\mu\nu} e_R\right) H F^{\mu\nu}$. The same operator also induces a contribution to the process $\mu^+\mu^- \to h\gamma$ that grows with energy, and thus can become dominant over the SM cross-section at a very high-energy collider. Neglecting all masses, we find the following total $\mu^+\mu^- \to h\gamma$ cross-section

$$\sigma_{h\gamma} = \frac{s}{48\pi}\frac{|C^\mu_{e\gamma}|^2}{\Lambda^4} \approx 0.7\,\mathrm{ab}\left(\frac{\sqrt{s}}{30\,\mathrm{TeV}}\right)^2\left(\frac{\Delta a_\mu}{3\times 10^{-9}},\right)^2 \tag{14}$$

where in the last equation we assumed no contribution to Δa_μ other than the one from $C^\mu_{e\gamma}$. Moreover, we included running effects for $C^\mu_{e\gamma}$, see eq. (13), from a scale $\Lambda \approx 100$ TeV. Notice that there is an identical contribution also to the process $\mu^+\mu^- \to Z\gamma$ since H contains the longitudinal polarizations of the Z. Given the scaling with energy of the reference integrated luminosity for a MuC [84] one gets about 60 total $h\gamma$ events at $\sqrt{s} = 30$ TeV.

The SM irreducible $\mu^+\mu^- \to h\gamma$ background is small, $\sigma^{\rm SM}_{h\gamma} \approx 2\times 10^{-2}\,\mathrm{ab}\left(\frac{30\,\mathrm{TeV}}{\sqrt{s}}\right)^2$, with the dominant contribution arising at one-loop [85] due to the muon Yukawa coupling suppression of the tree-level part. The main source of background comes from $Z\gamma$ events, where the Z boson is incorrectly reconstructed as a Higgs. This cross-section is large, due to the contribution from transverse polarizations. There are two ways to isolate the $h\gamma$ signal from the background: by means of the different angular distributions of the two processes – the SM $Z\gamma$ peaks in the forward region, while the signal is central – and by accurately distinguishing h and Z bosons from their decay products, e.g. by precisely reconstructing their invariant mass. To estimate the reach on Δa_μ we consider a cut-and-count experiment in the $b\bar b$ final state, which has the highest signal yield. The significance of the signal is maximized in the central region $|\cos\theta| \lesssim 0.6$. At 30 TeV one gets

$$\sigma^{\rm cut}_{h\gamma} \approx 0.53\,\mathrm{ab}\left(\frac{\Delta a_\mu}{3\times 10^{-9}}\right)^2, \qquad\qquad \sigma^{\rm cut}_{Z\gamma} \approx 82\,\mathrm{ab}\,. \tag{15}$$

Requiring at least one jet to be tagged as a b, and assuming a b-tagging efficiency $\epsilon_b = 80\%$, we find that a value $\Delta a_\mu = 3\times 10^{-9}$ can be tested at 95% C.L. at a 30 TeV collider if the probability of reconstructing a Z boson as a Higgs is less than 10%. The resulting number of signal events is $N_S = 22$, and $N_S/N_B = 0.25$. In figure 16 we show as a black line the 95% C.L. reach from $\mu^+\mu^- \to h\gamma$ on the anomalous magnetic moment as a function of the collider energy. Note that since the number of signal events scales as the fourth power of the center-of-mass energy, only a collider with $\sqrt{s} \gtrsim 30$ TeV will have the sensitivity to test the g-2 anomaly in this channel.

If the magnetic moment arises at one loop from one of the other operators in (12), their Wilson coefficients must be larger to reproduce the observed signal, and the NP will be easier to test at a MuC. In particular, we now derive the constraints on the semi-leptonic operators. The operator $O^{\mu t}_T$ that enters Δa_μ at one loop can be probed by $\mu^+\mu^- \to t\bar t$ (Fig. 15). Its contribution to the cross-section is

$$\sigma_{t\bar t} = \frac{s}{6\pi}\frac{|C^{\mu t}_T|^2}{\Lambda^4} N_c \approx 58\,\mathrm{ab}\left(\frac{\sqrt{s}}{10\,\mathrm{TeV}}\right)^2\left(\frac{\Delta a_\mu}{3\times 10^{-9}}\right)^2 \tag{16}$$

where in the last equality we have again taken $\Lambda \approx 100$ TeV so that $|\Delta a_\mu| \approx 3\times 10^{-9}\,(100\,\mathrm{TeV}/\Lambda)^2\,|C^{\mu t}_T|$. We estimate the reach on Δa_μ simply assuming an overall 50% efficiency for reconstructing the top quarks, and requiring a statistically significant deviation from the SM $\mu^+\mu^- \to t\bar t$ background, which

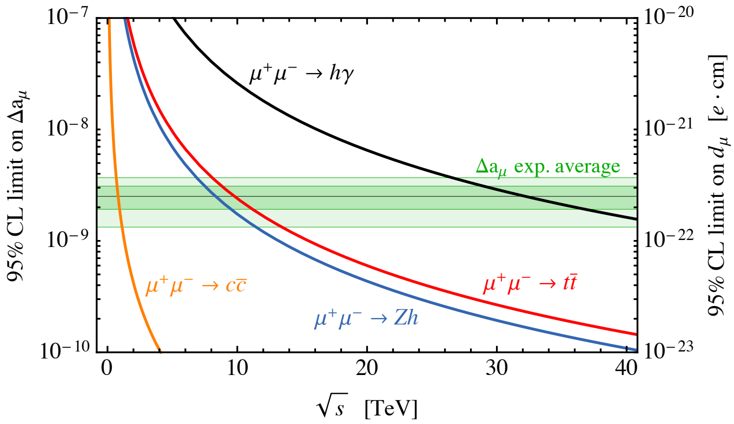

Fig. 16: Reach on the muon anomalous magnetic moment Δa_μ and muon EDM d_μ, as a function of the MuC collider center-of-mass energy $\sqrt{s}$, from the labeled processes.

has a cross-section $\sigma_{t\bar{t}}^{\rm SM} \approx 1.7\,\text{fb}\,\left(\frac{10\,\text{TeV}}{\sqrt{s}}\right)^2$. In Fig. 16 we show the 95% C.L. constraints on the top contributions to Δa_μ as red lines as a function of the collider energy. Note that this scenario can be probed at $\sqrt{s} = 10$ TeV. A similar analysis can be performed for semi-leptonic operator involving charm quarks. This case can be probed already at $\sqrt{s} = 1$ TeV as we can see in Fig. 16, orange line.

So far, we assumed CP conservation. If however the coefficients $C_{e\gamma}$, C_{eZ} or C_T are complex, the muon electric dipole moment (EDM) d_μ is unavoidably generated. Since the cross-sections in eq. (14) and (16) are proportional to the absolute values of the same coefficients, a MuC offers a unique opportunity to test also d_μ. The current experimental limit $d_\mu < 1.9 \times 10^{-19}\, e\,\text{cm}$ was set by the BNL E821 experiment [86] and the new E989 experiment at Fermilab aims to decrease this by two orders of magnitude [87]. Similar sensitivities could be reached also by the J-PARC g-2 experiment [88].

From the model-independent relation [89]

$$\frac{d_\mu}{\tan\phi_\mu} = \frac{\Delta a_\mu}{2m_\mu}\, e \simeq 3 \times 10^{-22} \left(\frac{\Delta a_\mu}{3\times 10^{-9}}\right) e\,\text{cm}\,, \tag{17}$$

where ϕ_μ is the argument of the dipole amplitude, the bounds on Δa_μ in figure 16 can be translated into a model-independent constraint on d_μ. We find that already a 10 TeV MuC can reach a sensitivity comparable to the ones expected at Fermilab [87] and J-PARC [88], while at a 30 TeV collider one gets the bound $d_\mu \lesssim 3 \times 10^{-22}\, e$ cm.

6.2 Direct searches

Here we show a model-exhaustive analysis of all possible BSM solutions to the g-2 anomaly to study production of the associated new states at future MuC. We then formulate a no-lose theorem for the discovery of new physics if the g-2 anomaly is confirmed and weakly coupled solutions below the GeV scale are excluded. We first find the highest possible mass scale of new physics subject only to perturbative unitarity, and optionally the requirements of minimum flavour violation and/or naturalness. Our results show that a 3 TeV MuC can discover all new physics scenarios in which Δa_μ is generated by SM singlets with masses above $\sim$ GeV (lighter singlets will be discovered by upcoming low-energy experiments). This includes the case when the singlets decay invisible, a scenario that can be challenging to probe at hadron colliders and low energy leptons colliders. Now, If new states with electroweak quantum numbers contribute to g-2, the minimal requirements of perturbative unitarity guarantee new charged states below ($\sim$ 100 TeV), but this is strongly disfavoured by stringent constraints on charged lepton flavour violating (LFV) decays. Reasonable new physics theories that satisfy LFV bounds by obeying Minimal Flavour Violation (MFV) and that avoid generating a hierarchy problem, not only for the Higgs

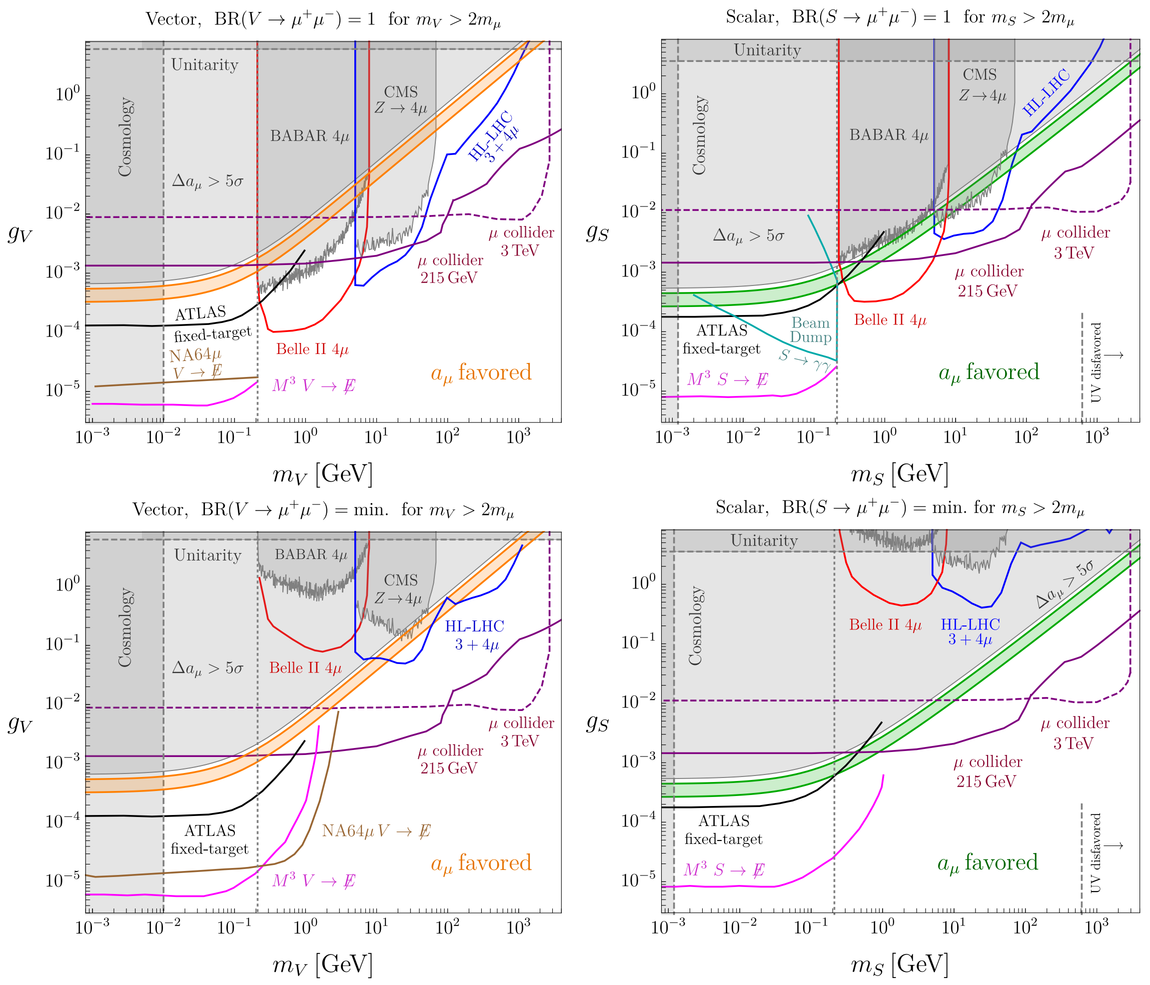

Fig. 17: Singlet models for g-2 and their probes at different masses, assuming 100% branching ratio to di-muons (top) and the minimum branching ratio to di-muon allowed by perturbativity [90].

but also for the muon mass, require the existence of at least one new charged state below ~ 10 TeV. This strongly motivates the construction of high-energy MuC.

Our model-exhaustive analysis starts with the question *What is the highest mass that new particles could have while still generating the measured BSM contribution to g-2?* Answering this question is important because knowing the highest mass scale can set the target for the center of mass energy of the MuC needed to detect these new particles. We assume that one-loop effects involving BSM states are responsible for the anomaly, since scenarios where new contributions only appear at higher loop order require a lower BSM mass scale to generate the required new contribution. We can, thus, organize all possible one-loop BSM contributions to Δa_μ into two classes: **Singlet Scenarios:** in which each BSM g-2 contribution only involves a muon and a new SM singlet boson that couples to the muon, and **Electroweak (EW) Scenarios:** in which new states with EW quantum numbers contribute to g-2.

Singlet mediators

Throughout this section *Singlet Models* refers to the family of models where Δa_μ is generated by a muon philic singlet, either scalar or vector (where μ_L and μ^c are the muon Weyl spinors)

$$g_S S(\mu_L\mu^c + \mu^{c\dagger}\mu_L^\dagger), \quad g_V V_\nu(\mu_L^\dagger\bar{\sigma}^\nu\mu_L + \mu^{c\dagger}\bar{\sigma}^\nu\mu^c)\,. \tag{18}$$

Realizations of these scenarios appear in multiple contexts. For example, vector singlets can be classified either into dark photon or $L_\mu - L_\tau$ like [91]. The former are solutions to g-2 where couplings between the vector and first generation fermions are generated via loop-induced kinetic mixing. These scenarios are all excluded [92, 93] or soon to be [94]. The second, $L_\mu - L_\tau$ like scenarios, are vectors that do not couple to first generation fermions. These are highly constrained and a combination of fixed target experiments and muon beam dumps could probe the remaining parameter space [95, 96]. As per singlet scalar UV completinos, one can have models with extra scalars and/or fermions that, after being integrated out, generate the dimension 5 operator $(S/\Lambda)\, H^\dagger L \mu^c$. Once the higgs gets a vev one reproduces the interaction in 18. These models are disfavored for large singlet masses [90].

Figure 17 shows the limits and projections on muon-philic vector (left) and scalar (right) singlets, assuming only di-muon decays where kinematically allowed. The green/orange bands represent the parameter space for which singlet scalars/vectors resolve g-2 within 2σ. Existing experimental limits are shaded in gray, while projections are indicated with colored lines. The M^3 [97], NA64μ [98], and ATLAS fixed-target [99] experiments probe invisibly-decaying singlets; projections here assume a 100% invisible branching fraction. The LHC limits and HL-LHC projections are obtained from $3\mu/4\mu$ muon searches. The purple muon collider projections are obtained from a combination of singlet+photon searches, and from deviations in angular observables of Bhabha scattering [83]. For scalar singlets whose width is determined entirely by the muon coupling (top right), we also show the projections for a beam dump search for $S \to \gamma\gamma$ [100] on the minimal assumption that the scalar-photon coupling arises solely from integrating out the muon. Similar beam dump searches involving $S \to e^+e^-$ decays below the $m_S < 2m_\mu$ threshold have also been proposed, but are not shown here because the signal is, in principle, unrelated to the singlet-muon coupling that resolves g-2. The bottom row shows same as the top row, but assuming that for $m_{S,V} > 2m_\mu$, the singlets have the *minimum* di-muon branching fraction consistent with unitarity. The curves which are unaffected by this change of muonic branching fraction correspond to searches that are insensitive to the singlet's decay modes. Projections for M^3, NA64μ, and ATLAS fixed-target experiments assume a $\simeq 100\%$ invisible branching fraction for $m_{S/V} > 2m_\mu$, which is model-dependent.

Electroweak mediators

Electroweak Scenarios can generate the necessary g-2 contribution even for NP much above the TeV scale. In particular, we carefully study simplified models featuring new scalars and fermions that yield the *largest possible BSM mass scale* able to account for the anomaly [82, 83]. Careful analysis of these scenarios allow us to derive our model-exhaustive upper bound on BSM particle masses responsible for Δa_μ. We also account for the possibility of many new states contributing to Δa_μ by considering $N_{\rm BSM} \geq 1$ copies of each BSM model being present simultaneously. Our results show that EW Scenarios must always have at least one new charged state lighter than the following upper bound:

$$M^{\rm max,X}_{\rm BSM,charged} \approx \left(\frac{2.8\times 10^{-9}}{\Delta a_\mu}\right)^{\frac{1}{2}} \times \begin{cases} (100\ {\rm TeV})\ N_{\rm BSM}^{1/2} & {\rm for}\quad X = ({\rm unitarity}^*) \\ (20\ {\rm TeV})\ N_{\rm BSM}^{1/2} & {\rm for}\quad X = ({\rm unitarity{+}MFV}) \\ (20\ {\rm TeV})\ N_{\rm BSM}^{1/6} & {\rm for}\quad X = ({\rm unitarity{+}naturalness}^*) \\ (9\ {\rm TeV})\ N_{\rm BSM}^{1/6} & {\rm for}\quad X = ({\rm unitarity{+}naturalness{+}MFV}), \end{cases} \tag{19}$$

where this upper bound is evaluated under four assumptions that the BSM solution to the g-2 anomaly must satisfy: perturbative unitarity only; unitarity + MFV; unitarity + naturalness (specifically, avoiding fine-tuning the Higgs and the muon mass); and unitarity + naturalness + MFV. The unitarity-only bound represents the very upper limit of what is possible within Quantum Field Theory, but realizing such high masses requires severe alignment, tuning or another unknown mechanism to avoid stringent constraints from charged lepton flavour-violating (CLFV) decays [101, 102]. We have therefore marked every scenario without MFV with a star (*) above, to indicate additional tuning or unknown flavour mechanisms that have to also be present.

Our results and those from the previous section have profound implications for the physics motivation of MuC. They allow us to formulate a no-lose theorem that can be broken down in chronological progression:

1. **Present day:** Confirmation of the $g-2$ anomaly.
2. **Discover or falsify low-scale Singlet Scenarios $\lesssim$ GeV:** If Singlet Scenarios with BSM masses below $\sim$ GeV generate the required Δa_μ contribution, multiple fixed-target and B-factory experiments are projected to discover new physics in the coming decade.
3. **Discover or falsify all Singlet Scenarios $\lesssim$ TeV:** If fixed-target experiments do not discover new BSM singlets that account for Δa_μ, a 3 TeV MC with $1\ \text{ab}^{-1}$ would be guaranteed to directly discover these singlets if they are heavier than $\sim$ 10 GeV. Even a lower-energy machine can be useful: a 215 GeV muon collider with $0.4\ \text{ab}^{-1}$ could directly observe singlets as light as 2 GeV.
4. **Discover non-pathological Electroweak Scenarios ($\lesssim$ 10 TeV):** If TeV-scale muon colliders do not discover new physics, the g-2 anomaly *must* be generated by EW Scenarios. In that case, all of our results indicate that in most reasonably motivated scenarios, the mass of new charged states cannot be higher than few $\times$ 10 TeV.
5. **Unitarity Ceiling ($\lesssim$ 100 TeV):** Even if such a high energy muon collider does not produce new BSM states directly, as we saw in the previous section, a 30 TeV machine would detect deviations in $\mu^+\mu^- \to h\gamma$, which probes the same effective operator generating g-2 at lower energies. This would provide high-energy confirmation of the presence of new physics.

If the g-2 anomaly is confirmed, our analysis and the results of the previous section show that finding the origin of this anomaly should be regarded as one of the most important physics motivations for an entire muon collider *program*. Indeed, a series of colliders with energies from the test-bed-scale $\mathcal{O}$(100 GeV) to the far more ambitious but still imaginable $\mathcal{O}$(10 TeV) scale and beyond has excellent prospects to discover the new particles necessary to explain this mystery.

6.3 Vector-like fermions

Simple explanations for g-2 involve extensions of the SM with new vector-like fermions (VLF) where the corrections to the muon magnetic moment are mediated by the SM Higgs and gauge bosons [103, 104]. These models generate effective interactions between the muon and multiple Higgs bosons leading to predictions for di- and tri-Higgs production at a MuC that are directly correlated with the corrections to Δa_μ [105]. Here we consider extensions of the SM with VLF doublets, $L_{L,R}$, and singlets $E_{L,R}$ with masses $M_{L,E}$, respectively. While in our main results we will assume that new L_L and E_R have the same quantum numbers as the SM leptons, we will comment on other possibilities later.

The Yukawa interactions of interest are the following

$$\mathcal{L} \supset -y_\mu \bar{l}_L \mu_R H - \lambda_E \bar{l}_L E_R H - \lambda_L \bar{L}_L \mu_R H - \lambda \bar{L}_L E_R H - \bar{\lambda} H^\dagger \bar{E}_L L_R + h.c., \tag{20}$$

where $l_L = (\nu_\mu, \mu_L)^T$, $L_{L,R} = (L^0_{L,R}, L^-_{L,R})^T$, and $H = (0,\ v + h/\sqrt{2})^T$ with $v = 174$ GeV. In the limit $v \ll M_{L,E}$, after integrating out the heavy leptons at tree level, Eq 20 becomes

$$\mathcal{L} \supset -y_\mu \bar{l}_L \mu_R H - \frac{m_\mu^{LE}}{v^3} \bar{l}_L \mu_R H (H^\dagger H) + h.c., \tag{21}$$

where

$$m_\mu^{LE} \equiv \frac{\lambda_L \bar{\lambda} \lambda_E}{M_L M_E} v^3 \tag{22}$$

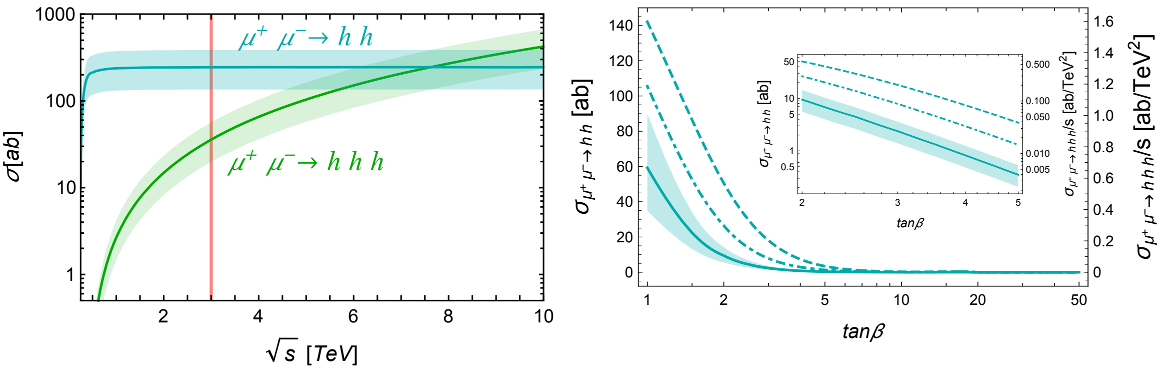

Fig. 18: *Left:* Cross sections for hh (cyan) and hhh (green) production as a function of $\sqrt{s}$ in models with VLF. *Right:* Cross sections for hh (left axis) and hhh (right axis) production as a function of $\tan\beta$ in models with VLF and 2HDM for $M_{L,E} \simeq m_{H,A,H^{\pm}}$. The dot-dashed and dashed lines correspond to the predictions corresponding to the central value of Δa_μ and $m_{H,A,H^\pm} = 3\times M_{L,E}$ and $m_{H,A,H^\pm} = 5\times M_{L,E}$, respectively. Both panels assume Δa_μ is within 1σ of the measured value (shaded ranges) [105].

is the contribution to the muon mass from mixing with new leptons. Mixing of the muon with heavy leptons also leads to modifications of the muon couplings to W, Z, and h, and generates new couplings of the muon to new leptons. Assuming that $v \ll M_{L,E}$, the total one-loop correction to g-2 induced by these effects is well approximated by [103, 104]

$$\Delta a_\mu = -\frac{1}{16\pi^2}\frac{m_\mu m_\mu^{LE}}{v^2}. \tag{23}$$

The explanation of the measured value of Δa_μ within 1σ requires that

$$m_\mu^{LE}/m_\mu = -1.07 \pm 0.25. \tag{24}$$

For couplings of $\mathcal{O}(1)$, Eq (24) can be achieved for new lepton masses even as heavy as 7 TeV while simultaneously satisfying current relevant constraints [106]. For couplings close to the limit of perturbativity, $\sqrt{4\pi}$, this range extends to close to 50 TeV. This far exceeds the reach of the LHC and even projected expectations of possible future proton-proton colliders, such as the FCC-hh. However, there are related signals that could be fully probed at, for example, a 3 TeV MuC through the effective interactions generated between the muon and multiple Higgs bosons. These interactions are all generated by Eq. 21 [105] and they lead to the following predictions

$$\sigma_{\mu^+\mu^-\to hh} = \frac{\left|\lambda_{\mu\mu}^{hh}\right|^2}{64\pi} = \frac{9}{64\pi}\left(\frac{m_\mu^{LE}}{v^2}\right)^2, \tag{25}$$

$$\sigma_{\mu^+\mu^-\to hhh} = \frac{\left|\lambda_{\mu\mu}^{hhh}\right|^2}{6144\pi^3}s = \frac{3}{4096\pi^3}\left(\frac{m_\mu^{LE}}{v^3}\right)^2 s. \tag{26}$$

Thus, considering Eq 23, we see that the effective interactions of the muon with the Higgs are completely fixed by the muon mass and the predicted value of Δa_μ. In Fig 18, we show the total $\mu^+\mu^- \to hh$ and $\mu^+\mu^- \to hhh$ cross sections at a MuC as a function of $\sqrt{s}$ calculated from the effective lagrangian and assuming that Δa_μ is achieved within 1σ (shaded ranges). Cross sections for a 3 TeV MuC are highlighted with the red line. We see that, for example, a MuC running at $\sqrt{s} = 3$ TeV with 1 ab^{-1} of integrated luminosity would see about 240 di-Higgs events and about 35 tri-Higgs events. It should be noted that already at $\sqrt{s} = 1$ TeV this is roughly 4 (3) orders of magnitude larger than $\mu^+\mu^- \to hh$ and $\mu^+\mu^- \to hhh$ in the SM. Note that di- and tri-Higgs signals produced from vector boson fusion in the SM appear with additional particles in the final state and can be easily vetoed in a dedicated analysis. Similarly, backgrounds involving the Z-boson which may be comparable at the level of cross sections, e.g. $\mu^+\mu^- \to Zh$ or $\mu^+\mu^- \to ZZ$, can also be easily suppressed via invariant mass cuts on the Z-boson masses once the relevant decays are taken into account in a given analysis.

Models with more exotic quantum numbers can also generate a similar correction to Δa_μ and, hence, similar predictions for di- and tri-Higgs cross sections. In total there are 5 different combinations of new lepton fields that can lead to mass-enhanced corrections to Δa_μ mediated by the SM Higgs. In each case, the correction as given in Eq 23 is simply multiplied by a corresponding c-factor. The resulting cross sections are then rescaled by a factor of $1/c^2$ compared to those in Fig 18. In Table 5, we list the 5 possible models, c-factor multiplying Eq 23, and corresponding predictions for di- and tri-Higgs cross sections for a MuC running at $\sqrt{s} = 3$ TeV, assuming $\Delta a_\mu \pm 1\sigma$. A MuC running even at moderate center-of-mass energies, $\sqrt{s} \sim 1 - 3$ TeV, can fully probe these scenarios.

Vector-like fermions and Two-Higgs-Doublet models

It is straightforward to extend the discussion from the previous section to a 2HDM (or any model where the Higgs acts as one component of the sector triggering EWSB) [106, 107]. For instance, in a type-II 2HDM where charged leptons couple exclusively to one Higgs doublet, H_d, (which can be achieved by assuming a Z_2 symmetry) the lagrangian in Eq. 1 from the previous section, is simply modified with the replacement $H \to H_d$. In this case both Higgs doublets develop a vev $\left\langle H_d^0 \right\rangle = v_d$ and $\left\langle H_u^0 \right\rangle = v_u$, where $\sqrt{v_d^2 + v_u^2} = v = 174$ GeV and $\tan\beta = v_u/v_d$. The effective interactions generated by integrating out heavy leptons is then

$$\mathcal{L} \supset y_\mu \bar{\mu}_L \mu_R H_d - \frac{m_\mu^{LE}}{v_d^3} \bar{\mu}_L \mu_R H_d (H_d^\dagger H_d). \tag{27}$$

Similar modifications to Z, W, and the SM-like Higgs couplings to the muon are also generated after EWSB. Including the additional corrections to Δa_μ from heavy charged and neutral Higgs bosons leads to [106, 107]

$$\Delta a_\mu = -\frac{1 + \tan^2\beta}{16\pi^2} \frac{m_\mu m_\mu^{LE}}{v^2}, \qquad m_\mu^{LE} \equiv \frac{\lambda_L \bar{\lambda} \lambda_E}{M_L M_E} v_d^3, \tag{28}$$

where we have assumed $M_{L,E} \simeq m_{H,A,H^\pm}$ for simplicity. The first term in Eq 28 results from the same loops as in the SM, i.e. involving the Z, W, and SM-like Higgs, whereas the second term, enhanced in comparison by $\tan^2\beta$, results from the additional contributions from the heavy Higgses. The corresponding requirement to satisfy Δa_μ within 1σ then becomes

$$m_\mu^{LE}/m_\mu = (-1.07 \pm 0.25)/(1 + \tan^2\beta). \tag{29}$$

Just as in the previous section, effective interactions between the muon and multiple Higgs bosons are generated via the single dimension-six operator in Eq 21. Thus, predictions for di- and tri-Higgs cross sections follow in the same way simply by replacing m_μ^{LE} with the corresponding definition in Eq 28. Considering Eq 29, it follows that $\sigma_{\mu^+\mu^- \to hh}$ and $\sigma_{\mu^+\mu^- \to hhh}$ cross sections in a type-II 2HDM decrease as $1/\tan^4\beta$.

In Fig 18, we show the $\tan\beta$ dependence of $\sigma_{\mu^+\mu^- \to hh}$ and $\sigma_{\mu^+\mu^- \to hhh}/s$ calculated from the effective lagrangian when Δa_μ is achieved within 1σ (shaded range) and $M_{L,E} \simeq m_{H,A,H^\pm}$. The dot-dashed and dashed lines correspond to the predictions corresponding to the central value of Δa_μ and $m_{H,A,H^\pm} = 3 \times M_{L,E}$ and $m_{H,A,H^\pm} = 5 \times M_{L,E}$, respectively. Its expected that future measurements of $h \to \mu{+}\mu^-$ will probe $\tan\beta$ up to ~ 5 and the inset zooms into this region [105].

Table 5: Quantum numbers of $L_{L,R} \oplus E_{L,R}$ under $SU(2) \times U(1)_Y$, corresponding c-factor for Δa_μ, and predictions for di- and tri-Higgs cross sections running at $\sqrt{s} = 3$ TeV, assuming $\Delta a_\mu \pm 1\sigma$.

$SU(2) \times U(1)_Y$	c	σ_{hh}(3 TeV)[ab]	σ_{hhh}(3 TeV)[ab]
$\mathbf{2}_{-1/2} \oplus \mathbf{1}_{-1}$	1	244^{+141}_{-109}	$35.8^{+20.8}_{-15.9}$
$\mathbf{2}_{-1/2} \oplus \mathbf{3}_{-1}$	5	10^{+6}_{-4}	$1.43^{+0.8}_{-0.6}$
$\mathbf{2}_{-3/2} \oplus \mathbf{1}_{-1}$	3	27^{+16}_{-12}	$4.0^{+2.3}_{-1.8}$
$\mathbf{2}_{-3/2} \oplus \mathbf{3}_{-1}$	3	27^{+16}_{-12}	$4.0^{+2.3}_{-1.8}$
$\mathbf{2}_{-1/2} \oplus \mathbf{3}_{0}$	1	244^{+141}_{-109}	$35.7^{+20.7}_{-15.9}$

For a MuC running at center-of-mass energy of 3 TeV with, for example, 1 ab^{-1} of luminosity 3 di-Higgs events are expected in these scenarios for $\tan\beta \simeq 3$. For tri-Higgs the same sensitivity does not extend MCh above $\tan\beta \simeq 1$. When $m_{H,A,H^\pm} = 5 \times M_{L,E}$, the corresponding sensitivities to $\tan\beta$ increase to about $\tan\beta \simeq 5$ and 2.5 for di-Higgs and tri-Higgs signals, respectively.

These conclusions also extend to models with additional scalars where the SM Higgs is only one component of the scalar sector responsible for EWSB. Mixing within the Higgs sector (e.g. $\tan\beta$ in a 2HDM) introduces a free parameter to the predictions and correlations between the muon magnetic moment and effective Higgs couplings. Thus, the corresponding predictions for di- and tri-Higgs signals at a MuC are not as sharp in these scenarios as compared to the SM. Though in a 2HDM the observables parametrically interpolate between the SM and models with scalars that do not participate in EWSB.

7 Lepton Flavour Universality and B physics

The rich set of observed deviations from SM predictions in rare semileptonic B-meson decays, induced by the $b \to s\mu^+\mu^-$ partonic transition, represent a compelling hint for new physics. The ratios R_K and R_{K^*}, relevant for testing Lepton Flavour Universality in B-meson decays, are defined as

$$R_K = \frac{\mathrm{BR}(B^+ \to K^+\mu^+\mu^-)}{\mathrm{BR}(B^+ \to K^+e^+e^-)}\,, \quad R_{K^\star} = \frac{\mathrm{BR}(B^0 \to K^{\star 0}\mu^+\mu^-)}{\mathrm{BR}(B^0 \to K^{\star 0}e^+e^-)}\,. \tag{30}$$

Due to highly suppressed hadronic uncertainties, such ratios are supposed to be theoretically clean and could thus be a clean signal of BSM-physics. Very recently, the LHCb collaboration reported the results of R_K-measurement (in the region $q^2 \in [1.1, 6]$ GeV^2) as [108]

$$R_K^{\mathrm{LHCb}} = 0.846^{+0.042+0.013}_{-0.039-0.012}\,, \tag{31}$$

which indicates a 3.1σ discrepancy from its SM prediction [109, 110]

$$R_K^{\mathrm{SM}} = 1.0003 \pm 0.0001\,. \tag{32}$$

Similarly, the LHCb Collaboration has also reported the results of R_{K^*}-measurement in two low-q^2 bins [111] ($q^2 \in [0.045, 1.1]$ GeV^2 and $q^2 \in [1.1, 6]$ GeV^2):

$$R_{K^*}^{\mathrm{LHCb}} = \begin{cases} 0.660^{+0.110}_{-0.070} \pm 0.024\,, \\ 0.685^{+0.113}_{-0.069} \pm 0.047\,, \end{cases} \tag{33}$$

which shows 2.2σ and 2.4σ deviations, respectively from their corresponding SM-predictions in each q^2 bin [112, 113]:

$$R_{K^\star}^{\mathrm{SM}} = \begin{cases} 0.92 \pm 0.02\,, \\ 1.00 \pm 0.01\,. \end{cases} \tag{34}$$

Furthermore, Belle has also presented their results on R_K [114] and R_{K^*} [115]. However, there are comparatively larger uncertainties than for the LHCb measurements. There are in fact only a few BSM possibilities which could resolve these $R_{K^{(*)}}$-anomalies. Before entering details, it is quite important to mention that an explanation of $R_{K^{(*)}}$ by modifying the $b \to s\mu^+\mu^-$ decay anticipates a better global-fit to other observables, as compared to altering the $b \to se^+e^-$ decay, reason why we focus on the former.

The effective Lagrangian responsible for semi-leptonic $b \to s\mu^+\mu^-$-transitions can be expressed as (V denotes the CKM-matrix)

$$\mathcal{L}^{\rm NP}_{b\to s\mu\mu} \supset \frac{4G_{\rm F}}{\sqrt{2}} V_{tb}V^*_{ts}\,(C^\mu_9 O^\mu_9 + C^\mu_{10}O^\mu_{10}) + \text{h.c.} \tag{35}$$

with the relevant operators

$$\begin{aligned} O^\mu_9 &= \frac{\alpha}{4\pi}\left(\bar{s}_{\rm L}\gamma_\mu b_{\rm L}\right)\left(\bar{\mu}\gamma^\mu\mu\right), \\ O^\mu_{10} &= \frac{\alpha}{4\pi}\left(\bar{s}_{\rm L}\gamma_\mu b_{\rm L}\right)\left(\bar{\mu}\gamma^\mu\gamma_5\mu\right). \end{aligned} \tag{36}$$

Using these operators to explain the anomalies leads to best-fit values of the Wilson-coefficients $C_9 = -C_{10} = -0.43$, with the 1σ range being $[-0.50, -0.36]$ [116, 117]. This corresponds to a new physics scale of $\Lambda = 39$ TeV. Perturbative unitarity analysis suggests new mass thresholds below $\lesssim 100$ TeV.

Should these hints for Lepton Flavour Universality be confirmed by upcoming measurements, a major goal of HEP will be to understand the nature of the underlying new physics. Given the high EFT scale required to fit the deviation it is possible, and likely, that such NP is too heavy to be observed at the LHC. A more powerful collider would therefore be needed. In this Section we find the reach of a MuC on the NP responsible for the B-anomalies, both from the EFT perspective as well as considering some of the NP scenarios more commonly known in the literature.

7.1 *Nightmare* scenario: contact interactions

In this Section we consider the pessimistic scenario where the new physics states responsible for the anomalies are much heavier than the colliders' energy reach for on-shell production even at future colliders.[3] Nonetheless, the effect of these new states can be captured by contact interactions that would leave a trace in the high-invariant mass tails at the energy frontier providing a complementary information about the new physics [121]. For example, measuring such interactions and establishing a correlation with the low-energy observables would exclude light mediators and potentially uncover other properties of new physics.

The most pessimistic case would be to assume that only the contact interaction behind the anomalies, $(\bar{s}_L\gamma_\alpha b_L)(\bar{\mu}_L\gamma^\alpha\mu_L)$, is important at high-$p_T$. However, realistic models in general also induce contributions to quark flavor conserving operators. We thus also consider the four-fermion operator $(\bar{b}_L\gamma_\alpha b_L)(\bar{\mu}_L\gamma^\alpha\mu_L)$. To summarise, the contact interactions we consider are:

$$\mathcal{L}_{\rm EFT} = C_{bb\mu\mu}\,(\bar{b}_L\gamma_\alpha b_L)(\bar{\mu}_L\gamma^\alpha\mu_L) + \left[C_{sb\mu\mu}\,(\bar{s}_L\gamma_\alpha b_L)(\bar{\mu}_L\gamma^\alpha\mu_L) + \text{h.c.}\right] \tag{37}$$

Here we calculate and compare the reach on these intereactions at the following colliders

[3] The set of such models is not any empty set. To name one explicit example, a scalar leptoquark mediator S_3 [118] with a conserved baryon and a muon number which would explain almost a minimal set of couplings needed to fit the anomaly [119] can be as heavy as 69 TeV and still pass all the complementary experimental bounds and perturbative unitarity [120]. This is far beyond the reach for on-shell production at any considered future collider.

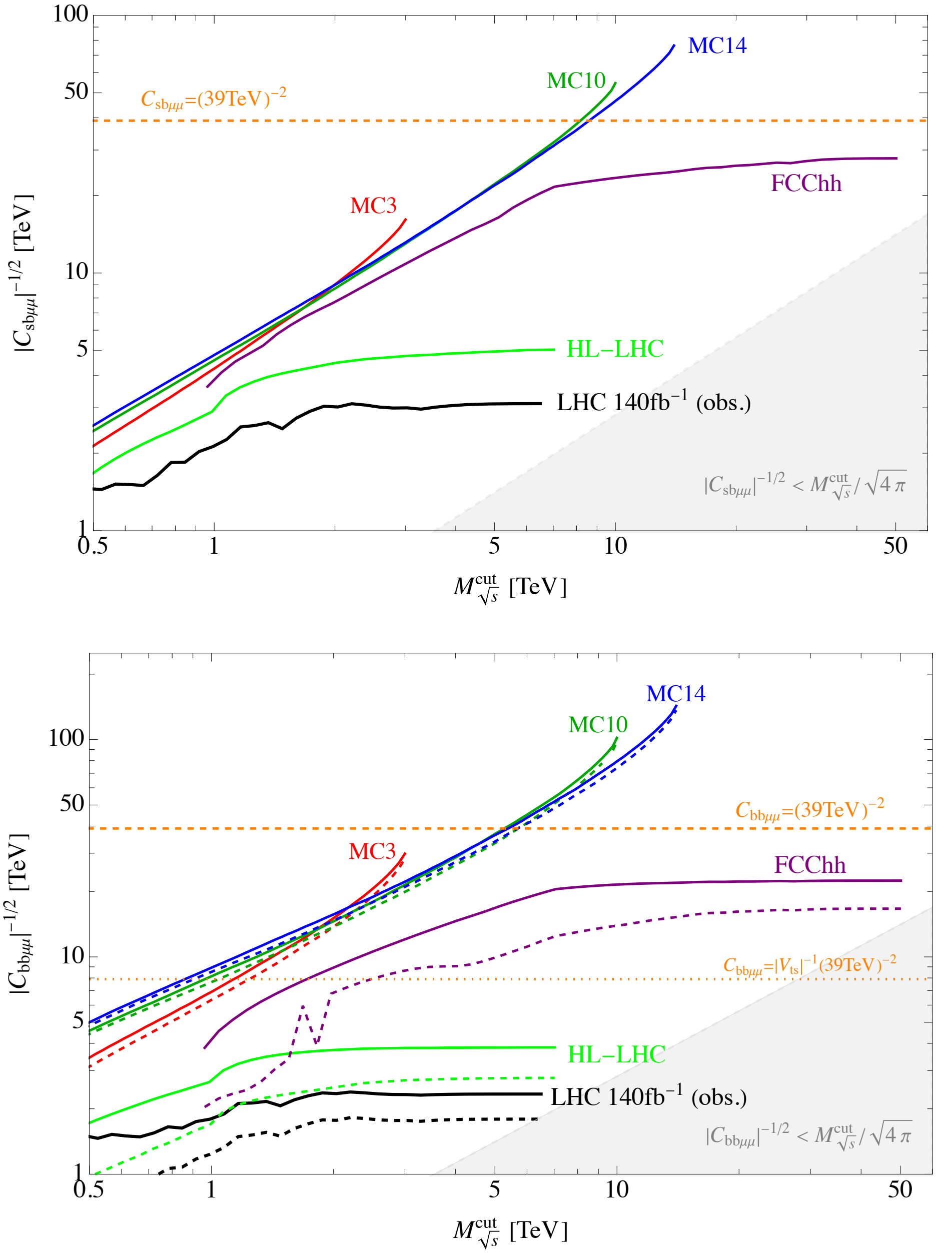

Fig. 19: Sensitivity reach (at 95% CL) for the $(\bar{s}_L\gamma_\alpha b_L)(\bar{\mu}_L\gamma^\alpha\mu_L)$ (top) and $(\bar{b}_L\gamma_\alpha b_L)(\bar{\mu}_L\gamma^\alpha\mu_L)$ (bottom) contact interactions as a function of the upper cut on the final-state invariant mass for various MuC, HL-LHC, FCC-hh, and the present LHC bounds. These are compared with values required to fit $b \to s\mu^+\mu^-$ anomalies without (dashed orange line) or with (dotted orange line) a flavor enhancement of the bb operator compared to the bs one. For the bottom plot solid (dashed) lines represent the limit for positive (negative) values of $C_{bb\mu\mu}$. The gray area represents a region where the EFT bounds are not valid (for a strongly coupled UV completion, for weakly coupled ones the area is larger).

Collider	C.o.m. Energy	Luminosity	Label
LHC Run-2 [122]	13 TeV	140 fb^{-1}	LHC
HL-LHC	14 TeV	6 ab^{-1}	HL-LHC
FCC-hh	100 TeV	30 ab^{-1}	FCC-hh
MuC	3 TeV	1 ab^{-1}	MC3
MuC	10 TeV	10 ab^{-1}	MC10
MuC	14 TeV	20 ab^{-1}	MC14

For the hadron colliders we study the high-energy di-muon production, $pp \to \mu^+\mu^-$, while, for the MuC we consider inclusive high-energy di-jet production via $\mu^-\mu^+ \to jj$. For MuC we take into account the full EW PDF of the muon, obtained by numerically solving the DGLAP evolution of the partonic distribution functions inside the muon using QED+QCD interactions below the EW scale and the full unbroken SM interactions above [123–125]. We checked that the purely QCD dijet cross section, initiated by quarks and gluons inside the muon, is always completely negligible with respect to the muon-initiated Drell-Yan one. On top of the statistical uncertainty, we include a 2% systematic uncertainty in each bin. While some improvement in sensitivity is expected by requiring one (or both) jet to be b-tagged, the overall picture will not change drastically for both hadron and MuC [126, 127], therefore we just consider the inclusive cross section at this point. For more details we refer to [128].

Our results are collected in Fig. 19, where we show the expected 95%CL sensitivity as a function of the upper cut on the invariant mass of the final state for different colliders. The present LHC bounds with 140 fb^{-1} of luminosity are shown in black [122]. The dashed orange line is the reference value for $C_{sb\mu\mu}$ required to fit the anomalies, while for $C_{bb\mu\mu}$ we also show as a dotted orange line a reference value where this flavor conserving interaction is enhanced by a factor of $1/|V_{ts}| \approx 25$ with respect to the flavor violating one, as expected in many realistic scenarios [129].

7.2 Z' models

In order to address the $R_{K^{(*)}}$-anomaly, there is a popular class of Z' scenarios. As a prototypical-model, we consider a Z' which dominantly couples to bs and $\mu^+\mu^-$, via left-handed currents[4]. One can achieve this by extending the SM with an extra $U(1)$ gauge group, which brings in a new Z' boson having a non-universal lepton-coupling and a flavor-changing quark-coupling. Here, we concentrate solely on the Lagrangian part relevant for $b \to s\mu^+\mu^-$-transitions, namely

$$\mathcal{L}_{Z'} \supset \left(\lambda^{\rm Q}_{ij}\bar{d}^i_{\rm L}\gamma^\mu d^j_{\rm L} + \lambda^{\rm L}_{\alpha\beta}\bar{\ell}^\alpha_{\rm L}\gamma^\mu \ell^\beta_{\rm L}\right) Z'_\mu\,, \tag{38}$$

where ℓ^i and d^i represent the corresponding generations of charged-lepton and down-type quark states.

Integrating out the Z' field yields the following effective-Lagrangian:

$$\begin{aligned}\mathcal{L}^{\rm eff}_{Z'} &= -\frac{1}{2M^2_{Z'}}\left(\lambda^{\rm Q}_{ij}\bar{d}^i_{\rm L}\gamma_\mu d^j_{\rm L} + \lambda^{\rm L}_{\alpha\beta}\bar{\ell}^\alpha_{\rm L}\gamma_\mu \ell^\beta_{\rm L}\right)^2 \\ &\supset -\frac{1}{2M^2_{Z'}}\left[\left(\lambda^{\rm Q}_{23}\right)^2\left(\bar{s}_{\rm L}\gamma_\mu b_{\rm L}\right)^2 + 2\lambda^{\rm Q}_{23}\lambda^{\rm L}_{22}\left(\bar{s}_{\rm L}\gamma_\mu b_{\rm L}\right)\left(\bar{\mu}_{\rm L}\gamma^\mu \mu_{\rm L}\right) + \text{h.c.}\right].\end{aligned} \tag{39}$$

Now one can obtain the relevant Wilson-coefficients at tree-level [cf. left-panel of Fig. 15] by matching onto the effective-Lagrangians for the low-energy observables at the scale $\left(\mu = M_{Z'}\right)$ as

$$C^\mu_9 = -C^\mu_{10} = -\frac{\pi}{\sqrt{2}G_{\rm F}M^2_{Z'}\alpha}\left(\frac{\lambda^{\rm Q}_{23}\lambda^{\rm L}_{22}}{V_{tb}V^*_{ts}}\right). \tag{40}$$

[4] Right-handed currents in the lepton-sector actually worsen the compatibility of $R_{K^{(*)}}$ explanation with the ΔM_s (mass-differences of neutral B-mesons) measurement [120], since they demand a larger Wilson-coefficient.

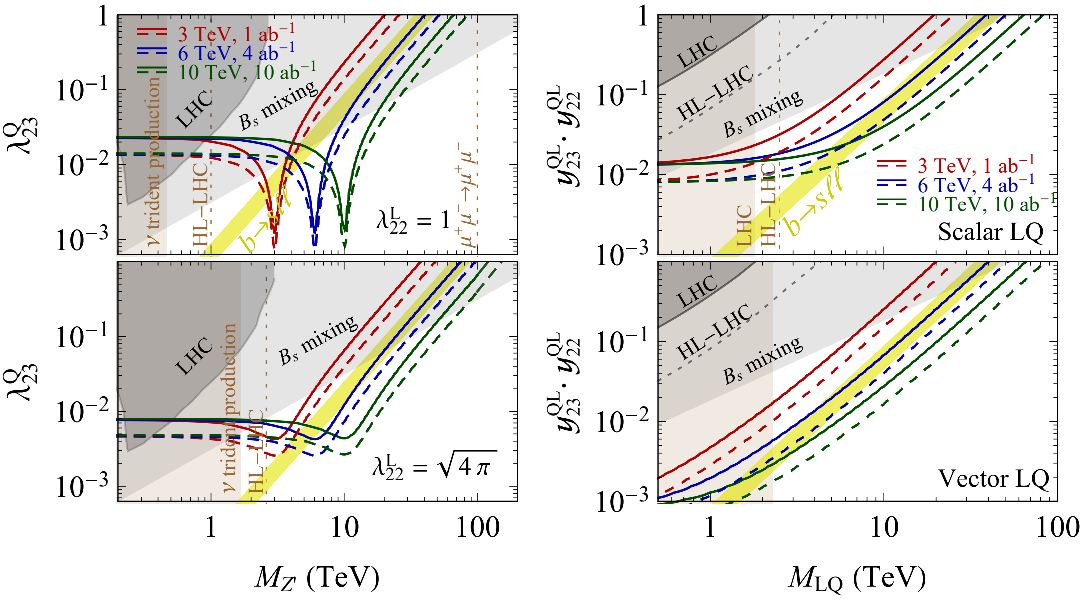

Fig. 20: *Left:* Sensitivities to the Z' model with $\lambda^{L}_{22} = 1$ (upper panel) and $\lambda^{L}_{22} = \sqrt{4\pi}$ (lower panel) via $\mu^+\mu^- \to b\bar{s}$ at a MuC with $\sqrt{s} = 3, 6, 10$ TeV (red, blue, green). Other limits include the neutrino trident production [95], LHC [131], HL-LHC [132], and B_s mixing [120]. *Right:* Sensitivities to the LQ model via $\mu^+\mu^- \to b\bar{s}$ at a MuC for scalar (upper) and vector (lower) LQ. Figures from Ref. [130].

The diagram for the Z' option at the MuC is shown in the left panel of Fig. 15, which is related to the simple Z'-mediated process $b \to s\mu^+\mu^-$ of $R_{K^{(*)}}$ anomaly by a crossing symmetry. This s-channel process enables a robust direct test to the Z' interpretation [130].

Because of the limited power of flavor reconstruction, the major background of the bs final state comes from the SM dijet signals, namely $\mu^+\mu^- \to jj$ with j being u, d, s, c and b. The final sensitivity is subject to the b-jet tagging efficiency and the mistag rate. We assume a conservative experimental performance, with the b-jet tagging efficiency being $\epsilon_b = 70\%$ [8] and mistag rates being $\epsilon_{uds} = 1\%$ and $\epsilon_c = 10\%$. While counting the signal events, we simply require that one of the jets is successfully tagged as a b jet, while the other is not. The t-jet should be able to be clearly separated from b-jet with proper cuts on the jet structure.

The sensitivity is studied at the parton level for the MuC setup $\sqrt{s} = 3$ TeV and $L = 1$ ab^{-1} by counting the event number with respect to the polar angle. We adopt the following chi-square

$$\chi^2 = \sum_i \frac{(N_i - \widetilde{N}_i)^2}{N_i + \epsilon^2 \cdot N_i^2} , \tag{41}$$

where i sums over polar angles with a bin size of $\cos\theta$ being 0.1, N_i is the predicted total event number of signal plus SM backgrounds, $\widetilde{N}_i$ is SM only event number, and we fix the possible systematic error ϵ as 0.1%.

The final sensitivity to Z' connecting the $\mu\mu$ and bs currents are shown in Fig. 20, left. The red curves mark the sensitivity of the MuC with $\sqrt{s} = 3$ TeV and $L = 1$ ab^{-1} if we take $\lambda^{L}_{22} = 1$ (upper panel) or $\lambda^{L}_{22} = \sqrt{4\pi}$ (lower panel). Note that large λ^{L}_{22} is needed because λ^{Q}_{23} is strongly constrained by $B_s - B_{\bar{s}}$ mixing. The solid and dashed curves represent the cases without and with flavor tagging, respectively. The parameter space of Z' explaining the $R_{K^{(*)}}$ anomaly is given as the yellow band, which is actually limited by neutrino trident production and B_s mixing. If $\lambda^{L}_{22} = 1$ is assumed, the Z' parameter space which survives in explaining the $R_{K^{(*)}}$ anomaly (yellow bands) can be largely covered.

Even though it is not shown here, we expect the radiative return process, $\mu^+\mu^- \to bs\gamma$, will explore the rest of the surviving parameter space. Moreover, we observe that with a higher COM energy, a higher Z' mass region can be probed. This is helpful to probe the $R_{K^{(*)}}$ anomaly when a larger $\lambda^{\rm L}_{22}$ is taken. For instance, for $\lambda^{\rm L}_{22} = \sqrt{4\pi}$ the MuC with $\sqrt{s} = 6$ TeV will rule out most of the favored parameter space.

7.3 Scalar Leptoquarks

In order to address the $R_{K^{(*)}}$-anomaly, there is another popular class of models in which leptoquarks (LQ) are applied. Here we briefly review these simplified models that can accommodate the $R_{K^{(*)}}$-anomaly. There are only four scalar LQ which can interact with the SM-fermions at renormalizable level. Interestingly, $S_3 \sim (3, 3, -1/3)$ can simultaneously address R_K and R_{K^*} and its constraints are not in conflict with the experimental data [133, 134]. Similarly, the vector LQ $U_1 \sim (3, 1, 2/3)$ can also provide a good fit for the $R_{K^{(*)}}$-anomaly. Note that it requires a proper UV-completion for theoretical consistency.

The relevant Lagrangian for S_3 can be written as:

$$\mathcal{L}_{S_3} = -M^2_{S_3} |S^a_3|^2 + y^{\rm LQ}_{i\alpha} \overline{Q^{c}}^{i} (\epsilon\sigma^a)\, L^\alpha S^a_3 + \text{h.c.}, \tag{42}$$

with lepton and quark-doublets $L^\alpha = (\nu^\alpha_{\rm L},\, \ell^\alpha_{\rm L})^{\rm T}$ and $Q^i = \left(V^*_{ji} u^j_{\rm L},\, d^i_{\rm L}\right)^{\rm T}$, and Pauli-matrices σ^a ($a = 1, 2, 3$; $\epsilon = i\sigma^2$). The LQ contributes to the Wilson-coefficients at tree-level [cf. Fig. 15] and one can identify:

$$C^\mu_9 = -C^\mu_{10} = \frac{\pi}{\sqrt{2} G_{\rm F} M^2_{S_3} \alpha} \left(\frac{y^{\rm LQ}_{32} y^{\rm LQ*}_{22}}{V_{tb} V^*_{ts}} \right). \tag{43}$$

In contrast to Z' scenario, the process mediated by LQ is t-channel [130]. Hence, we expect a different event distribution if the mediator mass is reachable by the colliding energy. If the mediator mass is large, we can still test the $R_{K^{(*)}}$ anomaly at the MuC but can no longer differentiate various models. In this regard, it is convenient to describe with an effective theory in terms of the Wilson coefficients C^μ_9 and C^μ_{10}. It is easy to find the cross section of $\mu^+\mu^- \to b\bar{s}$ to be

$$\sigma(s) = \frac{G^2_{\rm F} \alpha^2 |V_{tb} V^*_{ts}|^2 s}{8\pi^3} \left(|C^\mu_9|^2 + |C^\mu_{10}|^2 \right). \tag{44}$$

When the mediator mass is very large, the signal event number is fixed by the Wilson coefficients, regardless of the details of the UV completion. If we take the best-fit scenario of B anomaly fit, i.e., $C^\mu_9 = -C^\mu_{10} = -0.43$, we obtain the event number of bs as

$$\#\text{signal} \simeq 10^3 \left(\frac{\sqrt{s}}{6\ \text{TeV}} \right)^2 \left(\frac{L}{4\ \text{ab}^{-1}} \right). \tag{45}$$

The SM background of quark dijets without flavor tagging reads $1.2 \times 10^5 \cdot (6\ \text{TeV}/\sqrt{s})^2 \cdot (L/4\ \text{ab}^{-1})$. The signal is found to exceed the SM background uncertainty at around 3σ confidence level.

The sensitivity to the S_3 LQ model is shown in the upper-right panel of Fig. 20. The MuC with $\sqrt{s} = 3$ TeV and $L = 1\ \text{ab}^{-1}$ will reach the red curves. The solid and dashed curves stand for the cases without and with the flavor tagging procedure. For $\sqrt{s} = 3$ TeV, an upgrade of the luminosity $L = 1\ \text{ab}^{-1}$ by a factor of 4 to 8 or a better tagging efficiency is required to cover the LQ parameter space indicated by the $R_{K^{(*)}}$ anomaly.

Nevertheless, it is interesting to discuss the potential of MuC with other options. For the setup $\sqrt{s} = 6$ TeV and $L = 4\ \text{ab}^{-1}$, we find most of the parameter space suggested by the $R_{K^{(*)}}$ anomaly will be probed. For demonstration, we also show the case of U_1 vector LQ in the lower-right panel of Fig. 20, for which the setup $\sqrt{s} = 6$ TeV and $L = 4\ \text{ab}^{-1}$ can fully cover the indicated parameter space.

7.4 Vector Leptoquarks

We now focus on the phenomenology of the vector LQ known in the literature as U_1^μ, at a MuC. As a proof-of-principle, we [135] explore the reach of two benchmark MuC facilities (1 ab^{-1} at 3 TeV and 20 ab^{-1} at 14 TeV) for U_1^μ production and contribution to LFUV. The Lagrangian of this model includes

$$\mathcal{L}_{\text{LQ}} \supset \frac{g_U}{\sqrt{2}} U_1^\mu \beta_L^{ij} \bar{Q}_L^i \gamma_\mu L_L^j + \text{h.c.}, \tag{46}$$

where $g_U \beta_L^{ij}$ parametrizes the coupling of the vector LQ U_1 to a left-handed i-generation quark and j-generation massive lepton. This model can explain the observed anomaly if

$$\frac{\beta_L^{22} \beta_L^{32}}{m_{\text{LQ}}^2} \approx 1.98 \times 10^{-3}\ \text{TeV}^{-2}. \tag{47}$$

Note that each β_L^{ij} is a parameter of the theory. For concreteness, a multitude of coupling scenarios are considered, such as

$$\beta_L^{ij} = \begin{pmatrix} 0 & 0 & 0 \\ 0 & \beta_L^{22} = \beta_L^{32} & 0 \\ 0 & \beta_L^{32} & 0 \end{pmatrix}, \tag{48}$$

i.e. and equal coupling of U_1 to μs and μb, and zero coupling to other flavors of quarks and leptons. Other coupling schemes are considered to explore the phenomenological consequences, but the choice given in Eq. 48 provides the minimal structure to address the flavor anomalies.

To generate the events, three production mechanisms were considered: pair production, single production, and Drell-Yan.

Pair Production. This channel is dominated by producing two on-shell U_1s. These processes are initiated either by direct muon collisions or initial state vector boson fusion. A cut on the invariant mass of the bottom quark pair in the final state, m_{bb}, can significantly reduce the background. Note that pair production of U_1 from initial vector bosons is determined by its gauge interactions and it is independent of the β_L couplings to SM fermions.

Single Production. This channel has distinct phenomenology from the pair production one. While pair production falls off steeply once the two U_1s are not produced on-shell, the single production channel doesn't fall off until the mass threshold ($m_{\text{LQ}} = \sqrt{s}$). Additionally, the single-production diagrams all depend on β_L and lose sensitivity in the weak coupling region of parameter space. The background diagrams of this channel are similar to that from the pair-production channel, with one of the final state particles missing. Again we can leverage the different topology of the background and signal diagrams to impose appropriate cuts. For example, a cut on the angular distance between the two final b quarks and on the pseudorapidity of the final μ can significantly improve the signal-to-background ratio for this channel [135].

Drell-Yan. Finally, a t-channel exchange of the LQ can give rise to a final state with b-quark jets. This interferes with the s-channel SM signal. Depending on the mass of the U_1, the distribution of events in kinetic variable (e.g. η or p_T) can be very different. By binning the events in different η bins and fitting the distribution, the background and signal events can be more easily separated.

Combining the results of all production channels, the reach of a 3 and 14 TeV MuC in the mass m_{LQ} and coupling β_L^{32} for a U_1 model is shown in Fig. 21. In Ref. [135] four different flavor scenarios, i.e. texture of yukawa couplings, were considered. The plots here are reproduced with flavor scenario 2 ($\beta_L^{22} = \beta_L^{32}$) of Ref. [135].

Note that the pair-production channel is dominant and ultimately independent of β_L at sufficiently small couplings as the EW production takes over. We observe that with the cuts and the rudimentary analyses proposed in Ref. [135], the Drell-Yan-like channel has the best sensitivity for most of the parameter

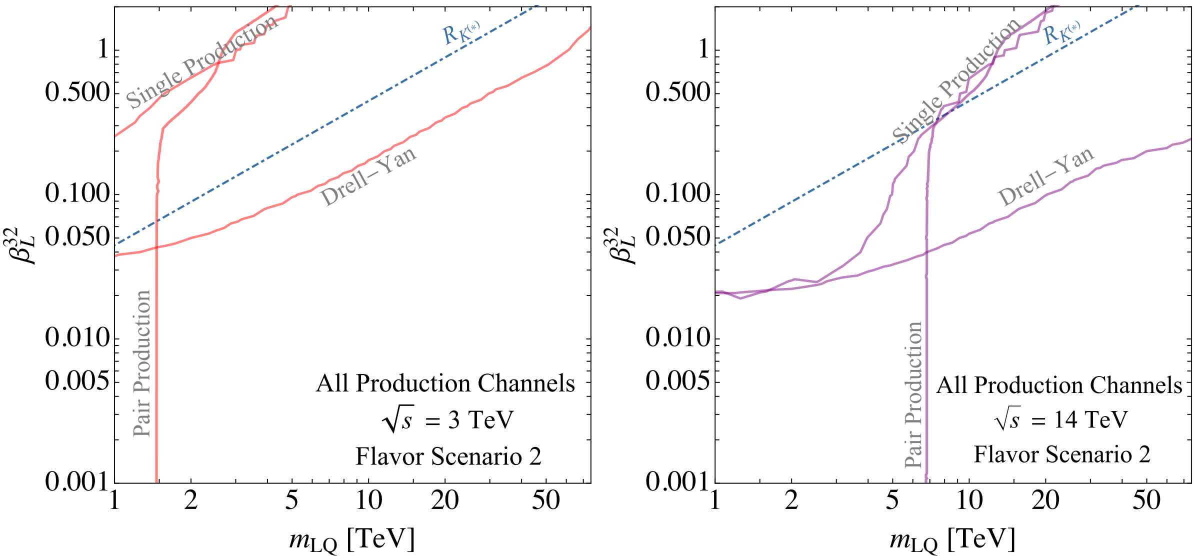

Fig. 21: The 5σ discovery reach of 3 (14) TeV MuC with 1 (20) ab^{-1} of data. The reach is calculated using the flavor scenario described in Eq. 48. The straight-line boundary of the pair-production channel corresponds to pure EW production, and is therefore independent of β_L. Figure taken from Ref. [135].

space for these choices of $\sqrt{s}$. In particular, we find that the line for the best fit to $R_{K^{(*)}}$ anomalies, see Eq. 47, can be probed even at a 3 TeV MuC. If the anomalies are supported by the upcoming LHCb or Belle II experiments, these results provide an irrefutable case for building a high energy MuC.

Since the construction of a future MuC has not begun, this analysis has not attempted to simulate systematics or detector effects. An attempt at emulating the systematics in searches for U_1 at a future MuC can be found in [130] . Inclusion of systematics and different statistical analysis led Ref. [130] to a slightly lower reach than shown in Fig. 21. Yet, both analyses agree that a MuC with a few to 10 TeV center of mass energy, and with predicted attainable luminosities [3], can cover the entire parameter space of U_1 that explains the flavor anomalies. Once the research and design of the collider is underway, further studies will be needed to refine the reach plot provided in this proof-of-concept study.

8 Lepton Flavour Violation

The SM exhibits a distinctive pattern of fermion masses and mixing angles, for which we currently have no deep explanation. Delicate symmetries also lead to a strong suppression of flavor-changing processes in the quark and lepton sectors, which may be reintroduced by new particles or interactions. The non-observation of such processes thus leads to some of the most stringent constraints on BSM physics, while a positive signal could give us insight into the observed structure of the SM. A number of precision experiments searching for lepton flavor violating (LFV) processes such as $\mu \to 3e$, $\tau \to 3\mu$ or μ-to-e conversion within atomic nuclei will explore these processes with orders of magnitude more precision in the coming decades [136]. As we will see, a high-energy MuC has the unique capability to explore the same physics — either via measuring effective interactions or by directly producing new states with flavor-violating interactions — at the TeV scale.

8.1 Effective LFV Contact Interactions

In this section, we study MuC bounds on $\mu\mu\ell_i\ell_j$-type contact interactions, and demonstrate the complementarity with precision experiments looking for lepton-flavor violating decays, as first studied in ref. [4]. We will focus on $\tau 3\mu$ and $\mu 3e$ operators, since constraints on them can be compared directly with the sensitivity from $\tau \to 3\mu$ and $\mu \to 3e$ decays. We parametrize the four-fermion operators

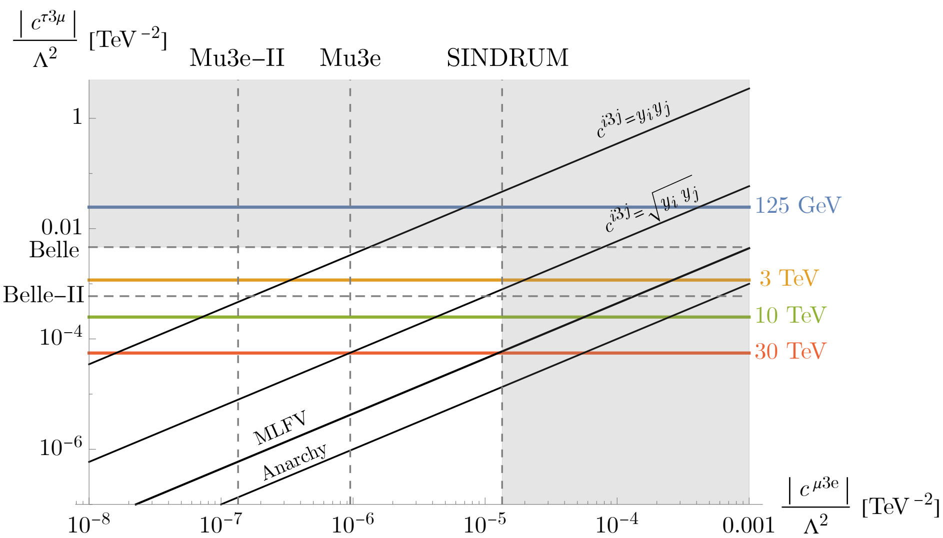

Fig. 22: Summary of MuC and low-energy constraints on flavor-violating 3-body lepton decays. The colored horizontal lines show the sensitivity to the $\tau 3\mu$ operator at various energies, all assuming 1 ab^{-1} of data. The dashed horizontal (vertical) lines show the current or expected sensitivity from $\tau \to 3\mu$ ($\mu \to 3e$) decays for comparison. The diagonal black lines show the expected relationship between different Wilson coefficients with various ansatz for the scaling of the flavor-violating operators (e.g., "Anarchy" assumes that all Wilson coefficients are $\mathcal{O}(1)$).

relevant for the $\tau \to 3\mu$ decay via

$$\mathcal{L} \supset V_{LL}^{\tau 3\mu} (\bar{\mu}\gamma^\mu P_L \mu)(\bar{\tau}\gamma_\mu P_L \mu) + V_{LR}^{\tau 3\mu} (\bar{\mu}\gamma^\mu P_L \mu)(\bar{\tau}\gamma_\mu P_R \mu) + (L \leftrightarrow R) + \text{h.c.}\,, \tag{49}$$

with an equivalent set for the $\mu \to 3e$ decay. We will assume all the $\tau 3\mu$ coefficients are equal: In what follows, we will assume all the $V_{ij}^{\tau 3\mu}$ coefficients are equal to $c^{\tau 3\mu}/\Lambda^2$, where $c^{\tau 3\mu}$ is a dimensionless coefficient and Λ is to be interpreted as the scale of new physics, and similarly for $\mu 3e$ coefficients.

At a MuC, the $\tau 3\mu$ coefficients are probed via $\mu^+\mu^- \to \mu\tau$. Our analysis closely follows an analogous study at an e^+e^- collider in ref. [137]. As discussed in ref. [4], the SM backgrounds from $\tau^+\tau^-$ and W^+W^- production can be substantially mitigated by a simple set of cuts, whereas the signal can be largely retained up to $\sim 10\%$ effects due to initial state radiation. The resulting bounds, assuming integrated luminosities of 1 ab^{-1} at 0.125, 3, 10 and 30 TeV are shown in Fig. 22, alongside current and future sensitivities of $\tau \to 3\mu$ and $\mu \to 3e$ experiments. A 3 TeV machine would set a direct bound at the same level as the future Belle II sensitivity.

Given an ansatz regarding the flavor structure, the constraints on the $\tau 3\mu$ operators can be compared to the constraints on the analogous $\mu 3e$ operator in the $\mu \to 3e$ decay. The diagonal lines in Fig. 22 show the expected relationship between the two Wilson coefficients for several different ansatz, including flavor anarchy (where all coefficients ~ 1), Minimal Leptonic Flavor Violation [138], or scalings with different powers of the involved Yukawa couplings. While muon decays set the strongest limits assuming anarchical coefficients, a MuC could set competitive constraints for other ansatz: in the most extreme case, where the Wilson coefficients scale like the product of the Yukawas, a 3 TeV machine would have sensitivity comparable to the final Mu3e sensitivity.

In addition to the $\tau 3\mu$ operators considered here, similar sensitivity should be attainable for the $\mu^+\mu^- \to \mu^\pm e^\mp$ process, as well as to the processes such as $\mu^+\mu^- \to \tau^\pm e^\mp$ that violate lepton flavor by two units. Overall, we see that a MuC would be capable of directly probing flavor-violating interactions that are quite complementary to future precision constraints.

8.2 Direct Probes: Lepton-Flavor Violation in the MSSM

An exciting possibility is that the flavor-changing processes that might be observed in low-energy experiments arise from loops of new particles near the TeV scale. As a motivated example, consider the MSSM. The scalar superpartners of the SM leptons can have soft supersymmetry-breaking contributions to their mass matrix that are off-diagonal in the SM lepton eigenbasis. As a result, the slepton interactions with the leptons will be flavor-violating and lead to processes such as muon-to-electron conversion and rare muon decays at one loop. In well-motivated constructions, the mixing between the selectron and smuon states can be quite large, as the low-energy processes are protected by a "Super-GIM" mechanism [139], allowing the new states to be near the TeV scale while consistent with current bounds.

A 3 TeV MuC would dramatically extend the reach for electroweak-charged superpartners beyond a TeV, raising the possibility of directly producing the new states responsible for lepton flavor-violation. Moreover, the unique environment of a MuC makes it possible to not only produce these new states, but measure their LFV interactions. This would provide detailed insight into both the mechanism of supersymmetry breaking and the origin of the flavor structure of the SM. A detailed investigation of these prospects is carried out in ref. [140];[5] here we briefly review their results for the 3 TeV case.

To understand the complementarity of low-energy cLFV probes and the MuC reach, we consider the scenario in which only the right-handed selectron and smuon, along with one light neutralino (which we will assume to be a pure bino with mass M_1) are in the spectrum. If the slepton masses $m_{\tilde{\ell}} > M_1$, the sleptons decay directly to a lepton and bino, and the LFV interactions can be measured directly via the pair-production process: $\mu^+\mu^- \to \tilde{e}^+_{1,2}\tilde{e}^-_{1,2} \to \mu^\pm e^\mp \chi^0_1\chi^0_1$, where the binos appear as missing momentum. In this simplified scenario, both the low-energy LFV processes and the pair-production process at a MuC depend only on the slepton masses and mixing angle, as well as M_1.

In Fig. 23, we show the 5σ reach for a 3 TeV MuC, assuming an average slepton mass of 1 TeV. The left panel shows the reach as a function of the mixing angle and mass-splitting, $\Delta m^2 = m^2_{\tilde{e},2} - m^2_{\tilde{e},1}$, with $M_1 = 500\,\mathrm{GeV}$. The right panel shows the constraints for fixed $\Delta m^2/\bar{m}^2 = 0.1$ in the M_1 vs. $\sin 2\theta_R$ plane. Large mixing angles are motivated in models involving gauge-mediated supersymmetry breaking (GMSB), indicated by the purple region, while larger mass splittings are motivated in scenarios where the messengers carry flavor-dependent charges, such as $L_\mu - L_\tau$, indicated by the blue regions (see ref. [140] for more details). The complementary constraints from low-energy experiments searching for $\mu \to e\gamma$, $\mu \to 3e$ decays or μ-to-e transitions are shown in blue, purple and green, respectively. We see that the MuC reach can extend to small mass splittings in the GMSB scenario, and can cover a substantial part of the most well-motivated parameter space.

8.3 Gauge $L_\mu - L_\tau$ Interactions

It is not straightforward to test the $L_\mu - L_\tau$ model at laboratories due to the preferred couplings to the second and third family leptons, unless we have a facility to directly collide muons.

We discuss in the following the potential of a MuC with a COM energy $\sqrt{s} = 3$ TeV and an integrated luminosity $L = 1\ \mathrm{ab}^{-1}$ in searching for Z' [141, 142] in the $L_\mu - L_\tau$ model. In particular, the parameter space which explains the $(g-2)_\mu$ as well as B-physics anomalies is found to be fully explored by such a facility given a reasonable integrated luminosity. The relevant interaction with the new boson Z' reads

$$\mathcal{L} \supset g' \left(\overline{\ell_{\mathrm{L}}} Q' \gamma^\mu \ell_{\mathrm{L}} + \overline{E_{\mathrm{R}}} Q' \gamma^\mu E_{\mathrm{R}} \right) Z'_\mu \,, \tag{50}$$

where g' stands for the coupling constant of gauged $L_\mu - L_\tau$ symmetry, $\ell \equiv (\nu, E)^{\mathrm{T}}$ is the lepton doublet with ν and E being the neutrino and the charged lepton, respectively, and $Q' = \mathrm{Diag}(0, 1, -1)$ represents the charge matrix in the basis of (e, μ, τ). The Z' will inevitably mix with the SM gauge bosons, i.e., γ

[5] These prospects were also reviewed in ref. [4].

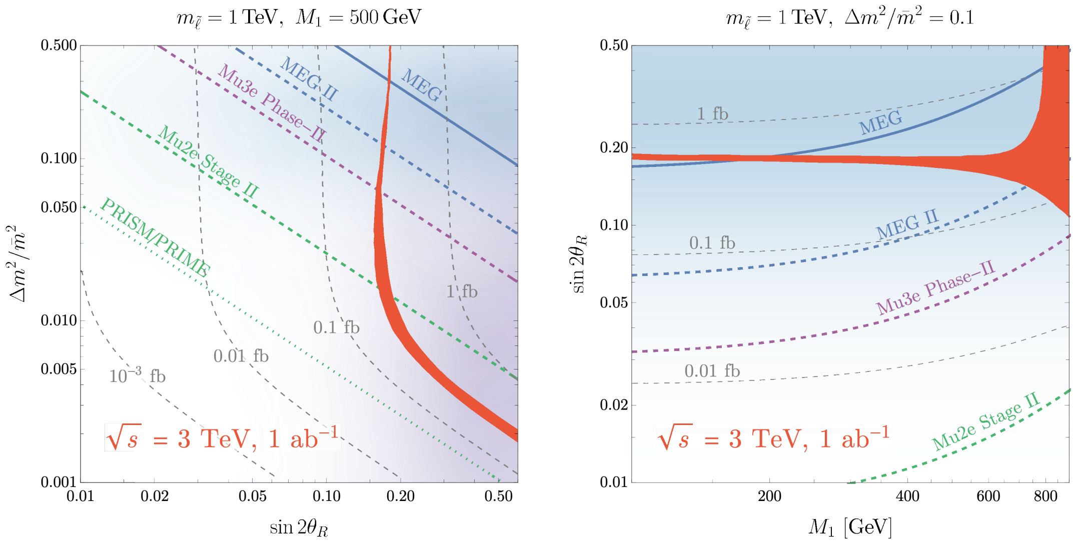

Fig. 23: Constraints on lepton flavor violation in the MSSM in the $\Delta m^2/\bar{m}^2$ vs. $\sin 2\theta_R$ plane (left) and the $\sin 2\theta_R$ vs. M_1 plane (right) from measurements of the slepton pair production process with flavor-violating final states (red band) at a 3 TeV MuC, assuming $1\,\mathrm{ab}^{-1}$ of luminosity. The width of the band represents the uncertainty on the reach from the measurement of the slepton and neutralino masses in flavor-conserving channels. The purple and blue shaded lightly shaded regions indicate parameters preferred in Gauge-Mediated Supersymmetry Breaking scenarios and flavor-dependent mediator scenarios, respectively. Both plots assume a mean slepton mass of 1 TeV. In the left plot we fix the neutralino mass $M_1 = 500\,\mathrm{GeV}$, while in the right figure $\Delta m^2/\bar{m}^2$ is fixed to 0.1. The current (solid) and expected (dashed, dotted) limits from low-energy lepton flavor violation experiments are indicated by the blue, purple and green lines.

and Z. We find that the mixing with γ is strongly suppressed by the Z' mass, while the mixing with Z can be relevant if their masses are of the similar order. For simplicity, we assume a negligible mixing in the following, which actually represents a conservative estimate to the sensitivity.

In such a setup, the Feynman diagrams for relevant processes are given in Fig. **??**. These processes include the final-state signatures of dimuon (+ photon), ditau (+ photon) as well as monophoton. Even though the process with initial photon radiation is of higher order compared to the trivial two-body scatterings, its impact is comparable and in some circumstances even larger than the two-body ones, due to the radiative return of resonant Z' production [143, 144].

The two-body scattering is very clean, as the final back-to-back dimuon or ditau carries all the energy delivered by the initial colliding muons. The only background of our concern should be the intrinsic SM processes, such as $\mu^+\mu^- \to \gamma/Z \to l^+l^-$ as well as t-channel exchanges. We will also benefit from the interference between the Z' and SM-mediated diagrams. For instance, the cross section for $\mu^+\mu^- \to \tau^+\tau^-$ is approximately $e^2g'^2/(4\pi s)$ for $s \gg M_{Z'}^2$ and $-e^2g'^2/(4\pi M_{Z'}^2)$ for $s \ll M_{Z'}^2$, which actually dominates over the Z'-only cross section $\propto g'^4$ when g' is small. The SM cross section approximately takes $\sim e^4/(8\pi s) \sim 10^4$ ab $(3\ \mathrm{TeV}/\sqrt{s})^2$. Hence we can readily estimate the excellent sensitivity to the gauge coupling even before the event generation:

$$g' < 3.4\times 10^{-2}\left(\frac{\sqrt{s}}{3\ \mathrm{TeV}}\right)^{\frac{1}{2}}\left(\frac{1\ \mathrm{ab}^{-1}}{L}\right)^{\frac{1}{4}}\max\left(1, \frac{M_{Z'}}{\sqrt{s}}\right). \tag{51}$$

To obtain the final sensitivity to the parameter space, we have to make a few assumptions to the particle identification and detection prospects. For the two-body scatterings, we assume the efficiency for dimuon identification to be 100% and that for ditau to be 70%, which is rather conservative. The

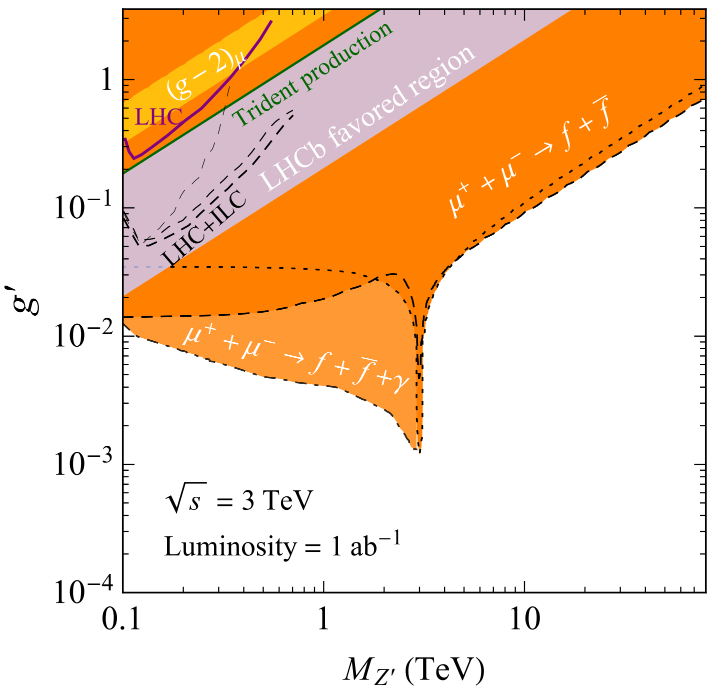

Fig. 24: The sensitivity of the MuC with the COM energy $\sqrt{s} = 3$ TeV and luminosity $L = 1$ ab^{-1}, given as orange regions. Other limits and projections are also shown for comparison. Our concerned parameter regions explaining the $(g-2)_\mu$ and B anomalies are given as yellow and blue bands, respectively. Figure from Ref. [141].

search of resonance for the radiative return process severely relies on the energy resolution of photon or equivalently dilepton. For photon, we adopt the energy resolution of the current CMS detector with $\mathrm{PbWO_4}$ crystals [145], and for dimuon we take $\Delta m_{\mu^+\mu^-} \simeq 5 \times 10^{-5}$ GeV$^{-1} \cdot s$ [146]. Moreover, a systematic uncertainty of 0.1% level is assumed.

The projected sensitivity is presented in Fig. 24. The limits using $\mu^+\mu^- \to \ell^+\ell^-$ (dashed and dotted curves for $\ell = \mu$ and τ, respectively) are given as the darker orange region, while the radiative return process yields the lighter orange region. Other limits and projections are also shown for comparison, such as $e^+e^- \to \mu^+\mu^- Z'$, $Z' \to \mu^+\mu^-$ from the BaBar experiment [147], the LHC searches [148, 149], the trident production in neutrino scattering experiments [95]. The parameter spaces which can explain the g-2 and B anomalies are shown as the yellow and blue bands, respectively. It is obvious that the parameter space of our concern with $M_{Z'} > 100$ GeV is entirely covered by the MuC setup $\sqrt{s} = 3$ TeV and $L = 1$ ab^{-1}.

9 Muon Yukawa Couplings

9.1 Modified muon-Higgs Coupling

The Higgs couplings to the second generation of SM fermions still remain to be measured precisely. Recently, the Higgs-charm coupling was observed to be $|\kappa_c| = \sqrt{2}|y_c|/m_c < 8.5$ at 95% confidence level by ATLAS [150]. In comparison, the Higgs-muon coupling can be measured more precisely due to the cleaner background of $H \to \mu^+\mu^-$. First evidence suggests its value to be of the order of magnitude predicted by the SM [151, 152], but $\mathcal{O}(100\%)$ deviations from the SM value are still possible. During the upcoming high-luminosity phase of the LHC, the muon Yukawa coupling can be pinned down to tens of percent, albeit in a model-dependent way [153].

A high-energy MuC with multi-TeV center-of-mass energy and high luminosity would allow to measure the Higgs-muon coupling in a model-independent way, directly probing the mass generation mechanism of the muon. Considering its general applicability, our proposal [154] can be extended to study related new-physics effects involving final states of charged leptons and jets.

The EFT parameterization

In the Higgs Effective Field Theory (HEFT), the physical Higgs singlet together with the triplet Goldstone bosons is introduced in a non-linear parameterization as

$$U = e^{i\phi^a \tau_a / v}, \text{ with } \phi^a \tau_a = \sqrt{2} \begin{pmatrix} \frac{\phi^0}{\sqrt{2}} & \phi^+ \\ \phi^- & -\frac{\phi^0}{\sqrt{2}} \end{pmatrix}. \tag{52}$$

The HEFT Lagrangian can describe a generic Yukawa sector as follows,

$$\mathcal{L}_{UH} \supset -\frac{v}{2\sqrt{2}} \left[\sum_{n \geq 0} y_n \left(\frac{H}{v} \right)^n (\bar{\nu}_L, \bar{\mu}_L)\, U\, (1 - \tau_3) \begin{pmatrix} \nu_R \\ \mu_R \end{pmatrix} + \text{ h.c.} \right]. \tag{53}$$

With these definitions, the muon mass and the prefactor of the Yukawa coupling are given by $m_\mu = y_0 v/\sqrt{2}$ and $\kappa_\mu = y_1 v/(\sqrt{2} m_\mu)$, respectively.

The case $y_1 = y_0 = y_\mu$ corresponds to the SM reference value, $\kappa_\mu = 1$. In a generic new-physics scenario, the relation between the coefficients y_0 and y_1 is unknown; it depends on the specific underlying dynamics. In the effective-theory description, new operators in the H/v expansion will appear as contact terms which directly couple the muon to Higgs or Goldstone bosons. By means of the Goldstone-Boson Equivalence Theorem (GBET), we can associate a modification of the muon-Higgs coupling y_μ with new contributions to multiple vector-boson production which generically can become large in the high-energy limit.

Alternatively, a new-physics contribution to the Yukawa interaction can be parameterized in terms of the Standard-Model Effective Field Theory (SMEFT) formalism. A generic Yukawa part of the Lagrangian takes the form

$$\mathcal{L}_\varphi \supset \left[-\bar{\mu}_L y_\mu \varphi \mu_R + \sum_{n=1}^{N} \frac{C_{\mu\varphi}^{(n)}}{\Lambda^{2n}} \left(\varphi^\dagger \varphi \right)^n \bar{\mu}_L \varphi \mu_R + \text{ h.c.} \right], \tag{54}$$

where

$$\varphi = \frac{1}{\sqrt{2}} \begin{pmatrix} \sqrt{2}\phi^+ \\ v + H + i\phi^0 \end{pmatrix}. \tag{55}$$

Higher-dimensional effective operators in the SMEFT Lagrangian ($n \geq 1$) result in modifications to the muon mass and the corresponding Yukawa coupling,

$$m_\mu = \frac{v}{\sqrt{2}} \left[y_\mu - \sum_{n=1}^{N} \frac{C_{\mu\varphi}^{(n)}}{\Lambda^{2n}} \frac{v^{2n}}{2^n} \right], \qquad \kappa_\mu = 1 - \frac{v}{\sqrt{2} m_\mu} \sum_{n=1}^{N} \frac{C_{\mu\varphi}^{(n)}}{\Lambda^{2n}} \frac{n v^{2n}}{2^{n-1}}, \tag{56}$$

respectively. In this approach, the SM reference value $\kappa_\mu = 1$ is reproduced if only a dimension-4 operator ($n = 0$) is present. Starting from dimension-6 operators, we receive new contributions to the muon-Higgs coupling. These are associated with contact terms involving Higgs or Goldstone bosons. They lead to an enhanced production of multi-boson final states in the high energy limit, in complete analogy with the HEFT formalism. Assuming a modification of the Yukawa coupling, we can translate an experimental bound on $\Delta\kappa_\mu$ to a new-physics scale Λ via (assuming $C_{\mu\varphi}^{(1)} \sim \mathcal{O}(1)$)

$$\Lambda \sim \sqrt{\frac{v^3}{\sqrt{2} m_\mu \Delta\kappa_\mu}}. \tag{57}$$

Multiple boson production

In the context of the above model-independent κ_μ parameterizations, in Ref. [154] we have extensively studied multi-boson production at high-energy MuC. We could demonstrate that at high collision energies, a modification of the Yukawa coupling can induce a significant enhancement of the multi-boson production rate that grows with energy. The effect becomes more striking for a final-state multiplicity of three or more bosons. It provides a unique opportunity to test the muon Yukawa coupling which is independent from the measurement via the Higgs decay to muons. Focusing on the examples of ZHH and WWH production, we have explored various relevant kinematic distributions in order to compute the achievable precision on the coupling and thus on the corresponding operator coefficients.

In this report, we extend the explicit coverage of multi-boson final states by presenting distributions of ZZH and ZZZ production, adopting a reference value of 10 TeV for the muon-collider c.m. energy. The inclusive boson angle θ_B, diboson distance R_{BB} and triboson invariant mass M_{3B} distributions are shown in Fig. 25, respectively. A few features stand out. First, we verify that for the annihilation process, the invariant mass M_{3B} sharply peaks at the collision energy $\sqrt{s}$, with a small spread as a consequence of the initial-state radiation (ISR). The vector-boson fusion contribution to the same three-boson final state mainly accumulates around the threshold. We can take advantage of this characteristic feature to filter the vector-boson funsion (VBF) background, by imposing an invariant mass cut such as $M > 0.8\sqrt{s}$, explicitly shown as the dashed lines in Fig. 25. Another feature that clearly discriminates the extreme cases of the SM $\kappa_\mu = 1$ vs. $\kappa_\mu = 0$ (*i.e.*, the BSM scenario with an order-one modification of the muon Yukawa coupling) is that $\kappa_\mu = 0$ enhances the annihilation to bosons mostly in the central region, while the SM produces a large fraction of the bosons in the forward region. With a reasonable acceptance cut $10^\circ < \theta_B < 170^\circ$ to require bosons to be detectable, we can further reduce the irreducible SM background. Finally, we have imposed a basic separation cut $R_{BB} > 0.4$, in order to resolve the final-state boson within a generic detector setup.

Assuming some deviation of multi-boson production from the SM background, we can estimate the sensitivity that follows from analyzing the tri-boson channels as $\mathcal{S} = S/\sqrt{B}$, where

$$S = N_{\kappa_\mu} - N_{\kappa_\mu=1},\ B = N_{\kappa_\mu=1} + N_{\text{VBF}}. \tag{58}$$

Regarding the energy dependence of this sensitity, the integrated luminosity is taken as quadratically scaling with energy, $\mathcal{L} = 10\ \text{ab}^{-1}(\sqrt{s}/10\ \text{TeV})^2$ [3]. We obtain the sensitivity contours that correspond to $\mathcal{S} = 2$ as shown in Fig. 26(a). We conclude that at a 3 TeV MuC, the muon Yukawa coupling can be probed by this method at the order of 100%. With an increased collision energy of 10 (30) TeV, this result can be improved to 10% (1%), respectively. Based on the translation in Eq.(57), the precision of this muon-Higgs coupling measurement can be translated into a Yukawa-sector new-physics scale of 10 (30) TeV to be probed at a 3 (10) TeV MuC, respectively.

9.2 Heavy Higgses through the Radiative Return Process

A unique feature of MuC is the possibility of generating s channel-resonant of Higgs boson [155–159]. However, when identifying the heavier additional (pseudoscalar) scalars, the lack of *a priori* knowledge of mass makes finding new particles very difficult. A wide range of new physics scenarios from supersymmetry (SUSY) to neutrino mass generative models, motivates an extended sector of basic scalars. Due to the weak couplings and sizable SM backgrounds, the LHC will have limited coverage for such search. At a future lepton collider is clean, and it would be straightforward to identify a heavy Higgs signal once produced on resonance [156].

The exact value of center-of-mass energy required for optimal detection of heavy Higgs depends on its unknown mass, particularly for the s-channel resonant production at a MuC. If we consider the associated production of a Higgs boson with other particles, the situation may improve. A compelling

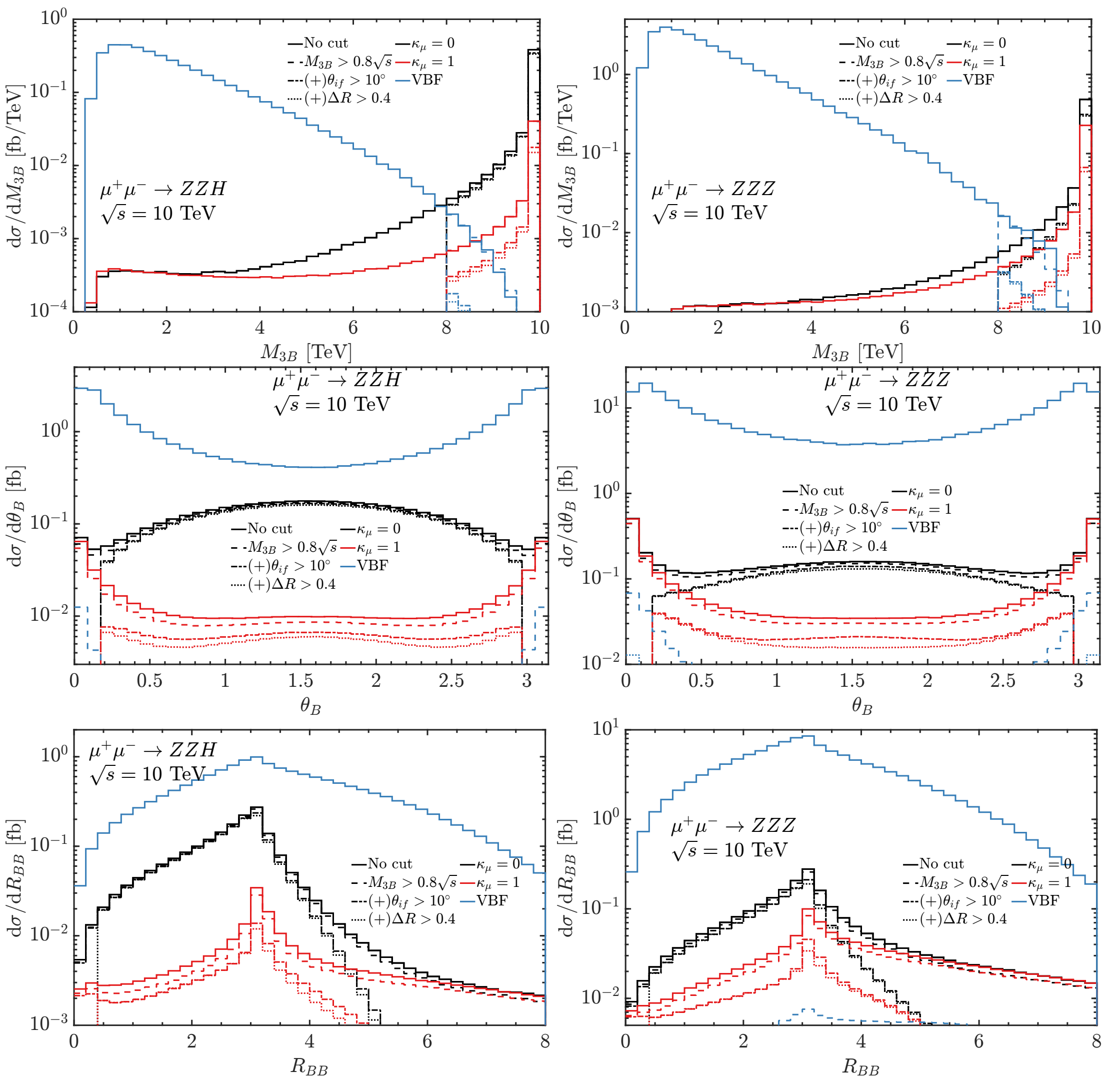

Fig. 25: The kinematic distributions $\theta_B, R_{BB}, M_{3B}(B = Z, H)$ of ZZH (left) and ZZZ (right) production at a $\sqrt{s} = 10$ TeV MuC.

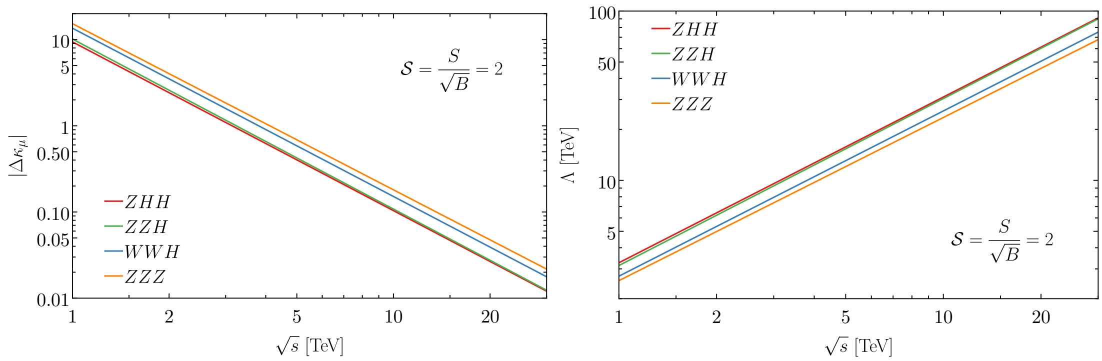

Fig. 26: (a) A high-energy MC's statistical sensitivity contour $\mathcal{S} = 2$ to probe the muon-Higgs coupling κ_μ based on the measurement of three-boson production. (b) The probe of new physics scale with the assumption in Eq. (57).

Table 6: Parametrization and their 2HDM models correspondence.

Coupling	$\kappa \equiv g/g_{\mathrm{SM}}$	Type-II & lepton-specific	Type-I & flipped
$g_{H\mu^+\mu^-}$	κ_μ	$\sin\alpha/\cos\beta$	$\cos\alpha/\sin\beta$
$g_{A\mu^+\mu^-}$	κ_μ	$\tan\beta$	$-\cot\beta$
g_{HZZ}	κ_Z	$\cos(\beta-\alpha)$	$\cos(\beta-\alpha)$
g_{HAZ}	$1-\kappa_Z^2$	$\sin(\beta-\alpha)$	$\sin(\beta-\alpha)$

process is the "radiative return" (RR) process,

$$\mu^+\mu^- \to \gamma H, \gamma A, \tag{59}$$

where H (A) is a neutral CP-even (CP-odd) Higgs state. When the center-of-mass energy of the MuC is above the heavy Higgs mass, the photon emission from the initial state enables an opportunity for the heavy Higgs boson to "back" to the resonance. In this case, we do not need to know the exact value of the (unknown) heavy scalar mass. We illustrate our main points in the context of two-Higgs-doublet models (2HDM) [160].

The relevant heavy Higgs boson couplings can be parametrized as

$$\mathcal{L}_{int} = -\kappa_\mu \frac{m_\mu}{v} H\bar{\mu}\mu + i\kappa_\mu \frac{m_\mu}{v} A\bar{\mu}\gamma_5\mu + \kappa_Z \frac{m_Z^2}{v} HZ^\mu Z_\mu + \frac{g\sqrt{(1-\kappa_Z^2)}}{2\cos\theta_W}(H\partial^\mu A - A\partial^\mu H)Z_\mu. \tag{60}$$

The two parameters κ_μ and κ_Z characterize the coupling strength relative to the SM Higgs boson couplings. The coupling κ_μ controls the heavy Higgs resonant production and the radiative return cross-sections. κ_Z controls the cross-sections for ZH associated production and heavy Higgs pair HA production. We use κ_μ as the common rescale parameter for the Yukawa couplings for both the CP-even H and the CP-odd A. Although, in principle, these couplings could be different. For the HAZ coupling we use the generic 2HDM relation: κ_Z is proportional to $\cos(\beta-\alpha)$ and the HAZ coupling is proportional to $\sin(\beta-\alpha)$. In the decoupling limit of 2HDM at large m_A, $\kappa_Z \equiv \cos(\beta-\alpha) \sim m_Z^2/m_A^2$ is highly suppressed and $\kappa_\mu \approx \tan\beta$ $(-\cot\beta)$ in Type-II and lepton-specific (Type-I and flipped) 2HDM. We show our choices of parameters and their 2HDM correspondences in Table. 6.

When kinematically allowed, the photon emission from the initial state enables an opportunity for the heavy Higgs boson "back" to resonance. The signature is quite striking: a monochromatic photon. The "recoil mass" would be a sharp resonant peak at $m_{H/A}$, standing out of the continuous background. The reconstruction of the heavy Higgs boson from its decay product provides an extra handle.

The characteristic of this RR signal is a photon with the energy given by

$$E_\gamma = \frac{\hat{s} - m_{H/A}^2}{2\sqrt{\hat{s}}}, \tag{61}$$

from which a recoil mass peaked at the heavy Higgs mass $m_{H/A}$ can be reconstructed. The energy of this photon is broadened by detector photon energy resolution, beam energy spread, additional (soft) ISR/FSR, and heavy Higgs width. The beam energy spread and additional soft ISR/FSR are GeV level [161]. When the Higgs boson is significantly below the beam energy, the recoil mass construction receives considerable smearing dominated by the photon energy resolution.

Besides the mass, the other most important parameter is its total width, which effectively smears the monochromatic photons. In Type-II 2HDM, $\kappa_\mu = \tan\beta$ in the decoupling limit. The total width is minimized when $\tan\beta = \sqrt{m_t/m_b}$ but typically O(GeV) to O(100 GeV).

The inclusive cross-section for the mono-photon background is substantial compared to the radiative return signal. The background is mainly from the Mṙoller scattering with ISR/FSR $\mu^+\mu^- \to$

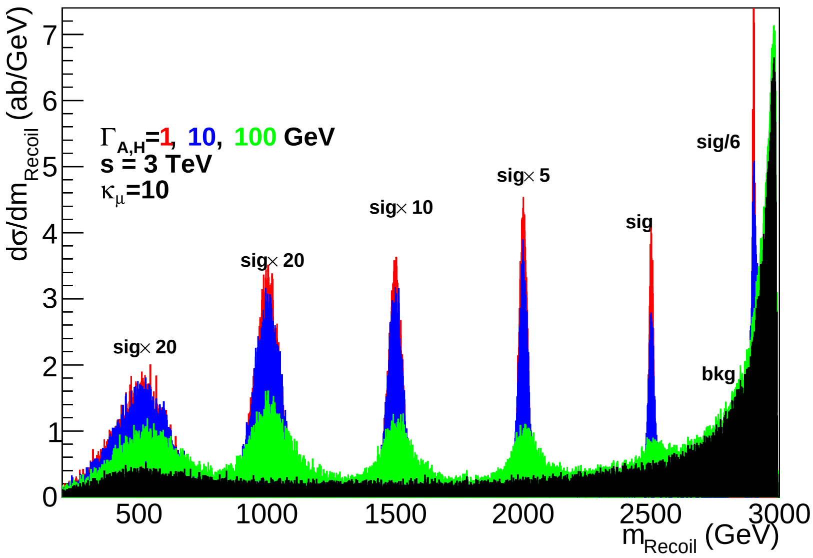

Fig. 27: Recoil mass distribution for heavy Higgs mass of 0.5, 1, 1.5, 2, 2.5, 2.9 TeV with a total width 1 (red), 10 (blue), and 100 (green) GeV at a 3 TeV MuC. ISR and FSR are included in this calculation. Background (black shaded region) includes all events with a photon of $p_T > 10$ GeV. Note that signal and background have different re-scale factors for clarity. This figure is obtained from [143] and more detailed discussion can be found there.

$\mu^+\mu^-\gamma$, and the W exchange with ISR $\mu^+\mu^- \to \nu\nu\gamma$. The signal background ratio is typically the order 10^{-3} for a 3 TeV MuC. Consequently, to discover through RR, we rely on some exclusive processes.

We adopt the Type-II 2HDM for concrete illustration and choose the $b\bar{b}$ final state as a benchmark with the decaying branching fraction be 80%. We also assume 80% b-tagging efficiency and require at least one b-jet tagged.

We use Madgraph5 [162] for parton level signal and background simulations and then Pythia [163] for ISR and FSR. We further implement detector smearing and beam energy spread. We show the recoil mass distribution at a 3 TeV MuC in Fig. 27. Both cross-sections of the signal and the background at fixed beam energy increase as the recoil mass increase from the photon emission. We can see clearly the pronounced mass peaks look and the RR process is an essential discovery production mechanism.

It is informative to put the reach of the two theory parameters side-by-side via the RR and pair production, as in Fig. 28. The shaded regions represent when the RR process dominants over the ZH associated production and HA pair production. The RR production mode covers a large region of κ_μ ($\tan\beta$ in Type II 2HDM). The closer the Higgs mass to the MuC energy threshold, the more critical the RR channel is than the ZH channel. Well below the threshold, these two processes scale the same way as $1/s$. The RR process is only dependent on κ_μ, while both ZH associated production and HA pair production mainly depend on κ_Z. The nearly flat region in the figure for 1.4 TeV heavy Higgs represents the good sensitivity from heavy Higgs pair production. The RR process is the leading channel for a heavy Higgs boson near the energy threshold and the decoupling regime of general Higgs extensions.

The currently observed SM-like Higgs boson tightly constrains the κ_Z region. The allowed parameter regions for 2HDM with current LHC data (solid) and projection are also shown in the figure for comparison. This illustrates that the RR processes are favored in all allowed 2HDM models.

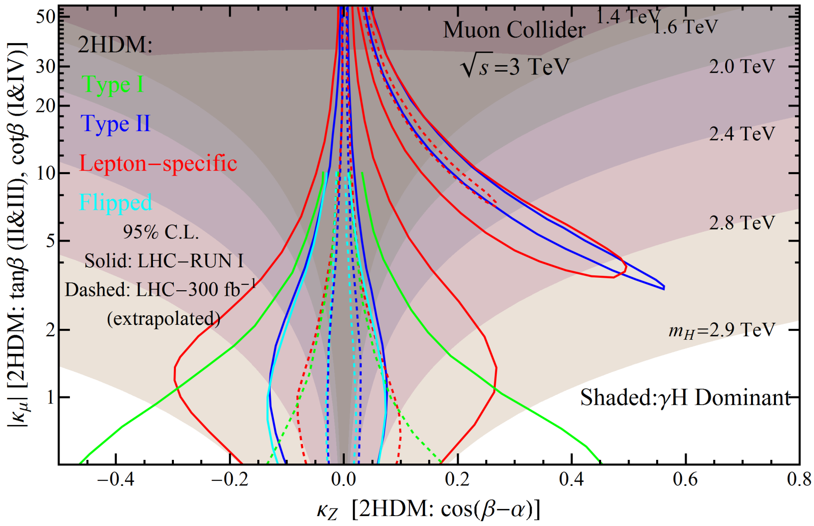

Fig. 28: Comparison of sensitivities between different production mechanisms in the parameter plane κ_μ-κ_Z for different masses of the heavy Higgs boson at the 3 TeV MuC. The shaded regions show a higher direct signal rate from the RR process than the ZH associated production and HA pair production channels. We also show the allowed parameter regions (extracted from Ref. [164]). This figure is obtained from [143] and more detailed discussion can be found there.

In summary, we studied the signature and sensitivity of heavy Higgs boson signals from three production modes at a high-energy MuC. More detailed discussions can be found in Ref. [143]. Compared to the s-channel resonance at $\sqrt{s} = m_h$, these different production mechanisms do not rely on *a priori* knowledge of the heavy Higgs mass. We find that radiative return is of particular interest, avoiding the scan process. A monochromatic photon characterizes this signal (γH). We show the coupling-mass parameter space κ_μ-m (SUSY equivalent of $\tan\beta - M_A$) covered by such search through RR process at a high energy MuC can substantially extend over the LHC projections. Compared with other modes of ZH and HA production at a lepton collider, the RR process is advantageous, especially for the decoupling regions in all 2HDM-like models. The RR process could undoubtedly provide us an attractive option compared to the traditional scanning procedure for heavy Higgs boson at a high energy MuC, enabling heavy Higgs discovery opportunities.

10 Dark Sectors

Dark particles can couple to SM states by means of effective higher dimensional operators, which are dominated by those of dimension five. These operators appear for instance in dark photon (DP) coupling to SM fermions via magnetic dipole interactions, as predicted by portal dark-sector models [165], or axion-like particles (ALP) to di-photon couplings, as a consequence of the $U(1)$ Peccei-Quinn anomaly.

On dimensional grounds, the leading production cross section of a dark particle in association with a photon at high energy tends to a constant proportional to $1/\Lambda^2$, with Λ the effective scale associated to the dimension five operators. This behavior must be compared to that of the cross section for dark particles production by renormalizable couplings to SM particles, the cross section of which is expected to decrease as $\sigma \sim 1/s$ at high center of mass (CM) energy $\sqrt{s}$. In addition, the corresponding cross section for the SM background, characterized by a photon plus a neutrino pair, scales as $1/s$ at high energy which leads to the enhanced ratio of signal over background at high energy for dark-particle productions in association to a photon. These features make a MuC with both high energy and high luminosity a very promising machine for the study of the dark sector [166].

We focus here on the annihilation of a muon pair into a light dark particle X and a photon γ [167]

$$\mu^+ \mu^- \to \gamma X \,, \tag{62}$$

the dark-sector particle behaving as missing energy inside the detector. As the dark particle is invisible and assumed to be light, the events shows up as a mono-chromatic single photons with almost half of the center-of-mass energy.

Experimental searches for the same mono-photon signature have been performed at the LEP [168–170], the Tevatron [171, 172] and the LHC [173, 174] though only providing rather weak bounds on their couplings to SM particles. We will show that a MuC with CM energy of 3 and 10 TeV offers a large potential to increase the sensitivity to this signal with respect to the aforementioned colliders.

Dark particles

We consider two possible candidates for the invisible state in the single photon signature: a massless, spin 1 particle (the DP) and a light pseudo-scalar particle (an ALP).

The DP A'_μ with field strength $F'^{\mu\nu}$ can couple to the muons via the magnetic-dipole interaction

$$\mathcal{L}_{\rm DP}^{\rm dipole} = \frac{1}{2\,\Lambda}\,(\bar{\mu}\,\sigma_{\mu\nu}\,\mu)\,F'^{\mu\nu}\,, \tag{63}$$

where $\sigma_{\mu\nu}$ is defined to be $i[\gamma^\mu, \gamma^\nu]/2$. The scale Λ modulates the strength of the interaction. In a UV completion of the theory this effective scale can be generated at one-loop by the exchange of heavy particles in the portal sector [165, 175]. The coupling in (63) is the only one in the case of a massless dark photon. On the other hand, in the case of a massive dark photon, in addition to the Pauli dipole term, an ordinary coupling to the vectorial muon current is also possible $\mathcal{L}_{\rm DP}^{\rm tree} = \varepsilon e(\bar{\mu}\,\gamma^\mu\,\mu)A'_\mu$, arising from a tree-level contribution of kinetic mixing of dark-photon with ordinary photon [176], that in the massive case cannot be rotated away. This Pauli operator has not been constrained by current massive DP searches because they have been performed at low-energies, where its effect is strongly suppressed. Therefore, we assume here, the interaction in (63) be the dominant mechanism also in production of a massive dark-photon at MuC.

The ALP a couples to the muons by means of the portal operator $\mathcal{L}_{\rm ALP}^{\rm muon} = (\bar{\mu}\,\gamma_5\gamma^\mu\,\mu)\,\partial_\mu a/\Lambda$ and to photons by means of

$$\mathcal{L}_{\rm ALP}^{\rm photon} = \frac{1}{\Lambda}\,a\,F^{\mu\nu}\widetilde{F}_{\alpha\beta}\,, \tag{64}$$

where $\widetilde{F}_{\alpha\beta} = 1/2\epsilon_{\alpha\beta\mu\nu}F^{\mu\nu}$ is the dual field strength of the photon, with $\epsilon_{\alpha\beta\mu\nu}$ the Levi-Civita antisymmetric tensor satisfying $\epsilon_{0123} = 1$. The scale Λ controls the strength of the interactions. However, in the high-energy regime the interaction with the muon axial current is chirally suppressed by terms proportional to the muon mass over energy [177] and so we retain only the interaction in (64) that significantly contributes to the cross section. Being (63) and (64) effective interactions, the Λ scale is assumed to be larger or at most of the same order as the CM energy.

Constraints

The SM process $\mu^+\mu^- \to \gamma\nu\bar{\nu}$ gives rise to the same signature as the signal and it provides the main source of background. The SM cross section grows with the CM energy but the number of events with a high-energy photon decreases [182, 183]. However, background events at the end of the photon energy spectrum around $E_\gamma = \sqrt{s}(1 - m_Z^2/s)/2$ are enhanced by the radiative return of the Z-boson pole. This feature reduces the sensitivity to the signal that—it being a two-body process—is centered in the same range of energies (for $s \gg m_Z^2$). Therefore a suitable statistical analysis is necessary in order to distinguish the signal from this background.

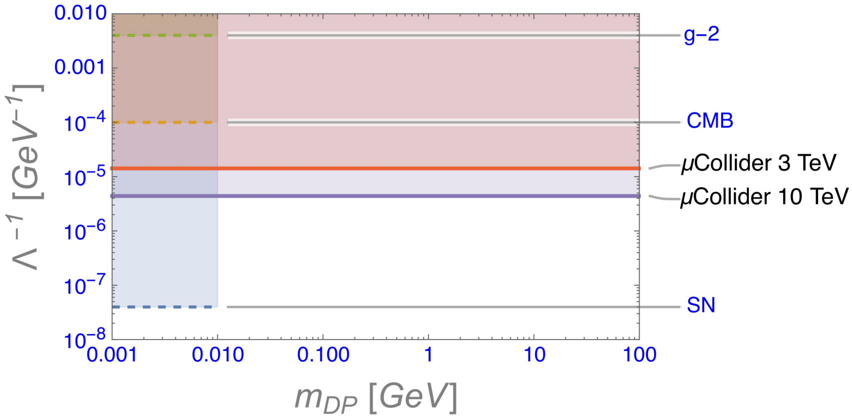

Fig. 29: Limits on $1/\Lambda$ scale for the dark-photon as a function of the dark-photon mass m_{DP}: for SN the scale of the coupling to muons has been set at $10^{7.4}$ GeV [178] by the effect of dark radiation on Supernovae dynamics. For CMB see [179]. For $g-2$ see [180, 181]. Comparable bounds hold for the ALP to muons because of the similar structure of the interaction vertex. For masses up to 100 GeV the μCollider limits are for all practical purposes mass independent.

Table 7: Explorable values of the effective energy scale Λ for DP and ALP (95% CL) for the two benchmark scenarios of the future MuC under consideration.

	DP		**ALP**	
Energy	3 TeV	10 TeV	3 TeV	10 TeV
Exclusion	141 TeV	459 TeV	112 TeV	375 TeV
Discovery	92 TeV	303 TeV	71 TeV	238 TeV

In our analysis [167], we consider two benchmark collider scenarios, namely with CM energy of 3 TeV and 10 TeV with total integrated luminosity of 1 ab^{-1} and 10 ab^{-1} respectively. Then, we study the generation of events with a single, monochromatic photon plus missing energy in the final states. The events for the signal and the background are generated by means of MADGRAPH5 [162]. A 10-GeV cut on the photon generated transverse momentum is imposed to remove most of the soft radiation. The output of MADGRAPH5 is automatically fed into PYTHIA [163] and the events thus generated are processed by the detector simulation. The full-simulated events are reconstructed with a particle-flow algorithm [184], which is integrated in the ILCSoft reconstruction software. A suitable choice of cuts on the photon energy and polar angle, to suppress the large background induced by the radiative return effect, has been implemented to increase signal over background sensitivity [167]. Results for the limits (95% CL) and discovery (5σ) for the largest Λ reachable are reported in Table I.

Finally, in Figs.29 and 30 the bounds for $1/\Lambda$ and the $g_{a\gamma}$ couplings respectively, are compared with current and future limits from low-energy, cosmological, astrophysical and collider physics, where the following notation is adopted for the coupling $g_{a\gamma} \equiv 4/\Lambda$ associated to the dipole operator in (63), in order to compare it with the common notation used in the various experiments.

When and if a signal is found, it will be important to know which dark sector particle is responsible for it. In [167] we show that a MuC operating at 3 or 10 TeV has the potential to distinguish the spin-0 ALP from the spin-1 DP scenario. For a common energy scale $\Lambda = 300$ TeV—about 200 events (which

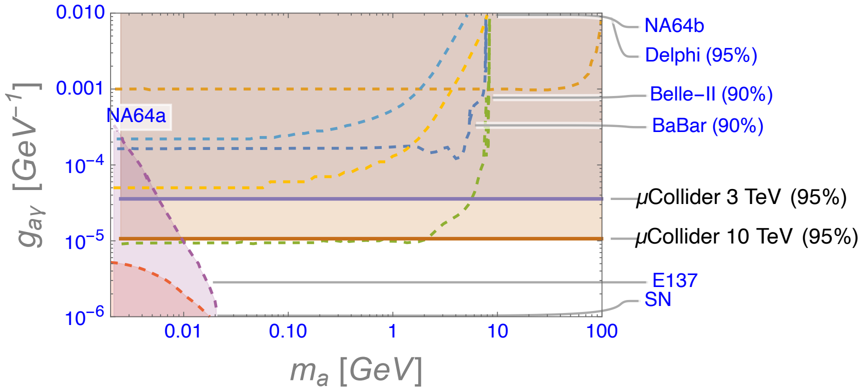

Fig. 30: Limits on $g_{a\gamma} = 4/\Lambda$ as a function of the ALP mass m_a: NA64a [185], Delphi [186] and BaBar [187] are actual limits. Belle-II [188, 189], NA64b [185] and μCollider [167] are future estimates. The limit indicated by E137 is the one from [190] as modified for a small (10^{-4}) visible branching fraction [177]. For masses up to 100 GeV the μCollider limits are for all practical purposes mass independent.

1404 can be accumulated in order five years) are required to separate the two spin scenarios at the 95% CL.

1405

11 Key findings

Higgs Physics

Higgs physics at high-energy muon colliders benefits mainly from the growth with the energy of the rates in vector-boson-fusion processes to close a comprehensive programe of measurements covering both single and multi-Higgs observables. With 1 ab^{-1} of collected luminosity, precision measurements of the single Higgs couplings at 3 TeV would significantly improve in many cases the percent-level knowledge gained from the HLLHC, and hence our sensitivity to the large class of BSM scenarios that predict modifications of the Higgs properties. Reaching a permille level precision in the couplings to WW^*, ZZ^* and $b\bar{b}$ would be possible by operating with even higher energies and luminosities, at 10 TeV with 10 ab^{-1}. It is still open for clarification, though, what would be the true potential of these high-energy muon colliders to measure certain Higgs couplings. This is the case of, for instance, the Top Yukawa, which could be accessible via measurements not only of $\mu^+\mu^- \to t\bar{t}h$ but, with higher rates, also via $VV \to t\bar{t}$ or, at 10 TeV, $VV \to t\bar{t}h$.

High energy muon colliders also open the stage for clean measurements of the Higgs trilinear, λ_3, and even the potential observation of processes sensitive to the quartic self-interaction. In what regards the 3 TeV option, we find that the precision in the determination of λ_3 would benefit substantially from an increase in the total luminosity by a factor$\sim$ 2 with respect to the proposed benchmark of 0.9 ab^{-1}, allowing a determination at the 15% level. Percent level uncertainties could be reached though by running at higher centre-of-mass energies $\sqrt{s} > 10$ TeV, and thus comparable or even beyond what would be possible at a 100 TeV pp machine.

We also covered in this report the capabilities of a low energy muon collider option operating at the Higgs pole, $\sqrt{s} = 125$ GeV. While this offers the possibility of obtaining a model independent determination of the Higgs width at the percent level, which is not possible at higher energies, and a subpercent determination of the muon Yukawa coupling, high luminosities ~ 20 fb^{-1} are required to achieve a precision in the determination of other Higgs couplings comparable to the Higgs factories proposed in the literature. While a measurement of Γ_H is important on its own, and this helps to resolve a very particular flat direction in the Higgs coupling analysis, the significance of this region of the parameter space from the point of view of learning from specific BSM scenarios is to be determined. It should also be noted that, while a model-independent determination of the Higgs width is not possible at the high-energy muon collider, this absence could be solved when combined with the informations that will be available from future e^+e^- Higgs factories.

Effective Field Theories

The overall reach in terms of constraining indirect effects of new physics at high-energy muon colliders goes beyond the exploration of effects in Higgs processes. A global assesment of the physics potential for indirect constraints at a high-energy muon collider was performed here within the framework of the dimension-six SMEFT. In the language of effective field fheories, one of the advantages of operating at Multi-TeV centre-of-mass energies is the augmented sensitivity to operators whose contributions relative to the SM to electroweak processes grow with the energy $\sim E_{\text{cm}}^2/\Lambda^2$. This is the case of, for instance, contributions in 2 to 2 fermion processes from four-fermion operators, which could be generated at low energies by a variety of heavy new particles. Such enhancement on the virtual effects of new resonances allow to set stringent bounds on their properties, even if experimental precision is limited, e.g. testing $\Lambda \sim 100$ TeV for percent-level precions measurements at $\sqrt{s} = 10$ TeV. Although the set of projections for measurements interpreted in the EFT framework at a high-energy muon collider is still limited, preventing a full exploration of the EFT parameter space, the results discussed here, which combine information from Higgs, difermion and diboson measurements, clearly indicate the potential for massive gains in terms of sensitivity to new BSM interactions with respect to the HLLHC, especially for those inducing the above-mentioned growing-with-energy effects. In particular, sensitivities to new physics interaction scales up to $\Lambda/\sqrt{c} \sim 30$ (100) TeV would be possible at $\sqrt{s}$ =3 (10) TeV.

The improvement in sensitivity with respect to the HLLHC is even more clear when interpreting the EFT results in terms of indirect constraints on specific scenarios, e.g. composite Higgs models, where a $\sqrt{s}$ =3 (10) TeV muon collider could test values of the typical mass of the composite sector, $m_\star$, in the range of $\sim$ 20-35 (50-90) TeV, depending on the value of the typical coupling $g_\star \in [1, 4\pi]$. For comparison, the corresponding HLLHC limits would reach the lower bound of the 3 TeV muon collider results. Similar conclusions can be derived for other SM extensions, as we saw for new heavy vector resonances where, for the simple case of a heavy replica of the $U(1)_Y$ vector boson, the HLLHC mass reach of $\sim$ 20 TeV could be extended up to few 100 TeV, for order one new physics couplings.

BSM - New Scalars

On top of the above mentioned investigations on the nature of the Higgs boson and the characterization of the 125 GeV symmetry breaking scalar of the SM, a very intriguing possibility of having multiple Higgs bosons can be explored at the 3 TeV muon collider. The 3 TeV muon collider generically has sensitivity to discover new Higgs bosons up to half of the center of mass energy when they can be produced in pairs via gauge interactions, e.g. for the pair production of charged Higgs bosons. For singly produced Higgs bosons, the reach in mass depends on the strength of the coupling that mediate the single production. In the simple examples of extended Higgs sectors featuring new singlet scalars coupled to the SM only via mixing with the Higgs boson, the 3 TeV muon collider is sensitive to new Higgs bosons up to around 2 TeV. This mass reach significantly extends that of the HL-LHC and complements the sensitivity from indirect probes such as Higgs couplings measurement. The 3 TeV muon collider, as it simultaneously operates as a Higgs factory at the intensity frontier and a exploration machine at the energy frontier, can provide multiple probes of new physics in the Higgs sector.

For particular interpretation of the searches of extra Higgs bosons, one can better quantify the impact of the 3 TeV muon collider. Major results are expected, leading to very significant progress about fundamental open issues of the SM. For instance the measurements of Higgs couplings and the direct search for new bosons can put very stringent bounds on models that modify the strength of the electroweak phase transition and essentially rule out scalars as possible agents of modification of the Higgs boson potential. In this particular class of models, a 3 TeV muon collider could have a nice interplay with gravity waves observations expected from the electroweak phase transition. The possibility that space-born gravity waves observatories will come online during the late 2030s marries nicely with the timeline of the 3 TeV muon collider as initial stage of a high energy exploration based on muon beams.

In addition, the thorough exploration of trans-TeV masses for new scalars is a significant step in the understanding of role of the Higgs boson in shaping fundamental interactions. For instance the role of the Higgs as symmetry breaking scalar can be further clarified by finding, or not finding, a new scalar in the TeV mass range. A discovery enabled by the 3 TeV muon collider would open up a vista on a whole new sector made of spin-0 particles. Such a finding would call for a deeper understanding of the origin of spin-0 particles and their possible point-like nature. Not finding a new scalar in the TeV mass range would stress even further the already peculiar role played by the Higgs boson in the SM, making each and every of its properties a key element to determine the scale of weak interactions, hence a test of our understanding of microscopic theories of its origin. In both cases the results from the 3 TeV muon collider will radically improve our understanding of weak interactions and symmetry breaking.

BSM - Dark Matter

A high energy muon collider has a great potential to probe dark matter particles, in particular weakly charged ones. The interesting mass range for this type of dark matter covers a rather large span from fractions of TeV up to fractions of PeV. The lighter dark matter candidates can be embedded in more ambitious BSM scenarios such as perturbative supersymmetric extensions of the SM in principle valid up to the ultimate short-scale. The heavier candidates, roughly above O(10) TeV, are typical of BSM constructions that feature non-perturbative regimes at some short distance above the weak scale. A 3 TeV muon collider has a potential to probe, and potentially discover, dark matter candidates around the TeV scale employing three different search modes: i) the direct search for signatures such as the stub-track of the higgsino dark matter candidate; ii) the direct and very general search for dark matter production in association with SM states, e.g. electroweak vector bosons; iii) the indirect search for precision effects beyond the SM from loops of weakly charged dark matter. Exclusions for the higgsino dark matter can be attained at the 3 TeV muon collider with 1 ab^{-1} from direct searches and corroborating evidence can be accumulated from other direct search channels and indirect precision effects. A discovery of this kind would hard to mistake as there are several sensitive probes measurable at the same time at the 3 TeV muon collider. A machine running around 3.5 TeV would have an even more impressive chance to discover this dark matter candidate, filling a gap in the reach of direct dark matter detection experiment based on ultra-low background underground experiments.

The long list of weakly charged dark matter candidates can be probed at higher energy muon colliders, with few candidates already in the reach of the 3 TeV machine. Increasing the energy and luminosity of upgrades of the first stage of the muon collider one can establish a systematic path to cover the entire list up of weakly charged dark matter candidates.

Very importantly for the livelihood of the field, the timeline for the realization of a high energy muon collider can interleave nicely with both direct and indirect searches of astrophysical dark matter. These experiments are expected to probe new ground in data-taking expected in the 2030s. After these new runs, there might be first claims for the observation of TeV scale dark matter, thus calling for action already during the next decade. A high energy muon collider would have a unique opportunity to clarify the veracity of these claims in a timely and accurate manner.

Conclusions - Muon-Specific Opportunities

Muon colliders have a clear advantage over any other collider when it comes to searches for new physics that interacts more with muons than with first-generation particles. Hints of the existence of this muon-philic new physics can be found in experimental anomalies like the muon g-2 and the B-meson decay anomalies, or in the Yukawa interactions of the Higgs. We have shown that a muon collider program starting at 3 TeV and scalating up to higher energies can establish a no-lose theorem for discovering the new physics responsible for the g-2 anomaly. A 3 TeV muon collider can discover all beyond the Standard Model scenarios in which g-2 is generated by singlet bosons with masses above $\sim$GeV (lighter singlets will be discovered by upcoming low-energy experiments). If new states with electroweak quantum numbers contribute to g-2 more powerful colliders are required. If this new physics is too heavy to be directly produced, a 30 TeV muon collider is guaranteed to find deviations in higgs+gamma production due to the same physics responsible to g-2. This strongly motivates the construction of high energy muon colliders with energies $\sim$1-10 TeV. Regardless of what each of these colliders find, each will make invaluable contributions to allow us to understand the precise nature of the new physics behind g-2 (in some cases by directly producing new states and in some others by indirect signals in e.g. multi-higgs or higgs+X production). Therefore, this truly is a no-lose theorem for the discovery of new physics, the greatest imaginable motivation for a heroic undertaking like the construction of a revolutionary new type of particle collider.

If the new physics responsible for the B meson anomalies is due to *only* the specific four-fermion operators that are used to fit the data (the *nightmare scenario*), then a 3 TeV muon collider can probe a significant portion of the parameter space, whereas a 8 TeV collider would be necessary to entirely probe this scenario. Specific models aimed to address these anomalies generate a series of processes beyond those from the contact interactions of the nightmare scenario. For this reason these models are more *discoverable* than the nightmare scenario and a muon collider with multi-TeV energies can probe them. Finally, if one parametrizes muon portal new physics with higher dimensional operators that generate lepton flavor violating interactions, modified muon-higgs yukawas, and muon-dark portal particles interactions, then muon colliders with enegies between 3-10 TeV can probe new physics scales between 10-1000 TeV. This is in some cases comparable with the reach of searches for lepton flavor violation processes at flavor factories; some of the measurements that are sensitive to the highest new physics scales in high energy physics.

Acknowledgements

[82,191] We would like to thank the LHC experimental Collaborations and the WLCG for their essential support. We are especially grateful for the efforts by the computing, generator and validation groups who were instrumental for the creation of large simulation samples. We thank the detector upgrade groups as well as the physics and performance groups for their input. Not least, we thank the many colleagues who have provided useful comments on the analyses.

References

[1] *The international muon collider collaboration*, https://muoncollider.web.cern.ch.

[2] N. Surname, *Muon colldiers physics summary*, (2022) , arXiv:2202.yyyy [hep-ph].

[3] J. P. Delahaye, M. Diemoz, K. Long, B. Mansoulié, N. Pastrone, L. Rivkin, D. Schulte, A. Skrinsky, and A. Wulzer, *Muon Colliders*, arXiv:1901.06150 [physics.acc-ph].

[4] H. Al Ali et al., *The Muon Smasher's Guide*, arXiv:2103.14043 [hep-ph].

[5] A. Costantini, F. De Lillo, F. Maltoni, L. Mantani, O. Mattelaer, R. Ruiz, and X. Zhao, *Vector boson fusion at multi-TeV muon colliders*, JHEP **09** (2020) 080, arXiv:2005.10289 [hep-ph].

[6] D. Buttazzo, R. Franceschini, and A. Wulzer, *Two Paths Towards Precision at a Very High Energy Lepton Collider*, arXiv:2012.11555 [hep-ph].

[7] D. Buttazzo, D. Redigolo, F. Sala, and A. Tesi, *Fusing Vectors into Scalars at High Energy Lepton Colliders*, ArXiv e-prints (July, 2018) , arXiv:1807.04743 [hep-ph].

[8] W. Liu and K.-P. Xie, *Probing electroweak phase transition with multi-TeV muon colliders and gravitational waves*, arXiv:2101.10469 [hep-ph].

[9] M. Ruhdorfer, E. Salvioni, and A. Weiler, *A Global View of the Off-Shell Higgs Portal*, arXiv e-prints (Oct., 2019) , arXiv:1910.04170 [hep-ph].

[10] T. Han, S. Li, S. Su, W. Su, and Y. Wu, *Heavy Higgs Bosons in 2HDM at a Muon Collider*, arXiv:2102.08386 [hep-ph].

[11] S. Bottaro, D. Buttazzo, M. Costa, R. Franceschini, P. Panci, D. Redigolo, and L. Vittorio, *Closing the window on WIMP Dark Matter*, Eur. Phys. J. C **82** (2022) no. 1, 31, arXiv:2107.09688 [hep-ph].

[12] T. Han, Z. Liu, L.-T. Wang, and X. Wang, *WIMPs at High Energy Muon Colliders*, Phys. Rev. D **103** (2021) no. 7, 075004, arXiv:2009.11287 [hep-ph].

[13] L. Di Luzio, R. Gröber, and G. Panico, *Probing new electroweak states via precision measurements at the LHC and future colliders*, JHEP **01** (2019) 011, arXiv:1810.10993 [hep-ph].

[14] R. Capdevilla, F. Meloni, R. Simoniello, and J. Zurita, *Hunting wino and higgsino dark matter at the muon collider with disappearing tracks*, JHEP **06** (2021) 133, arXiv:2102.11292 [hep-ph].

[15] CLICdp, CLIC Collaboration, T. K. Charles et al., *The Compact Linear Collider (CLIC) - 2018 Summary Report*, arXiv:1812.06018 [physics.acc-ph].

[16] V. D. Barger, M. S. Berger, J. F. Gunion, and T. Han, *s channel Higgs boson production at a muon muon collider*, Phys. Rev. Lett. **75** (1995) 1462–1465, arXiv:hep-ph/9504330.

[17] V. D. Barger, M. S. Berger, J. F. Gunion, and T. Han, *Higgs Boson physics in the s channel at* $\mu^+\mu^-$ *colliders*, Phys. Rept. **286** (1997) 1–51, arXiv:hep-ph/9602415.

[18] J. de Blas et al., *The CLIC Potential for New Physics*, arXiv:1812.02093 [hep-ph].

[19] J. de Blas et al., *Higgs Boson Studies at Future Particle Colliders*, JHEP **01** (2020) 139, arXiv:1905.03764 [hep-ph].

[20] R. K. Ellis et al., *Physics Briefing Book: Input for the European Strategy for Particle Physics Update 2020*, arXiv:1910.11775 [hep-ex].

[21] N. Surname, *Simulated Detector Performance at the Muon Collider*, (2022) , arXiv:2202.yyyy [hep-ph].

[22] N. Surname, *Promising Technologies and R&D Directions for the Future Muon Collider*, (2022) , arXiv:2202.yyyy [hep-ph].

[23] N. V. Mokhov and S. I. Striganov, *Detector Background at Muon Colliders*, Phys. Procedia **37** (2012) 2015–2022, arXiv:1204.6721 [physics.ins-det].

[24] M. Forslund and P. Meade, *In preparation*, arXiv:22xx.xxx [hep-ph].

[25] T. Han, D. Liu, I. Low, and X. Wang, *Electroweak couplings of the Higgs boson at a multi-TeV muon collider*, Phys. Rev. D **103** (2021) no. 1, 013002, arXiv:2008.12204 [hep-ph].

[26] FCC Collaboration, A. Abada et al., *FCC Physics Opportunities: Future Circular Collider Conceptual Design Report Volume 1*, Eur. Phys. J. C **79** (2019) no. 6, 474.

[27] M. Chiesa, F. Maltoni, L. Mantani, B. Mele, F. Piccinini, and X. Zhao, *Measuring the quartic Higgs self-coupling at a multi-TeV muon collider*, JHEP **09** (2020) 098, arXiv:2003.13628 [hep-ph].

[28] J. de Blas, J. Gu, and Z. Liu, *In preparation*, arXiv:2203.xxx [hep-ph].

[29] J. de Blas et al., *HEPfit: a code for the combination of indirect and direct constraints on high energy physics models*, Eur. Phys. J. C **80** (2020) no. 5, 456, arXiv:1910.14012 [hep-ph].

[30] M. Cepeda et al., *Report from Working Group 2: Higgs Physics at the HL-LHC and HE-LHC*, CERN Yellow Rep. Monogr. **7** (2019) 221–584, arXiv:1902.00134 [hep-ph].

[31] M. Farina, G. Panico, D. Pappadopulo, J. T. Ruderman, R. Torre, and A. Wulzer, *Energy helps accuracy: electroweak precision tests at hadron colliders*, Phys. Lett. B **772** (2017) 210–215, arXiv:1609.08157 [hep-ph].

[32] R. Franceschini, G. Panico, A. Pomarol, F. Riva, and A. Wulzer, *Electroweak Precision Tests in High-Energy Diboson Processes*, JHEP **02** (2018) 111, arXiv:1712.01310 [hep-ph].

[33] S. Chen, A. Gliotti, R. Rattazzi, L. Ricci, and A. Wulzer, *In preparation*, arXiv:2203.xxx [hep-ph].

[34] G. Branco, P. Ferreira, L. Lavoura, M. Rebelo, M. Sher, et al., *Theory and phenomenology of two-Higgs-doublet models*, Phys.Rept. **516** (2012) 1–102, arXiv:1106.0034 [hep-ph].

[35] N. Craig, J. Hajer, Y.-Y. Li, T. Liu, and H. Zhang, *Heavy Higgs bosons at low* $\tan\beta$*: from the LHC to 100 TeV*, JHEP **01** (2017) 018, arXiv:1605.08744 [hep-ph].

[36] J. Kalinowski, W. Kotlarski, T. Robens, D. Sokolowska, and A. F. Zarnecki, *Exploring Inert Scalars at CLIC*, arXiv:1811.06952v1 [hep-ph].

[37] J. Kalinowski, T. Robens, D. Sokolowska, and A. F. Zarnecki, *IDM Benchmarks for the LHC and Future Colliders*, Symmetry **13** (2021) no. 6, 991, arXiv:2012.14818 [hep-ph].

[38] CLICdp Collaboration, J. Klamka and A. F. Zarnecki, *Pair-production of the charged IDM scalars at high energy CLIC*, arXiv:2201.07146 [hep-ph].

[39] X. Cid Vidal et al., *Report from Working Group 3: Beyond the Standard Model physics at the HL-LHC and HE-LHC*, CERN Yellow Rep. Monogr. **7** (2019) 585–865, arXiv:1812.07831 [hep-ph].

[40] S. Bottaro, D. Buttazzo, M. Costa, R. Franceschini, P. Panci, D. Redigolo, and L. Vittorio, *in progress*, .

[41] R. Franceschini and X. Zhao, *in progress*, .

[42] D. Curtin et al., *Long-Lived Particles at the Energy Frontier: The MATHUSLA Physics Case*, Rept. Prog. Phys. **82** (2019) no. 11, 116201, arXiv:1806.07396 [hep-ph].
[43] J. Alimena et al., *Searching for long-lived particles beyond the Standard Model at the Large Hadron Collider*, J. Phys. G **47** (2020) no. 9, 090501, arXiv:1903.04497 [hep-ex].
[44] J. Hisano, S. Matsumoto, M. Nagai, O. Saito, and M. Senami, *Non-perturbative effect on thermal relic abundance of dark matter*, Phys. Lett. B **646** (2007) 34–38, arXiv:hep-ph/0610249.
[45] ATLAS Collaboration, G. Aad et al., *Search for long-lived charginos based on a disappearing-track signature using 136 fb^{-1} of pp collisions at $\sqrt{s}$ = 13 TeV with the ATLAS detector*, arXiv:2201.02472 [hep-ex].
[46] ATLAS Collaboration, *Search for long-lived charginos based on a disappearing-track signature in pp collisions at $\sqrt{s} = 13$ TeV with the ATLAS detector*, JHEP **06** (2018) 022, arXiv:1712.02118 [hep-ex].
[47] ATLAS Collaboration, *Search for charginos nearly mass degenerate with the lightest neutralino based on a disappearing-track signature in pp collisions at $\sqrt(s)$=8 TeV with the ATLAS detector*, Phys. Rev. D **88** (2013) no. 11, 112006, arXiv:1310.3675 [hep-ex].
[48] CMS Collaboration, *Search for disappearing tracks in proton-proton collisions at $\sqrt{s} = 13$ TeV*, Phys. Lett. B **806** (2020) 135502, arXiv:2004.05153 [hep-ex].
[49] CMS Collaboration, *Search for disappearing tracks in proton-proton collisions at $\sqrt{s} = 8$ TeV*, JHEP **01** (2015) 096, arXiv:1411.6006 [hep-ex].
[50] ATLAS Collaboration, *ATLAS sensitivity to winos and higgsinos with a highly compressed mass spectrum at the HL-LHC*, . https://cds.cern.ch/record/2647294.
[51] S. Agostinelli et al., GEANT4 – *a simulation toolkit*, Nucl. Instrum. Meth. A **506** (2003) 250.
[52] N. V. Mokhov and C. C. James, *The MARS Code System User's Guide Version 15(2016)*, .
[53] ILC Collaboration, G. Aarons et al., *ILC Reference Design Report Volume 4 - Detectors*, arXiv:0712.2356 [physics.ins-det].
[54] Muon g-2 Collaboration, G. W. Bennett et al., *Final Report of the Muon E821 Anomalous Magnetic Moment Measurement at BNL*, Phys. Rev. D **73** (2006) 072003, arXiv:hep-ex/0602035.
[55] Muon g-2 Collaboration, T. Albahri et al., *Measurement of the anomalous precession frequency of the muon in the Fermilab Muon g-2 Experiment*, Phys. Rev. D **103** (2021) no. 7, 072002, arXiv:2104.03247 [hep-ex].
[56] Muon g-2 Collaboration, B. Abi et al., *Measurement of the Positive Muon Anomalous Magnetic Moment to 0.46 ppm*, Phys. Rev. Lett. **126** (2021) no. 14, 141801, arXiv:2104.03281 [hep-ex].
[57] T. Aoyama, M. Hayakawa, T. Kinoshita, and M. Nio, *Complete Tenth-Order QED Contribution to the Muon g-2*, Phys. Rev. Lett. **109** (2012) 111808, arXiv:1205.5370 [hep-ph].
[58] C. Gnendiger, D. Stöckinger, and H. Stöckinger-Kim, *The electroweak contributions to $(g-2)_\mu$ after the Higgs boson mass measurement*, Phys. Rev. D **88** (2013) 053005, arXiv:1306.5546 [hep-ph].
[59] A. Keshavarzi, D. Nomura, and T. Teubner, *Muon $g-2$ and $\alpha(M_Z^2)$: a new data-based analysis*, Phys. Rev. D **97** (2018) no. 11, 114025, arXiv:1802.02995 [hep-ph].
[60] M. Davier, A. Hoecker, B. Malaescu, and Z. Zhang, *A new evaluation of the hadronic vacuum polarisation contributions to the muon anomalous magnetic moment and to $\boldsymbol{\alpha(m_Z^2)}$*, Eur. Phys. J. C **80** (2020) no. 3, 241, arXiv:1908.00921 [hep-ph]. [Erratum: Eur.Phys.J.C 80, 410 (2020)].
[61] A. Kurz, T. Liu, P. Marquard, and M. Steinhauser, *Hadronic contribution to the muon anomalous magnetic moment to next-to-next-to-leading order*, Phys. Lett. B **734** (2014) 144–147, arXiv:1403.6400 [hep-ph].

[62] K. Melnikov and A. Vainshtein, *Hadronic light-by-light scattering contribution to the muon anomalous magnetic moment revisited*, Phys. Rev. D **70** (2004) 113006, arXiv:hep-ph/0312226.
[63] J. Bijnens, N. Hermansson-Truedsson, and A. Rodríguez-Sánchez, *Short-distance constraints for the HLbL contribution to the muon anomalous magnetic moment*, Phys. Lett. B **798** (2019) 134994, arXiv:1908.03331 [hep-ph].
[64] V. Pauk and M. Vanderhaeghen, *Single meson contributions to the muon's anomalous magnetic moment*, Eur. Phys. J. C **74** (2014) no. 8, 3008, arXiv:1401.0832 [hep-ph].
[65] I. Danilkin and M. Vanderhaeghen, *Light-by-light scattering sum rules in light of new data*, Phys. Rev. D **95** (2017) no. 1, 014019, arXiv:1611.04646 [hep-ph].
[66] P. Roig and P. Sanchez-Puertas, *Axial-vector exchange contribution to the hadronic light-by-light piece of the muon anomalous magnetic moment*, Phys. Rev. D **101** (2020) no. 7, 074019, arXiv:1910.02881 [hep-ph].
[67] G. Colangelo, M. Hoferichter, A. Nyffeler, M. Passera, and P. Stoffer, *Remarks on higher-order hadronic corrections to the muon g−2*, Phys. Lett. B **735** (2014) 90–91, arXiv:1403.7512 [hep-ph].
[68] A. Gérardin, H. B. Meyer, and A. Nyffeler, *Lattice calculation of the pion transition form factor with $N_f = 2 + 1$ Wilson quarks*, Phys. Rev. D **100** (2019) no. 3, 034520, arXiv:1903.09471 [hep-lat].
[69] E.-H. Chao, R. J. Hudspith, A. Gérardin, J. R. Green, H. B. Meyer, and K. Ottnad, *Hadronic light-by-light contribution to $(g-2)_\mu$ from lattice QCD: a complete calculation*, Eur. Phys. J. C **81** (2021) no. 7, 651, arXiv:2104.02632 [hep-lat].
[70] Fermilab Lattice, LATTICE-HPQCD, MILC Collaboration, B. Chakraborty et al., *Strong-Isospin-Breaking Correction to the Muon Anomalous Magnetic Moment from Lattice QCD at the Physical Point*, Phys. Rev. Lett. **120** (2018) no. 15, 152001, arXiv:1710.11212 [hep-lat].
[71] Budapest-Marseille-Wuppertal Collaboration, S. Borsanyi et al., *Hadronic vacuum polarization contribution to the anomalous magnetic moments of leptons from first principles*, Phys. Rev. Lett. **121** (2018) no. 2, 022002, arXiv:1711.04980 [hep-lat].
[72] RBC, UKQCD Collaboration, T. Blum, P. A. Boyle, V. Gülpers, T. Izubuchi, L. Jin, C. Jung, A. Jüttner, C. Lehner, A. Portelli, and J. T. Tsang, *Calculation of the hadronic vacuum polarization contribution to the muon anomalous magnetic moment*, Phys. Rev. Lett. **121** (2018) no. 2, 022003, arXiv:1801.07224 [hep-lat].
[73] D. Giusti, V. Lubicz, G. Martinelli, F. Sanfilippo, and S. Simula, *Electromagnetic and strong isospin-breaking corrections to the muon $g-2$ from Lattice QCD+QED*, Phys. Rev. D **99** (2019) no. 11, 114502, arXiv:1901.10462 [hep-lat].
[74] PACS Collaboration, E. Shintani and Y. Kuramashi, *Hadronic vacuum polarization contribution to the muon $g-2$ with 2+1 flavor lattice QCD on a larger than (10 fm)^4 lattice at the physical point*, Phys. Rev. D **100** (2019) no. 3, 034517, arXiv:1902.00885 [hep-lat].
[75] Fermilab Lattice, LATTICE-HPQCD, MILC Collaboration, C. T. H. Davies et al., *Hadronic-vacuum-polarization contribution to the muon's anomalous magnetic moment from four-flavor lattice QCD*, Phys. Rev. D **101** (2020) no. 3, 034512, arXiv:1902.04223 [hep-lat].
[76] A. Gérardin, M. Cè, G. von Hippel, B. Hörz, H. B. Meyer, D. Mohler, K. Ottnad, J. Wilhelm, and H. Wittig, *The leading hadronic contribution to $(g-2)_\mu$ from lattice QCD with $N_\mathrm{f} = 2 + 1$ flavours of $O(a)$ improved Wilson quarks*, Phys. Rev. D **100** (2019) no. 1, 014510, arXiv:1904.03120 [hep-lat].
[77] D. Giusti and S. Simula, *Lepton anomalous magnetic moments in Lattice QCD+QED*, PoS

LATTICE2019 (2019) 104, arXiv:1910.03874 [hep-lat].

[78] S. Borsanyi et al., *Leading hadronic contribution to the muon magnetic moment from lattice QCD*, Nature **593** (2021) no. 7857, 51–55, arXiv:2002.12347 [hep-lat].

[79] E34 Collaboration, Y. Sato, *Muon g-2/EDM experiment at J-PARC*, PoS **KMI2017** (2017) 006.

[80] G. Abbiendi et al., *Measuring the leading hadronic contribution to the muon g-2 via μe scattering*, Eur. Phys. J. C **77** (2017) no. 3, 139, arXiv:1609.08987 [hep-ex].

[81] W. Buchmuller and D. Wyler, *Effective Lagrangian Analysis of New Interactions and Flavor Conservation*, Nucl. Phys. B **268** (1986) 621–653.

[82] R. Capdevilla, D. Curtin, Y. Kahn, and G. Krnjaic, *Discovering the physics of $(g-2)_\mu$ at future muon colliders*, Phys. Rev. D **103** (2021) no. 7, 075028, arXiv:2006.16277 [hep-ph].

[83] R. Capdevilla, D. Curtin, Y. Kahn, and G. Krnjaic, *A No-Lose Theorem for Discovering the New Physics of $(g-2)_\mu$ at Muon Colliders*, arXiv:2101.10334 [hep-ph].

[84] Muon Collider Collaboration, D. Schulte, *The International Muon Collider Collaboration*, JACoW **IPAC2021** (2021) THPAB017.

[85] A. Abbasabadi, D. Bowser-Chao, D. A. Dicus, and W. W. Repko, *Higgs photon associated production at $e\bar{e}$ colliders*, Phys. Rev. D **52** (1995) 3919–3928, arXiv:hep-ph/9507463.

[86] Muon (g-2) Collaboration, G. W. Bennett et al., *An Improved Limit on the Muon Electric Dipole Moment*, Phys. Rev. D **80** (2009) 052008, arXiv:0811.1207 [hep-ex].

[87] Muon g-2 Collaboration, R. Chislett, *The muon EDM in the g-2 experiment at Fermilab*, EPJ Web Conf. **118** (2016) 01005.

[88] T. P. Gorringe and D. W. Hertzog, *Precision Muon Physics*, Prog. Part. Nucl. Phys. **84** (2015) 73–123, arXiv:1506.01465 [hep-ex].

[89] G. F. Giudice, P. Paradisi, and M. Passera, *Testing new physics with the electron g-2*, JHEP **11** (2012) 113, arXiv:1208.6583 [hep-ph].

[90] R. Capdevilla, D. Curtin, Y. Kahn, and G. Krnjaic, *Systematically Testing Singlet Models for $(g-2)_\mu$*, arXiv:2112.08377 [hep-ph].

[91] A. Greljo, Y. Soreq, P. Stangl, A. E. Thomsen, and J. Zupan, *Muonic Force Behind Flavor Anomalies*, arXiv:2107.07518 [hep-ph].

[92] M. Bauer, P. Foldenauer, and J. Jaeckel, *Hunting All the Hidden Photons*, JHEP **07** (2018) 094, arXiv:1803.05466 [hep-ph].

[93] P. Ballett, M. Hostert, S. Pascoli, Y. F. Perez-Gonzalez, Z. Tabrizi, and R. Zukanovich Funchal, *Z's in neutrino scattering at DUNE*, Phys. Rev. D **100** (2019) no. 5, 055012, arXiv:1902.08579 [hep-ph].

[94] G. Mohlabeng, *Revisiting the dark photon explanation of the muon anomalous magnetic moment*, Phys. Rev. D **99** (2019) no. 11, 115001, arXiv:1902.05075 [hep-ph].

[95] W. Altmannshofer, S. Gori, M. Pospelov, and I. Yavin, *Neutrino Trident Production: A Powerful Probe of New Physics with Neutrino Beams*, Phys. Rev. Lett. **113** (2014) 091801, arXiv:1406.2332 [hep-ph].

[96] G. Krnjaic, G. Marques-Tavares, D. Redigolo, and K. Tobioka, *Probing Muonphilic Force Carriers and Dark Matter at Kaon Factories*, Phys. Rev. Lett. **124** (2020) no. 4, 041802, arXiv:1902.07715 [hep-ph].

[97] Y. Kahn, G. Krnjaic, N. Tran, and A. Whitbeck, *M^3: a new muon missing momentum experiment to probe $(g-2)_?$ and dark matter at Fermilab*, JHEP **09** (2018) 153, arXiv:1804.03144 [hep-ph].

[98] S. N. Gninenko, D. V. Kirpichnikov, and N. V. Krasnikov, *Probing millicharged particles with NA64 experiment at CERN*, Phys. Rev. D **100** (2019) no. 3, 035003, arXiv:1810.06856 [hep-ph].

[99] I. Galon, E. Kajamovitz, D. Shih, Y. Soreq, and S. Tarem, *Searching for muonic forces with the ATLAS detector*, Phys. Rev. D **101** (2020) no. 1, 011701, arXiv:1906.09272 [hep-ph].

[100] C.-Y. Chen, M. Pospelov, and Y.-M. Zhong, *Muon Beam Experiments to Probe the Dark Sector*, Phys. Rev. D **95** (2017) no. 11, 115005, arXiv:1701.07437 [hep-ph].

[101] L. Calibbi and G. Signorelli, *Charged Lepton Flavour Violation: An Experimental and Theoretical Introduction*, Riv. Nuovo Cim. **41** (2018) no. 2, 71–174, arXiv:1709.00294 [hep-ph].

[102] BaBar Collaboration, B. Aubert et al., *Searches for Lepton Flavor Violation in the Decays $\tau^\pm \to e^\pm\gamma$ and $\tau^\pm \to \mu^\pm\gamma$*, Phys. Rev. Lett. **104** (2010) 021802, arXiv:0908.2381 [hep-ex].

[103] K. Kannike, M. Raidal, D. M. Straub, and A. Strumia, *Anthropic solution to the magnetic muon anomaly: the charged see-saw*, JHEP **02** (2012) 106, arXiv:1111.2551 [hep-ph]. [Erratum: JHEP 10, 136 (2012)].

[104] R. Dermisek and A. Raval, *Explanation of the Muon g-2 Anomaly with Vectorlike Leptons and its Implications for Higgs Decays*, Phys. Rev. D **88** (2013) 013017, arXiv:1305.3522 [hep-ph].

[105] R. Dermisek, K. Hermanek, and N. McGinnis, *Di-Higgs and tri-Higgs boson signals of muon g-2 at a muon collider*, Phys. Rev. D **104** (2021) no. 9, L091301, arXiv:2108.10950 [hep-ph].

[106] R. Dermisek, K. Hermanek, and N. McGinnis, *Muon g-2 in two-Higgs-doublet models with vectorlike leptons*, Phys. Rev. D **104** (2021) no. 5, 055033, arXiv:2103.05645 [hep-ph].

[107] R. Dermisek, K. Hermanek, and N. McGinnis, *Highly Enhanced Contributions of Heavy Higgs Bosons and New Leptons to Muon $g-2$ and Prospects at Future Colliders*, Phys. Rev. Lett. **126** (2021) no. 19, 191801, arXiv:2011.11812 [hep-ph].

[108] LHCb Collaboration, R. Aaij et al., *Test of lepton universality in beauty-quark decays*, arXiv:2103.11769 [hep-ex].

[109] C. Bobeth, G. Hiller, and G. Piranishvili, *Angular distributions of $\bar{B} \to \bar{K}\ell^+\ell^-$ decays*, JHEP **12** (2007) 040, arXiv:0709.4174 [hep-ph].

[110] M. Bordone, G. Isidori, and A. Pattori, *On the Standard Model predictions for R_K and R_{K^*}*, Eur. Phys. J. C **76** (2016) no. 8, 440, arXiv:1605.07633 [hep-ph].

[111] LHCb Collaboration, R. Aaij et al., *Test of lepton universality with $B^0 \to K^{*0}\ell^+\ell^-$ decays*, JHEP **08** (2017) 055, arXiv:1705.05802 [hep-ex].

[112] B. Capdevila, A. Crivellin, S. Descotes-Genon, J. Matias, and J. Virto, *Patterns of New Physics in $b \to s\ell^+\ell^-$ transitions in the light of recent data*, JHEP **01** (2018) 093, arXiv:1704.05340 [hep-ph].

[113] A. K. Alok, B. Bhattacharya, A. Datta, D. Kumar, J. Kumar, and D. London, *New Physics in $b \to s\mu^+\mu^-$ after the Measurement of R_{K^*}*, Phys. Rev. D **96** (2017) no. 9, 095009, arXiv:1704.07397 [hep-ph].

[114] Belle Collaboration, A. Abdesselam et al., *Test of lepton flavor universality in $B \to K\ell^+\ell^-$ decays*, arXiv:1908.01848 [hep-ex].

[115] Belle Collaboration, A. Abdesselam et al., *Test of lepton flavor universality in $B \to K^*\ell^+\ell^-$ decays at Belle*, arXiv:1904.02440 [hep-ex].

[116] W. Altmannshofer and P. Stangl, *New physics in rare B decays after Moriond 2021*, Eur. Phys. J. C **81** (2021) no. 10, 952, arXiv:2103.13370 [hep-ph].

[117] J. Aebischer, W. Altmannshofer, D. Guadagnoli, M. Reboud, P. Stangl, and D. M. Straub, *B-decay discrepancies after Moriond 2019*, Eur. Phys. J. C **80** (2020) no. 3, 252, arXiv:1903.10434 [hep-ph].

[118] V. Gherardi, D. Marzocca, and E. Venturini, *Low-energy phenomenology of scalar leptoquarks at one-loop accuracy*, JHEP **01** (2021) 138, arXiv:2008.09548 [hep-ph].

[119] A. Greljo, P. Stangl, and A. E. Thomsen, *A model of muon anomalies*, Phys. Lett. B **820** (2021)

136554, arXiv:2103.13991 [hep-ph].
[120] L. Di Luzio, M. Kirk, A. Lenz, and T. Rauh, *ΔM_s theory precision confronts flavour anomalies*, JHEP **12** (2019) 009, arXiv:1909.11087 [hep-ph].
[121] A. Greljo and D. Marzocca, *High-p_T dilepton tails and flavor physics*, Eur. Phys. J. C **77** (2017) no. 8, 548, arXiv:1704.09015 [hep-ph].
[122] CMS Collaboration, A. M. Sirunyan et al., *Search for resonant and nonresonant new phenomena in high-mass dilepton final states at $\sqrt{s}$ = 13 TeV*, JHEP **07** (2021) 208, arXiv:2103.02708 [hep-ex].
[123] T. Han, Y. Ma, and K. Xie, *High energy leptonic collisions and electroweak parton distribution functions*, Phys. Rev. D **103** (2021) no. 3, L031301, arXiv:2007.14300 [hep-ph].
[124] T. Han, Y. Ma, and K. Xie, *Quark and gluon contents of a lepton at high energies*, JHEP **02** (2022) 154, arXiv:2103.09844 [hep-ph].
[125] F. Garosi, D. Marzocca, and S. Trifinopoulos, *(in progress)*, .
[126] Y. Afik, S. Bar-Shalom, J. Cohen, and Y. Rozen, *Searching for New Physics with $b\bar{b}\ell^+\ell^-$ contact interactions*, Phys. Lett. B **807** (2020) 135541, arXiv:1912.00425 [hep-ex].
[127] D. Marzocca, U. Min, and M. Son, *Bottom-Flavored Mono-Tau Tails at the LHC*, JHEP **12** (2020) 035, arXiv:2008.07541 [hep-ph].
[128] A. Azatov, F. Garosi, A. Greljo, D. Marzocca, J. Salko, and S. Trifinopoulos, *New physics in R_K: FCC-hh or a Muon Collider (in progress)*, .
[129] D. Buttazzo, A. Greljo, G. Isidori, and D. Marzocca, *B-physics anomalies: a guide to combined explanations*, JHEP **11** (2017) 044, arXiv:1706.07808 [hep-ph].
[130] G.-y. Huang, S. Jana, F. S. Queiroz, and W. Rodejohann, *Probing the RK(*) anomaly at a muon collider*, Phys. Rev. D **105** (2022) no. 1, 015013, arXiv:2103.01617 [hep-ph].
[131] B. Allanach, F. S. Queiroz, A. Strumia, and S. Sun, *Z' models for the LHCb and $g-2$ muon anomalies*, Phys. Rev. D **93** (2016) no. 5, 055045, arXiv:1511.07447 [hep-ph]. [Erratum: Phys.Rev.D 95, 119902 (2017)].
[132] F. del Aguila, M. Chala, J. Santiago, and Y. Yamamoto, *Collider limits on leptophilic interactions*, JHEP **03** (2015) 059, arXiv:1411.7394 [hep-ph].
[133] F. S. Queiroz, K. Sinha, and A. Strumia, *Leptoquarks, Dark Matter, and Anomalous LHC Events*, Phys. Rev. D **91** (2015) no. 3, 035006, arXiv:1409.6301 [hep-ph].
[134] A. Angelescu, D. Bečirević, D. A. Faroughy, and O. Sumensari, *Closing the window on single leptoquark solutions to the B-physics anomalies*, JHEP **10** (2018) 183, arXiv:1808.08179 [hep-ph].
[135] P. Asadi, R. Capdevilla, C. Cesarotti, and S. Homiller, *Searching for leptoquarks at future muon colliders*, JHEP **10** (2021) 182, arXiv:2104.05720 [hep-ph].
[136] A. Baldini et al., *A submission to the 2020 update of the European Strategy for Particle Physics on behalf of the COMET, MEG, Mu2e and Mu3e collaborations*, arXiv:1812.06540 [hep-ex].
[137] B. Murakami and T. M. P. Tait, *Searching for lepton flavor violation at a future high energy e+e- collider*, Phys. Rev. D **91** (2015) 015002, arXiv:1410.1485 [hep-ph].
[138] V. Cirigliano, B. Grinstein, G. Isidori, and M. B. Wise, *Minimal flavor violation in the lepton sector*, Nucl. Phys. B **728** (2005) 121–134, arXiv:hep-ph/0507001.
[139] N. Arkani-Hamed, H.-C. Cheng, J. L. Feng, and L. J. Hall, *Probing lepton flavor violation at future colliders*, Phys. Rev. Lett. **77** (1996) 1937–1940, arXiv:hep-ph/9603431.
[140] S. Homiller, Q. Lu, and M. Reece, *to appear*, .
[141] G.-y. Huang, F. S. Queiroz, and W. Rodejohann, *Gauged $L_\mu - L_\tau$ at a muon collider*, Phys. Rev. D **103** (2021) no. 9, 095005, arXiv:2101.04956 [hep-ph].

[142] W. Liu, K.-P. Xie, and Z. Yi, *Testing leptogenesis at the LHC and future muon colliders: a Z' scenario*, arXiv:2109.15087 [hep-ph].

[143] N. Chakrabarty, T. Han, Z. Liu, and B. Mukhopadhyaya, *Radiative Return for Heavy Higgs Boson at a Muon Collider*, Phys. Rev. D **91** (2015) no. 1, 015008, arXiv:1408.5912 [hep-ph].

[144] M. Karliner, M. Low, J. L. Rosner, and L.-T. Wang, *Radiative return capabilities of a high-energy, high-luminosity e^+e^- collider*, Phys. Rev. D **92** (2015) no. 3, 035010, arXiv:1503.07209 [hep-ph].

[145] CMS Collaboration, S. Chatrchyan et al., *The CMS Experiment at the CERN LHC*, JINST **3** (2008) S08004.

[146] A. Freitas, *Weakly coupled neutral gauge bosons at future linear colliders*, Phys. Rev. D **70** (2004) 015008, arXiv:hep-ph/0403288.

[147] BaBar Collaboration, J. Lees et al., *Search for a muonic dark force at BABAR*, Phys. Rev. D **94** (2016) no. 1, 011102, arXiv:1606.03501 [hep-ex].

[148] E. Ma, D. Roy, and S. Roy, *Gauged L(mu) - L(tau) with large muon anomalous magnetic moment and the bimaximal mixing of neutrinos*, Phys. Lett. B **525** (2002) 101–106, arXiv:hep-ph/0110146.

[149] J. Heeck and W. Rodejohann, *Gauged $L_\mu - L_\tau$ Symmetry at the Electroweak Scale*, Phys. Rev. D **84** (2011) 075007, arXiv:1107.5238 [hep-ph].

[150] ATLAS Collaboration, G. Aad et al., *Direct constraint on the Higgs-charm coupling from a search for Higgs boson decays into charm quarks with the ATLAS detector*, arXiv:2201.11428 [hep-ex].

[151] ATLAS Collaboration, G. Aad et al., *A search for the dimuon decay of the Standard Model Higgs boson with the ATLAS detector*, Phys. Lett. B **812** (2021) 135980, arXiv:2007.07830 [hep-ex].

[152] CMS Collaboration, A. M. Sirunyan et al., *Evidence for Higgs boson decay to a pair of muons*, JHEP **01** (2021) 148, arXiv:2009.04363 [hep-ex].

[153] ATLAS Collaboration, *Projections for measurements of Higgs boson signal strengths and coupling parameters with the ATLAS detector at a HL-LHC*, http://cds.cern.ch/record/1956710, Oct, 2014.

[154] T. Han, W. Kilian, N. Kreher, Y. Ma, J. Reuter, T. Striegl, and K. Xie, *Precision test of the muon-Higgs coupling at a high-energy muon collider*, JHEP **12** (2021) 162, arXiv:2108.05362 [hep-ph].

[155] T. Han and Z. Liu, *Direct Measurement of the Higgs Boson Total Width at a Muon Collider*, Phys.Rev. **D87** (2013) 033007, arXiv:1210.7803 [hep-ph].

[156] E. Eichten and A. Martin, *The Muon Collider as a H/A factory*, Phys.Lett. **B728** (2014) 125–130, arXiv:1306.2609 [hep-ph].

[157] Y. Alexahin, C. M. Ankenbrandt, D. B. Cline, A. Conway, M. A. Cummings, et al., *Muon Collider Higgs Factory for Snowmass 2013*, arXiv:1308.2143 [hep-ph].

[158] M. Greco, T. Han, and Z. Liu, *ISR effects for resonant Higgs production at future lepton colliders*, Phys. Lett. B **763** (2016) 409–415, arXiv:1607.03210 [hep-ph].

[159] J. de Blas, J. Gu, and Z. Liu, *Understanding the Higgs Precision at resonant muon collider Higgs factory*, .

[160] H. Haber, G. L. Kane, and T. Sterling, *The Fermion Mass Scale and Possible Effects of Higgs Bosons on Experimental Observables*, Nucl.Phys. **B161** (1979) 493.

[161] J.-P. Delahaye, C. Ankenbrandt, A. Bogacz, S. Brice, A. Bross, et al., *Enabling Intensity and Energy Frontier Science with a Muon Accelerator Facility in the U.S.: A White Paper Submitted

to the 2013 U.S. Community Summer Study of the Division of Particles and Fields of the Amer, arXiv:1308.0494 [physics.acc-ph].

[162] J. Alwall, M. Herquet, F. Maltoni, O. Mattelaer, and T. Stelzer, *MadGraph 5 : Going Beyond*, JHEP **1106** (2011) 128, arXiv:1106.0522 [hep-ph].

[163] T. Sjostrand, S. Mrenna, and P. Z. Skands, *PYTHIA 6.4 Physics and Manual*, JHEP **0605** (2006) 026, arXiv:hep-ph/0603175 [hep-ph].

[164] V. Barger, L. L. Everett, H. E. Logan, and G. Shaughnessy, *Scrutinizing h(125) in Two Higgs Doublet Models at the LHC, ILC, and Muon Collider*, arXiv:1308.0052 [hep-ph].

[165] B. A. Dobrescu, *Massless gauge bosons other than the photon*, Phys. Rev. Lett. **94** (2005) 151802, arXiv:hep-ph/0411004.

[166] K. Long, D. Lucchesi, M. Palmer, N. Pastrone, D. Schulte, and V. Shiltsev, *Muon colliders to expand frontiers of particle physics*, Nature Phys. **17** (2021) no. 3, 289–292, arXiv:2007.15684 [physics.acc-ph].

[167] M. Casarsa, M. Fabbrichesi, and E. Gabrielli, *Mono-chromatic single photon events at the muon collider*, arXiv:2111.13220 [hep-ph].

[168] OPAL Collaboration, G. Abbiendi et al., *Search for anomalous photonic events with missing energy in e^+e^- collisions at $\sqrt{s} = 130, 136$ and 183 GeV*, Eur. Phys. J. C **8** (1999) 23–40, arXiv:hep-ex/9810021.

[169] L3 Collaboration, P. Achard et al., *Single photon and multiphoton events with missing energy in e^+e^- collisions at LEP*, Phys. Lett. B **587** (2004) 16–32, arXiv:hep-ex/0402002.

[170] DELPHI Collaboration, J. Abdallah et al., *Photon events with missing energy in e+ e- collisions at s**(1/2) = 130-GeV to 209-GeV*, Eur. Phys. J. C **38** (2005) 395–411, arXiv:hep-ex/0406019.

[171] CDF Collaboration, T. Aaltonen et al., *Search for large extra dimensions in final states containing one photon or jet and large missing transverse energy produced in $p\bar{p}$ collisions at $\sqrt{s}$ = 1.96-TeV*, Phys. Rev. Lett. **101** (2008) 181602, arXiv:0807.3132 [hep-ex].

[172] D0 Collaboration, V. M. Abazov et al., *Search for large extra dimensions via single photon plus missing energy final states at $\sqrt{s}$ = 1.96-TeV*, Phys. Rev. Lett. **101** (2008) 011601, arXiv:0803.2137 [hep-ex].

[173] ATLAS Collaboration, M. Aaboud et al., *Search for new phenomena in events with a photon and missing transverse momentum in pp collisions at $\sqrt{s} = 13$ TeV with the ATLAS detector*, JHEP **06** (2016) 059, arXiv:1604.01306 [hep-ex].

[174] CMS Collaboration, A. M. Sirunyan et al., *Search for new physics in final states with a single photon and missing transverse momentum in proton-proton collisions at $\sqrt{s}$ = 13 TeV*, JHEP **02** (2019) 074, arXiv:1810.00196 [hep-ex].

[175] E. Gabrielli, B. Mele, M. Raidal, and E. Venturini, *FCNC decays of standard model fermions into a dark photon*, Phys. Rev. D **94** (2016) no. 11, 115013, arXiv:1607.05928 [hep-ph].

[176] B. Holdom, *Two U(1)'s and Epsilon Charge Shifts*, Phys. Lett. B **166** (1986) 196–198.

[177] L. Darmé, F. Giacchino, E. Nardi, and M. Raggi, *Invisible decays of axion-like particles: constraints and prospects*, JHEP **06** (2021) 009, arXiv:2012.07894 [hep-ph].

[178] R. Bollig, W. DeRocco, P. W. Graham, and H.-T. Janka, *Muons in Supernovae: Implications for the Axion-Muon Coupling*, Phys. Rev. Lett. **125** (2020) no. 5, 051104, arXiv:2005.07141 [hep-ph]. [Erratum: Phys.Rev.Lett. 126, 189901 (2021)].

[179] F. D'Eramo, R. Z. Ferreira, A. Notari, and J. L. Bernal, *Hot Axions and the H_0 tension*, JCAP **11** (2018) 014, arXiv:1808.07430 [hep-ph].

[180] M. Pospelov, *Secluded U(1) below the weak scale*, Phys. Rev. D **80** (2009) 095002, arXiv:0811.1030 [hep-ph].

[181] M. Escudero, D. Hooper, G. Krnjaic, and M. Pierre, *Cosmology with A Very Light $L_\mu - L_\tau$ Gauge Boson*, JHEP **03** (2019) 071, arXiv:1901.02010 [hep-ph].

[182] L. Bento, J. C. Romao, and A. Barroso, *e+ e- —> gamma + MISSING NEUTRALS: NEUTRINO VERSUS PHOTINO PRODUCTION*, Phys. Rev. D **33** (1986) 1488.

[183] F. A. Berends, G. J. H. Burgers, C. Mana, M. Martinez, and W. L. van Neerven, *Radiative Corrections to the Process $e^+e^- \to$ Neutrino Anti-neutrino γ*, Nucl. Phys. B **301** (1988) 583–600.

[184] J. S. Marshall and M. A. Thomson, *The Pandora Software Development Kit for Pattern Recognition*, Eur. Phys. J. C **75** (2015) no. 9, 439, arXiv:1506.05348 [physics.data-an].

[185] NA64 Collaboration, D. Banerjee et al., *Search for Axionlike and Scalar Particles with the NA64 Experiment*, Phys. Rev. Lett. **125** (2020) no. 8, 081801, arXiv:2005.02710 [hep-ex].

[186] DELPHI Collaboration, J. Abdallah et al., *Search for one large extra dimension with the DELPHI detector at LEP*, Eur. Phys. J. C **60** (2009) 17–23, arXiv:0901.4486 [hep-ex].

[187] BaBar Collaboration, J. P. Lees et al., *Search for Invisible Decays of a Dark Photon Produced in e^+e^- Collisions at BaBar*, Phys. Rev. Lett. **119** (2017) no. 13, 131804, arXiv:1702.03327 [hep-ex].

[188] Belle-II Collaboration, W. Altmannshofer et al., *The Belle II Physics Book*, PTEP **2019** (2019) no. 12, 123C01, arXiv:1808.10567 [hep-ex]. [Erratum: PTEP 2020, 029201 (2020)].

[189] M. J. Dolan, T. Ferber, C. Hearty, F. Kahlhoefer, and K. Schmidt-Hoberg, *Revised constraints and Belle II sensitivity for visible and invisible axion-like particles*, JHEP **12** (2017) 094, arXiv:1709.00009 [hep-ph]. [Erratum: JHEP 03, 190 (2021)].

[190] J. D. Bjorken, S. Ecklund, W. R. Nelson, A. Abashian, C. Church, B. Lu, L. W. Mo, T. A. Nunamaker, and P. Rassmann, *Search for Neutral Metastable Penetrating Particles Produced in the SLAC Beam Dump*, Phys. Rev. D **38** (1988) 3375.

[191] D. Pagani and M. Zaro, *One-loop electroweak Sudakov logarithms: a revisitation and automation*, JHEP **02** (2022) 161, arXiv:2110.03714 [hep-ph].